Stephen F. Austin State University

SFA ScholarWorks

Spring 5-2024

Depositional Facies and Petrophysical Characterization of the Leonardian Carbonate (Lower Clear Fork), Tex-Mex, S.E. Field, Central Basin Platform, West Texas

Seyram Nyamasekpor
Stephen F. Austin State University, seyram.nyamey@gmail.com

Depositional Facies and Petrophysical Characterization of the Leonardian Carbonate (Lower Clear Fork), Tex-Mex, S.E. Field, Central Basin Platform, West Texas

Creative Commons License

DEPOSITIONAL FACIES AND PETROPHYSICAL CHARACTERIZATION OF THE

LEONARDIAN CARBONATE (LOWER CLEAR FORK), TEX-MEX, S.E. FIELD,

CENTRAL BASIN PLATFORM, WEST TEXAS

By

SEYRAM NYAMASEKPOR, Bachelor of Science

Presented to the Faculty of the Graduate School of

Stephen F. Austin State University

In Partial Fulfillment

Of the Requirements

For the Degree of

Master of Science

STEPHEN F. AUSTIN STATE UNIVERSITY

MAY 2024

DEPOSITIONAL FACIES AND PETROPHYSICAL CHARACTERIZATION OF THE
LEONARDIAN CARBONATE (LOWER CLEAR FORK), TEX-MEX, S.E. FIELD,
CENTRAL BASIN PLATFORM, WEST TEXAS

By

SEYRAM NYAMASEKPOR, Bachelor of Science

APPROVED:

_____
Dr. Julie Bloxson, Thesis Director

_____
Dr. R. LaRell Nielson, Committee Member

_____
Dr. Melinda Faulkner, Committee Member

_____
Dr. Robert Friedfeld, Committee Member

_____
Forrest Lane, Ph. D.
Dean of Research and Graduate Studies

ABSTRACT

The Lower Clear Fork from Tex-Mex, S.E. Field on the Central Basin Platform is a typical complex reservoir that displays high heterogeneity in lithological and petrophysical properties. The unit represents a producing reservoir succession of Leonardian platform carbonates deposited in shallow marine water during the Early Permian. The sediment of the Lower Clear Fork is composed of a mixed succession of dolomite interbedded with anhydrite, minor clay minerals, and siliciclastics. The high heterolithic nature of the reservoir makes efficient recovery of hydrocarbons difficult. This situation requires an understanding of the variability in depositional facies in terms of mineralogy, depositional textures and structures, and an assessment of its petrophysical properties. As of December 2023, cumulative production of hydrocarbon from the Tex-Mex, S.E. Field reached about 88,308 barrels of oil equivalent.

The study at Tex-Mex, S.E. Field utilized 338.9 ft (103.3 m) of Lower Clear Fork cored sample, core data, and wireline data from a key well. Key data utilized included core descriptions, wireline logs, routine core analysis data, petrographic thin sections, and whole rock mineralogical data from X-ray Diffraction. These data helped to (1) determine the paleoenvironments under which the Lower Clear Fork sediments were deposited, (2) build a core-calibrated petrophysical mineral model of the Lower Clear Fork from wireline logs and XRD mineralogy, and (3) assess the petrophysical properties of the Lower Clear Fork reservoir.

The integration of core/log analysis, XRD data, routine core data, and petrographic observations revealed seven (7) facies regrouped into four (4) major facies associations each representing the mineralogy, sedimentary textures, pore characteristics, and paleodepositional environment. The Lower Clear Fork, a second-order Leonardian sequence represents facies transitioning from dolomitized inner to ramp crest facies (skeletal/peloidal wackestone to grain-dominated packstone) in the lower part, to dolomitized restricted lagoon and tidal flats/sabkha facies (dolomudstone/anhydrite) in the upper part. The petrophysical characteristics of the Lower Clear Fork reservoir were dominantly controlled by post-depositional processes that altered the primary carbonate mineralogy and pore development. The principal diagenetic processes included reflux dolomitization, gypsum precipitation (later transformed into anhydrite), and dissolution of anhydrite and dolomite cement.

Mineralogical results revealed the dominance of dolomite, anhydrite with minor amounts of clay, and siliciclastics. Calibrated porosity values within the interval vary from 0.5% to 10%, while Klinkenberg permeability was in the range of 10^{-4} mD to 17.6 mD. The Lower Clear Fork facies showed dominance of high water saturation values, reaching up to 95.4%, and comparatively low oil saturation levels, peaking at a value of 14.4% in the dolopackstone facies. Overall, the Lower Clear Fork reservoir is of low quality, however, the grain-rich dolopackstone facies offered the most favorable reservoir properties when compared with other facies in the interval.

DEDICATION

This thesis is dedicated to my beloved parents, siblings, and friends, whose acts of kindness, steadfast support, and prayers were the guiding pillars that carried me through my academic journey. Their unwavering presence and assistance have been instrumental, and I wholeheartedly acknowledge that without their enduring love and encouragement, I would not have reached the place I am today. I also express my deepest gratitude to Hellen Adzo Djabeng, whose love, understanding, and encouragement have been my inspiration every step of the way. With heartfelt appreciation and profound gratitude, I dedicate this thesis to them.

ACKNOWLEDGEMENTS

TABLE OF CONTENTS

LIST OF FIGURES

LIST OF TABLES

LIST OF EQUATIONS

LIST OF ABBREVIATIONS

bbl.   Barrel

Bbbl.   Billion Barrels

BOE   Barrels of oil equivalent

BVW   Bulk Volume of Water (Porosity * Water Saturation)

CBP   Central Basin Platform

CSV   Comma-Separated Values

CT   Computed Tomography

EOR   Enhanced Oil Recovery

GR   Gamma Ray

K   Permeability

ϕ Porosity

LCLF   Lower Clear Fork

IP   Interactive Petrophysics Software

MMbbl.   Million Barrels

MCF   1000 cubic feet of natural gas

MICP   Mercury Injection Capillary Pressure

MSFL	Micro-Spherically Focused Log
OOIP	Original Oil in Place
PB	Permian Basin
PPL	Plain Polarized Light
XPL	Cross Polarized Light
PEF	Photoelectric Factor (Log)
PhiT	Total Porosity
RCAL	Routine Core Analysis
Rxo	Resistivity of the Flushed Zone (Invaded zone)
Rmf	Resistivity of the Mud Filtrate
Rt	True Resistivity of the Formation
SEM	Scanning Electron Microscopy
SGR	Spectra Gamma Ray
SWT	Total Water Saturation
S_w	Water Saturation
S_{oil}	Oil Saturation
Tex-Mex, S.E.	Texas-Mexico, South-East Field
XRD	X-ray Diffraction

UV	Ultraviolet Light
Vclay	Volume of Clay
V_{clayGR}	Volume of Clay (from Gamma Ray)
WL	White Light (Plain)

1. INTRODUCTION

The Lower Clear Fork is a productive hydrocarbon reservoir occurring within the Clear Fork Group carbonates, deposited in shallow water during the Leoardian stage (Leonardian - North American; Cisuralian Epoch, Kungurian in age (stage) - International). The Leonardian stage was marked by global changes in climate and sea level (Montañez et al., 2007). The Lower Clear Fork is part of the Leonardian succession which is composed of an assemblage of platform, marginal, and basinal deposits forming significant Leonardian reservoirs extending across West Texas and New Mexico (Figure 1.1; Ruppel, 2020; Ruppel & Jones, 2006). These reservoirs have been a target for drilling and production activities for a century in the Permian Basin.

In the Permian Basin, the Leonardian succession is as thick as 2500 ft [762 m] (Ruppel et al., 2002). Tyler et al., (1984) identified these reservoirs as restricted platform systems that possess distinct attributes that make them a low-quality reservoir, such as low recovery efficiencies, dolomitized with associated evaporites, and low permeability and porosity values (Figure 1.2). However, according to Holtz et al. (1992), the original oil in place at discovery was estimated to be more than 14.5 billion barrels of oil (Bbbl), accounting for about 15% of the total in-place resources within the Permian Basin (Figure 1.2). As of the year 2000, these carbonates provided more than 3.1 Bbbl of oil, amounting to about 10% of the total resources recovered from the Permian Basin (Dutton et al., 2005).
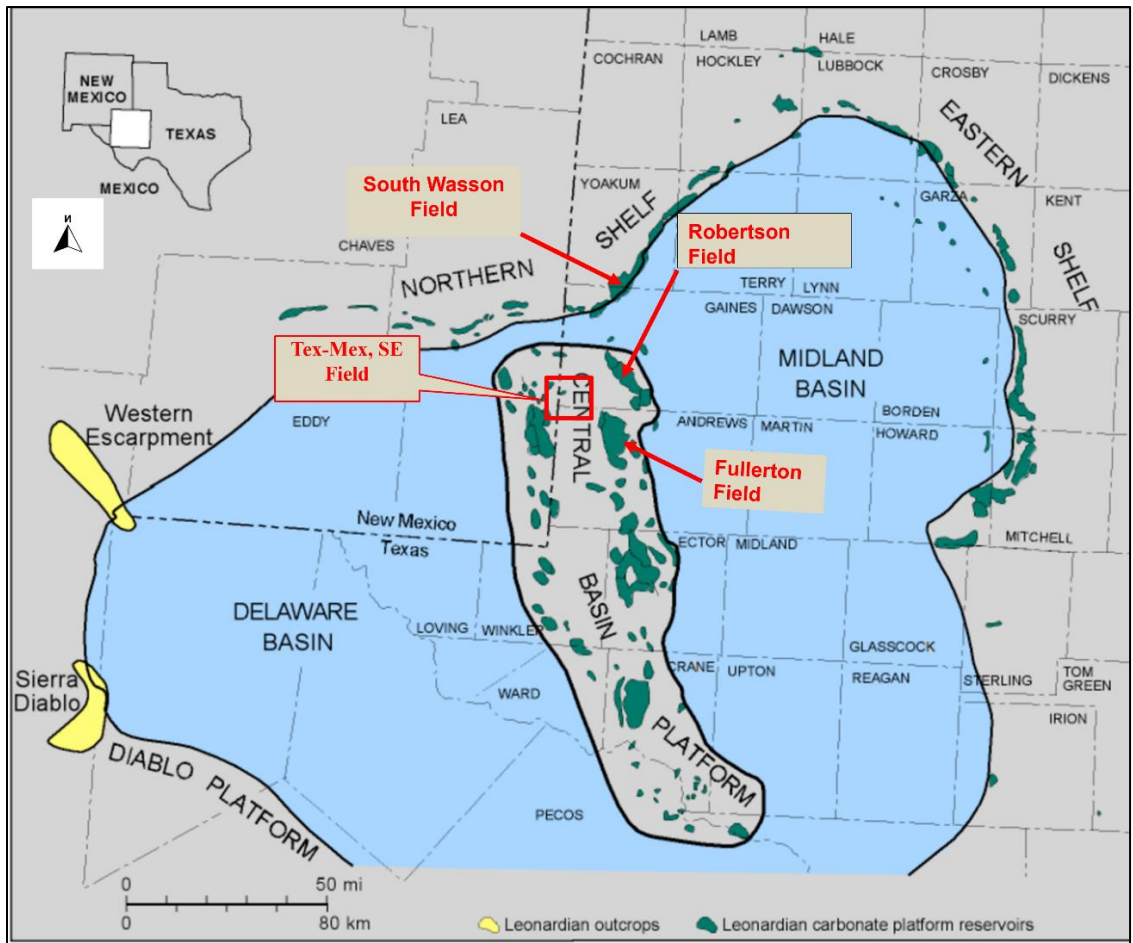
Figure 1.1. Regional map of the Permian Basin showing Leonardian carbonate platform reservoirs and its outcrop analogs from Sierra Diablo and Guadalupe Mountains. Tex-Mex, S.E. Field area outlined in red. (Modified from Ruppel & Jones, 2006).
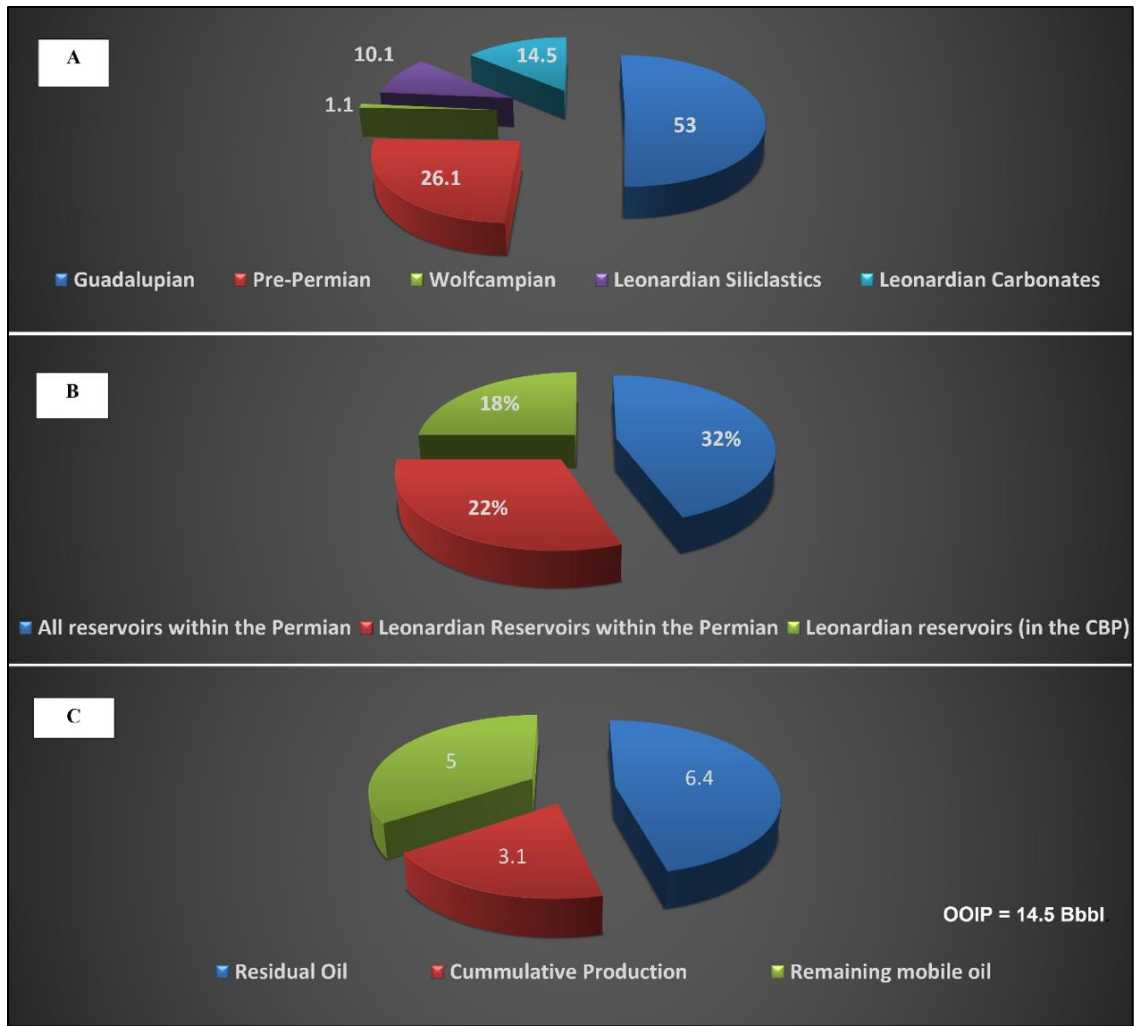
Figure 1.2. Leonardian reservoirs statistics in the Permian Basin at the end of the year 2002. (A) Distribution of original oil in place (Bbbl.). (B) Recovery efficiencies of reservoirs. (C) Volumetrics in Bbbl for the Leonardian reservoirs. (Historical numbers for the charts adapted from Ruppel et al., 2002).

The estimates from Dutton et al. (2005) and Holtz et al., (1992) put the recovery efficiencies of the Leonardian carbonate reservoirs within the Central Basin Platform (CBP) and the Permian Basin to about 18% and 22%, respectively, of the original oil in place (Figure 1.2). These recovery estimates are significantly lower than the approximated 32% average recovery rate for all carbonate reservoirs in the Permian Basin due to the high lithologic heterogeneity in the Leonardian carbonate reservoirs (Montgomery, 1998; Tyler et al., 1984). The high lithologic heterogeneity is attributable to the variation in the depositional facies (both vertical and lateral) caused by high-frequency, cyclic deposition in low-energy carbonate platform environments and by equally complex post-depositional diagenesis. This reasoning has been corroborated by authors including Holtz et al. (1992), Ruppel (1992), and Ruppel & Jones (2006). Though exhibiting low recovery efficiencies, studies confirmed that Leonardian reservoirs are ranked second for conventional reservoirs in the Permian Basin (Dutton et al., 2005; Ruppel, 2020).

Consequently, the Leonardian Lower Clear Fork reservoir displays a wide range of lithological and reservoir properties that impede efficient hydrocarbon recovery in the Permian Basin. However, technological advancements in horizontal drilling and hydraulic fracturing have been applied in the Permian Basin since the late 1980s and early 1990s to help maximize the recovery of hydrocarbons from these reservoirs beyond what can be achieved with primary recovery methods. To deploy these key technologies, there is a need to understand the geological and petrophysical characteristics of these reservoirs.

This study investigates the depositional facies, petrophysical, and mineralogical properties of the Lower Clear Fork reservoir from the Tex-Mex, S.E. Field. The investigation involves the integration of core, wireline data interpretation, and parameters extracted from sedimentological data and petrographic thin sections.

1.1. Objectives and Purpose

This study seeks to examine and improve the geologic understanding of the Lower Clear Fork reservoir in Tex-Mex, S.E. Field, Central Basin Platform in west Texas (Figure 1.1). This work can also aid in enhanced exploration and production of the remaining hydrocarbons in place. These objectives were as follows:

1) Determine the major depositional facies and related environments in which the Lower Clear Fork carbonates from Tex-Mex, S.E. Field were deposited.

2) Build a mineral model to determine the mineralogical composition of the Lower Clear Fork carbonates from Tex-Mex, S.E. Field using wireline logs from the Peterson 1P well and calibrating the interpretations with core-derived XRD data.

3) Assess the petrophysical properties from wireline interpretation and match the results to core-derived petrophysical data of the Lower Clear Fork interval in Tex-Mex, S.E. Field.

1.2. Study Area

The Tex-Mex, S.E. Field area, covers Andrews and Gaines County in west Texas and southeastern New Mexico and is a producing oil and gas field on the Central Basin Platform in the Permian Basin. The primary wireline logs and core samples used in this study were from the key well, Peterson 1P, located on section 17, Block A-27 PSL Survey, A-407 in southern Gaines County (Figure 1.3).
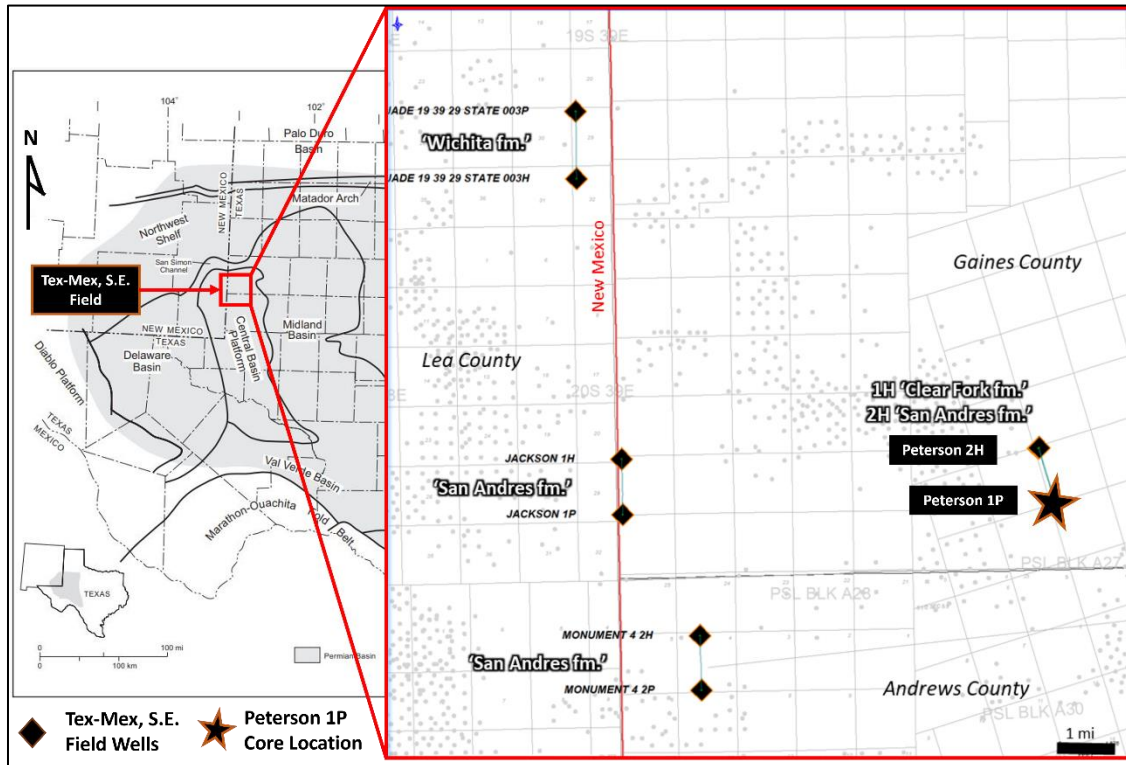
Figure 1.3. Location map showing of the Tex-Mex, S.E. Field showing well and cores. The light gray dots denote wells drilled in the area. The Permian Basin map was modified from Dutton et al., (2004). The Tex-Mex, S.E. Field outline is approximated as the red square, and its location was based on data and information provided by Sozo Natural Resources.

The field, with an initial lease area of 1 square mile (640 acres) was initially owned by RGX Energy LLC from Midland, Texas until it was acquired by Sozo Naural Resources. The permit to drill the well was approved in November 2017 and spudded in April 2018. Three months on, the first oil production was recorded (Enverus Inc., 2024). Figure 1.4 shows the production statistics from the Tex-Mex, S.E. Field since it began production in July 2018.

In the field area, outcrops of the Leonardian platform carbonates are not exposed. The Leonardian outcrops in the Permian Basin are limited to the western and southern mountains - Glass Mountains to the south and Guadalupe Mountains to the west (Figure 1.1). The Tex-Mex, S.E. Field has three production zones, the San Andres, the Lower Clear Fork, and the Wichita Formation.
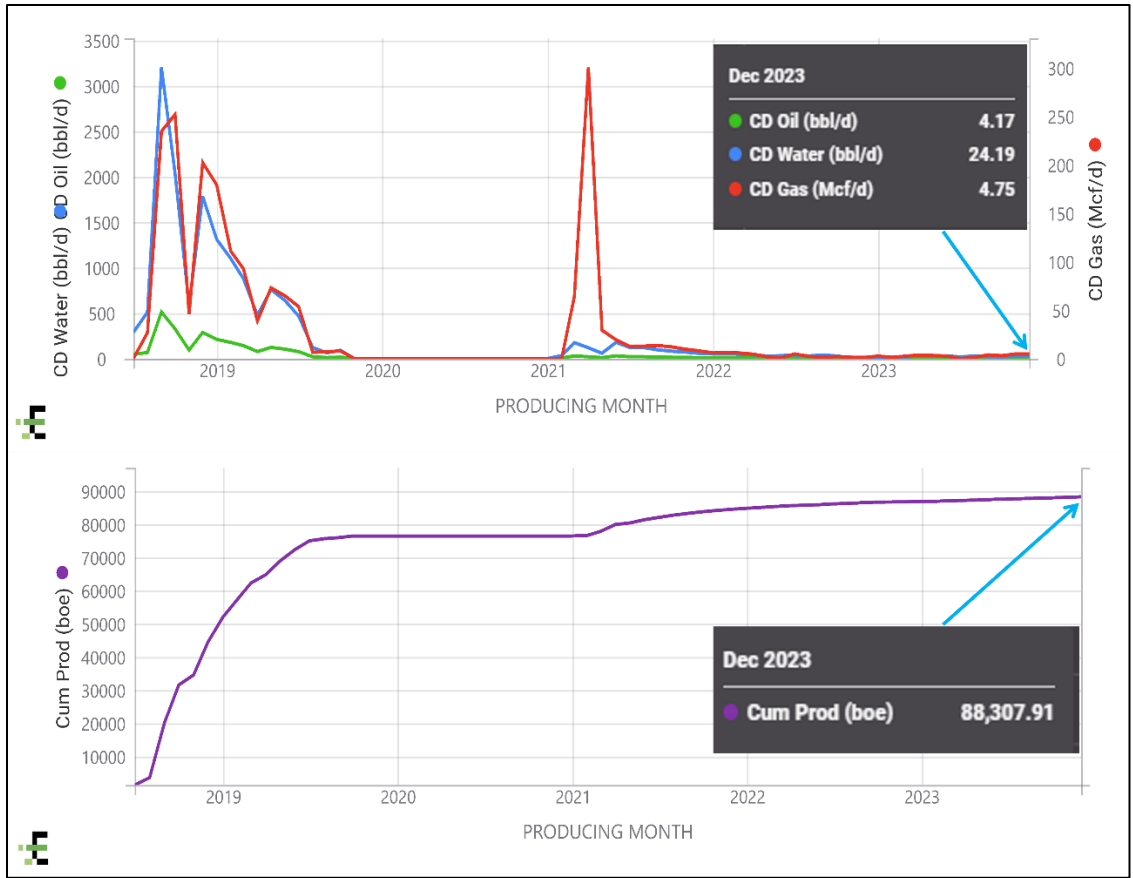
Figure 1.4. Hydrocarbon production from the study well in the Tex-Mex, SE Field (Peterson 1P). The top graph shows the cumulative distribution of water, oil, and gas production from the well per day. The bottom graph shows the cumulative production in barrels of oil equivalent tracked from July 2018 to December 2023. (Source: Enverus Prism Analytics, last accessed on February 23, 2024).

1.3. Previous Work

The Clear Fork carbonate reservoirs situated on the Central Basin Platform have been the subject of research in recent years. While few studies have been conducted on these reservoir successions, it is important to recognize that these studies were comprehensive and detailed. The reference to the name "Clear Fork Group" was originally used by Cummins (1890) for outcrops found along the Clear Fork of Brazos River (north of Abilene, Texas). A year later, Cummins (1891) formalized and fully described the Clear Fork strata. In the North-Central Texas area, Cummins described the composition of the Clear Fork as dominantly red mudstone, with minor amounts of gray mudstone, deposited on coastal plains and mudflats, fluvial-channel origin sandstones, and thin but laterally extensive beds of intertidal to shallow-subtidal dolomite (Chaney & Dimichele 2007).

Published works by P.B. King and others, King, (1942) and King et al., (1965) on the stratigraphy of the Permian Basin carried out in the 1930's documented fundamental geologic information on the Permian Basin area. King's original work on the outcrops at Victorio Peak, an equivalent of the subsurface Clear Fork Group, Abo, and Wichita Group at the Guadalupe and Sierra Diablo Mountain described the Lower Clear Fork as shallow-water-platform dolostone.

Work by Silver & Todd (1969) discussed the cyclic nature of the Permian Shelf sediments on the Northern Shelf of the Midland Basin. Their work recognized three major cycles and five basic lithofacies within the Clear Fork Group. These lithofacies included

9

shelf evaporite-carbonate, shelf clastics, shelf-margin carbonate, basin carbonate, and basin clastics.

Mazzullo (1982) and Mazzullo & Reid (1989) discussed the overviews of Lower Leonardian stratigraphy, reservoir potential, and depositional systems in the Midland Basin using seismic interpretations, well-cuttings, and wireline logs. Their findings established that the Leonardian strata from the platform to the basin are a complex wedge of carbonate, evaporite, and siliciclastic rocks representing different depositional systems. Their work also recognized that the progradation of the Lower Clear Fork was cyclic and mostly rapid during the periods of sea level rise and fall.

Ruppel et al. (2000) and Kerans et al. (2000) studied the depositional setting, facies, and stratal architecture of the Lower Clear Fork and Abo at the Sierra Diablo Mountains of west Texas, an outcrop analog of the producing subsurface Clear Fork reservoirs. Their study revealed that karsting significantly affected both the Abo Formation and the overlying Lower Clear Fork succession. Ruppel (2002) described the facies, cyclicity, and diagenesis in the Glorieta and Upper Clear Fork at Monahans Clear Fork field on the Central Basin platform. Their model suggested that the Clear Fork reservoir development was caused by cyclic deposition and diagenesis driven by episodic sea level rise and fall.

Ruppel & Jones (2006) and Ruppel & Harrington (2012) conducted comprehensive investigations into the facies and sequence stratigraphy which they presented in the latest work on critical tools for reservoir framework definition at the Fullerton Clear Fork

reservoir. Their work highlighted that the Leonardian reservoir succession across the broader Permian Basin comprises the base of Guadalupian San Andres, Glorieta, Clear Fork Group (Lower, Middle, and Upper Clear Fork), and Wichita/Abo Formations. The reservoir architecture in the Lower Clear Fork predominantly comprises altenating peritidal-tidal flat and subtidal facies, that occurred mainly during late transgression and early highstand. Notably, the most substantial porosity and permeability development within the Lower Clear Fork is linked to incompletely dolomitized grain-rich packstones and grainstones. Also, their study revealed a well-developed cyclicity in the deposition of the sediments.

2. GEOLOGIC SETTING

This section provides an overview of the regional geologic history, development, and structural setting of the Permian Basin. The major tectonic events that shaped the sedimentary development of the Permian Basin are summarized in Table 2.1. Leonardian stratigraphy and the depositional setting of the Lower Clear Fork are also discussed.

2.1. Geological Development of the Permian Basin

The Permian Basin is a complex Paleozoic sedimentary basin spanning an area of 11,583 squared miles (300,000 km^2) covering west Texas and southeastern New Mexico of the United States (Galley, 1958; Ward et al., 1986). The basin is found in the foreland of the Marathon-Ouachita orogenic belt (Fairhurst et al., 2021). The Permian Basin is filled with Phanerozoic carbonates, evaporites, and siliciclastics to a maximum depth of 33,136.5 ft (10,100 m) (Frenzel et al., 1988). Generally, the tectonic evolution of the current Permian Basin can be put into three stages – The Cambrian to Mississipian (Tobosa Stage), Mississipian to Early Permian (Collision Phase), and then Early Permian to current - structural stable phase and deposition of carbonates and clastics (Hills, 1984).

Table 2.1. Tectonic events in the Permian Basin. The yellow and blue colors denote major activities that led to the creation of the current Permian Basin configuration. Tectonic information was gathered from Adams (1965), Frenzel et al. (1988), and Hills (1984).

AGE			TECTONIC EVENTS/ACTIVITIES OF THE PERMIAN BASIN
CENOZOIC	Tert.		
			Laramide Orogeny
MESOZOIC	Cretac.		Sea Level Rise/Transgression
			Thin Sediment deposition in the Permian
	Jura.		Exposure of the Permian Basin
	Tri.		Regional Deposition in the Permian Basin
PALEOZOIC	Permian	Ochoan	Evaporite deposition
		Guad	Filling of the remnant of the Midland Basin
		Leo	Restriction of marine circulation and the start of evaporites precipitation. Continuation of rapid subsidence and deposition of fine-grained sediments on the basin floor; carbonates and intercalated siliciclastics accumulation on the platforms.
		Wolf	
	Carb.	Penn.	Development of shallow water platforms and carbonate shelves around the basin. Marathon-Ouachita Orogeny (Collision North America and South American plates) Collision of North America and Gondwana Land (South America and Africa) (Hercynian Orogeny) * Central Basin Platform Uplifted
		Miss.	
	Devo.		Sea Level Fall/Regression
	Silu.		Regional Subsidence & Filling of the Tobosa Basin
	Ordov.		
	Cambrain		Trangression of the sea/marine

13

2.1.1. Tobosa Stage: Cambrian to Mississippian

According to Galley (1958), during the Early Paleozoic Era, what is currently known as the Permian Basin was originally a shallow, broad, and gently dipping depression known as the Tobosa Basin. At this time, Tobosa was characterized by weak crustal extension and exhibited a low subsidence rate. Tobosa, otherwise referred to as the Ancestral Permian Basin, however, remained relatively stable from its formation until partitioning into the current Permian configuration – Delaware Basin to the west, median uplifted Central Basin Platform, and Midland Basin to the east (Frenzel et al., 1988). The ancestral Tobosa, and its evolutionary stages into the current Permian Basin configuration during the Early Paleozoic Era, are shown in Figure 2.1.

From the Early Ordovician through the Devonian, the Tobosa Basin experienced regional subsidence and consequent sediment deposition of widespread and relatively uniform shelf carbonates and thin basinal shales (Hills, 1984). In the Early Ordovician, the Ellenburger Sea deposited a wedge of sediments across the Texas-New Mexico area. In the offshore areas, evenly bedded shelf carbonates were deposited on the thin near-shore clastics. The basal coarse-grained clastics were derived from the weathering of the underlying basement. The carbonate shelves, including the Eastern and Northern Shelf, were wide and shallow (Hills, 1984). The Early to Middle Mississippian was marked by thicker depositions of brown and dark-gray shales along the axis of the Tobosa, filling the starved depressions created during the Devonian (Adams, 1965).
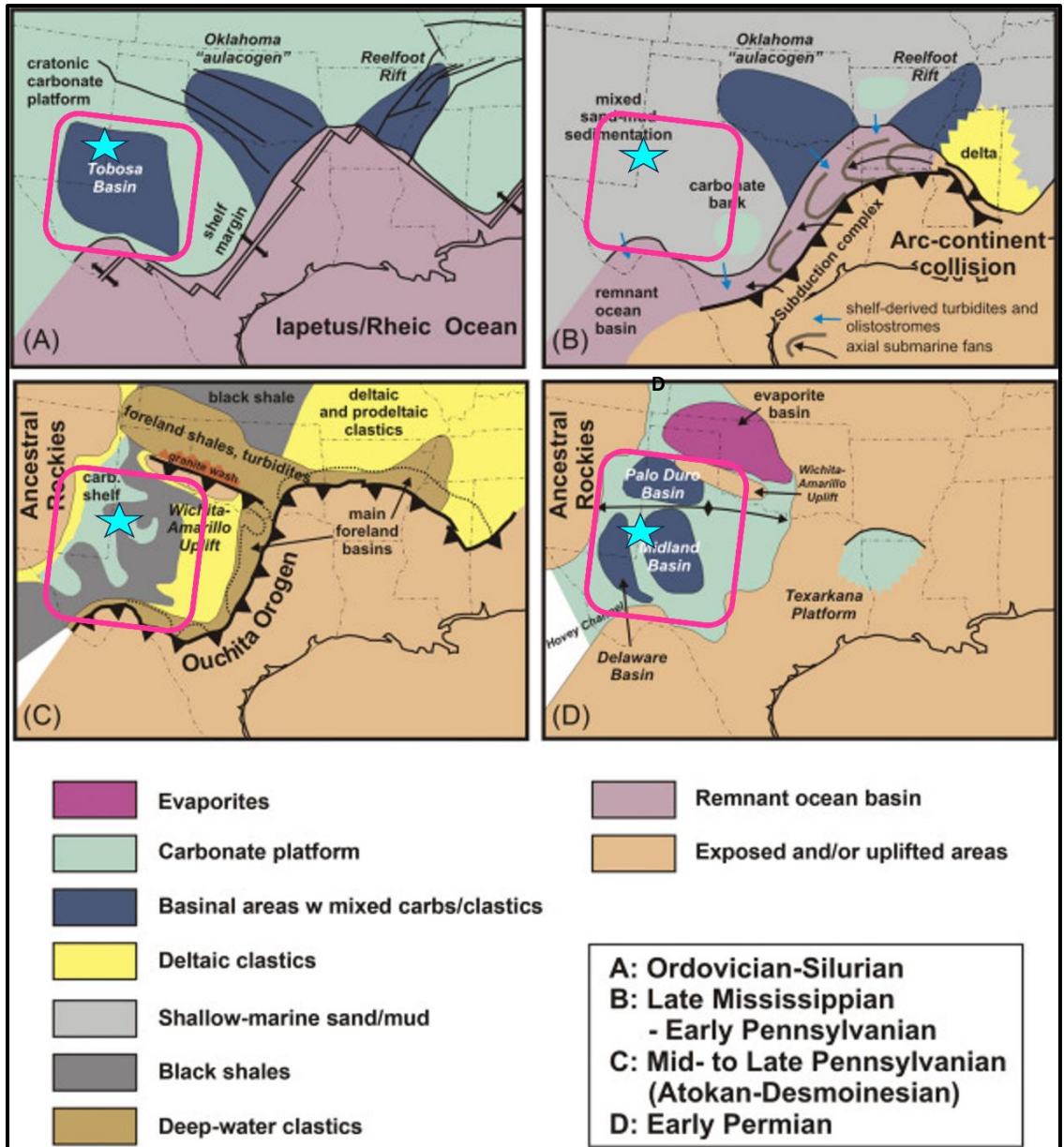
Figure 2.1. Tectonic development of the Permian Basin from its ancestral Tobosa Basin from Ordovician through the Early Permian. The red square shows the Tobosa/Permian Basin outline and the green star indicates the approximate location of the Tex-Mex, S.E. Field. Figures adapted from (Miall, 2008).

2.1.2. Collision Stage: Late Mississippian to Early Permian

The architecture of the current Permian Basin comprising the two sags (the Delaware and Midland basins) and the uplifted median portion (Central Basin Platform) was established in a collisional event known as the "Hercynian Orogeny" during the Mississippian. The Hercynian Orogeny was occasioned by the collision of the North American plate with the South American and African continental plates (Gondwana Land) (Horak, 1985). The Marathon-Ouachita Orogeny was an associated event that involved the collision of the North American with the South American continental plates that gave rise to the Ouachita-Marathon fold belt. The compression from the southwest end of the basin caused faulting and folding resulting in the uplift of the Central Basin (Frenzel et al., 1988). The collision also created the Ozona Arch, the Val Verde Basin, and partitioned the ancestral Tobosa Basin into the current configuration (Figure 5; Adams, 1965; Hills, 1984).

In the Early Pennsylvanian (Figure 2.2A), sedimentation began in the Permian Basin with rapid subsidence of basins and shelf areas. During this time, carbonate sediments were deposited over the Eastern Shelf, the Central Basin Platform, and the Northern Shelf while organic-rich shale deposition occurred predominantly in the basinal areas (Galley, 1958; Hoak et al., 1998). The rapid subsidence of the basinal areas created deeper areas unfavorable for limestone deposition. Following the deposition, these carbonate reefs broke apart due to accelerated tectonic activities and subsidence in the surrounding basinal regions, including the Marathon fold belt (Ewing, 2016; Hills, 1984).
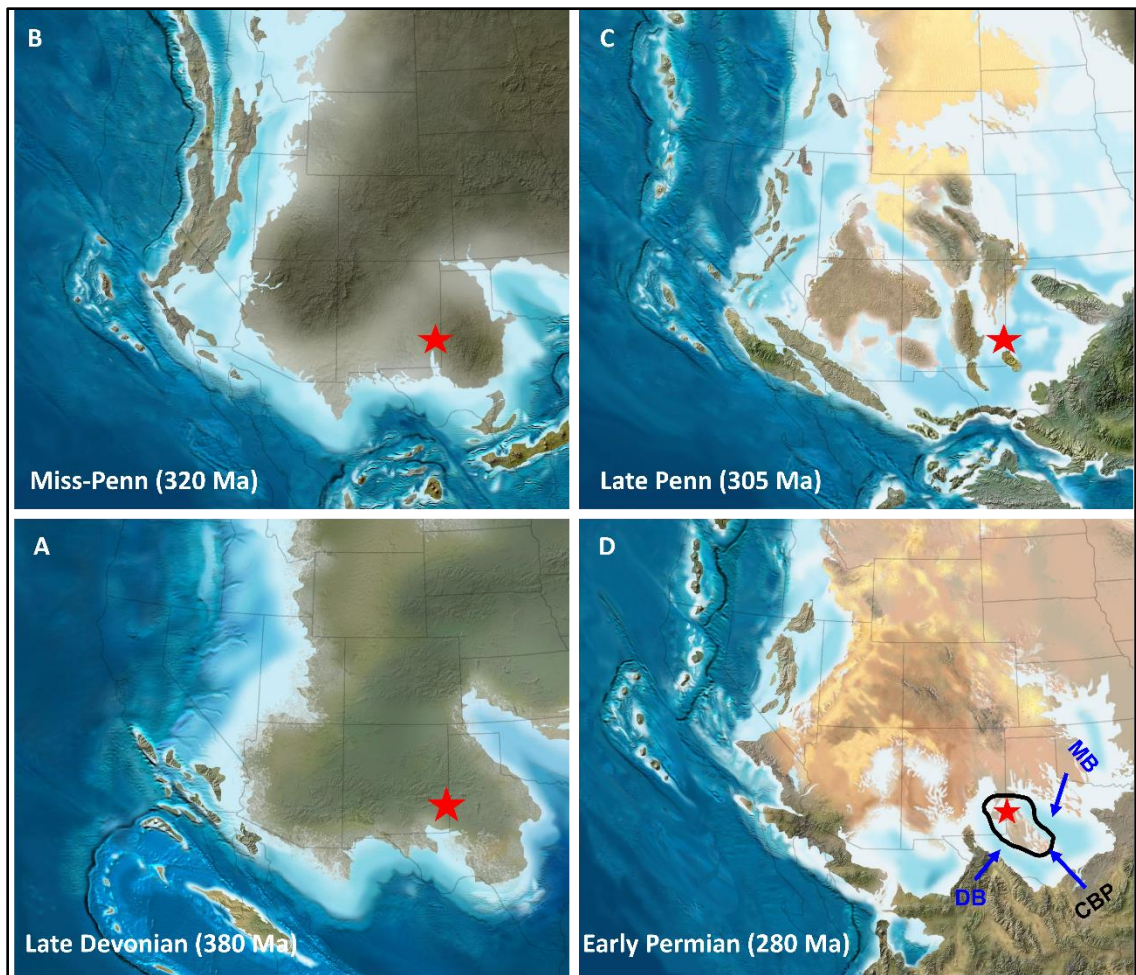
Figure 2.2. Paleogeographic maps showing depositional environment changes in the Permian Basin area from the Late Devonian through the Early Permian period (Red star is the approximate location of Tex-Mex, S.E. Field). The dark blue colors of the paleogeographic maps represent deep marine (abyssal) areas; Light blue colors represent shallow seas (shelf); Brown and Army green colors represent coastal plains/terrestrial environments. DB = Delaware Basin; MB = Midland Basin; CBP = Central Basin Platform location pointed by the blue arrow (Paleomaps adapted from Blakey, 2013).

17

2.1.3. Permian to Stable Stage: Early Permian to Current

In the Early Permian, rapid subsidence progressed with an accumulation of about 8,000 feet (2,440 m) of turbidites resulting in compressional stresses in the underlying rocks (Adams, 1965). The uplifted Central Platform enabled the development of extensive reefs (platform carbonates) and the building of shelf margins around the Delaware and Midland Basin edges during the Pennsylvanian-Wolfcampian. However, the depocenters of the basinal areas were filled with deep-water siliciclastics (Hills, 1984). At the same time, carbonates and intercalated siliciclastics accumulated in the platform areas (Adams, 1965).

The Early Permian period experienced icehouse conditions from the Late Mississippian transitioning to an arid greenhouse and warmer climate by the end of the Permian period (Montañez et al., 2007). The resulting sea level fluctuations at high frequency during the period marked the high cyclicity in the carbonates deposited on the platform (Mazzullo & Reid, 1989; Silver & Todd, 1969). In the Leonardian, the circulation of marine water ceased marking the start of evaporite precipitation in the Permian Basin (Hills, 1972). Subsequently in the Middle Permian, the subsidence rate reduced drastically with reduced sediment supply as a result of leveling of the mountains on the west and northwest. The deposits in the basinal areas largely consisted of fine-grained sandstone, dark limestone, and shale. On the eastward, the slow rising of the median ridge was completely capped by bedded shelf limestones.

According to Adams (1965), the name "Central Basin Platform" is generally applied to the intra-basin limestone bank.

During Guadalupian time, subsidence in the basinal areas slowed down. From Ward et al., (1986), carbonate accumulation in the Eastern shelf, Midland Basin, and Central Basin Platform ceased and instead became sites of cyclical deposition of sandstone, anhydrite, and halite. Finally in the Ochoan Epoch, the Delaware Basin was filled with thick evaporite deposits. At the close of the Permian, the entire area rose above sea level (Galley, 1958; 1971). A cross-section of the Permian configuration is shown in Figure 2.3. The Central Basin Platform represents the uplifted portion of the current Permian Basin configuration.
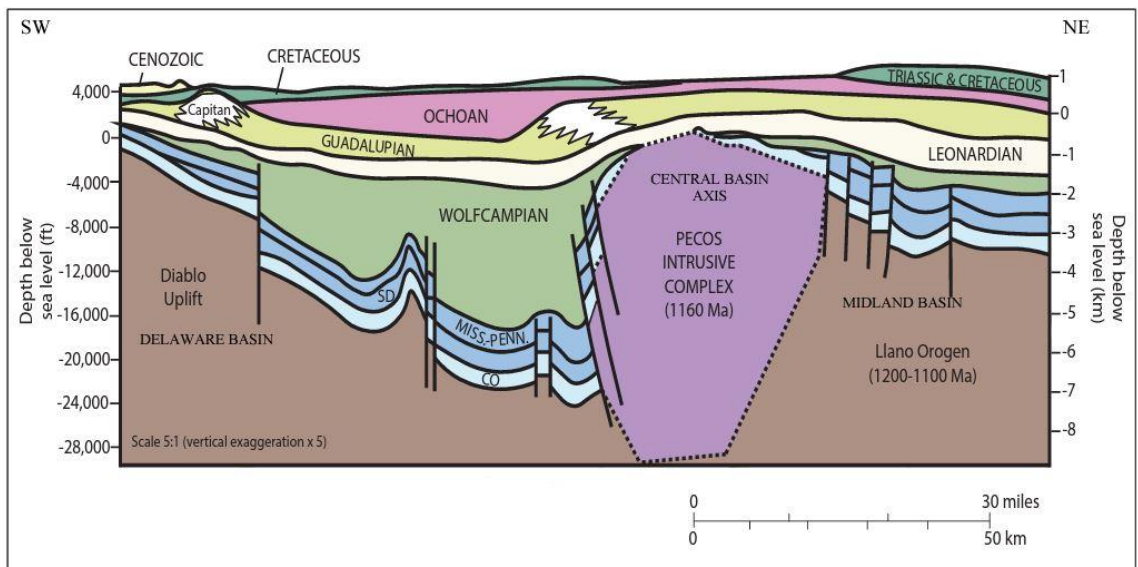
Figure 2.3. Southwest-northeast cross-section of the current Permian Basin crustal configuration. Vertical Exaggeration for the cross section is 5x. (Ewing, 2016).

2.2. Leonardian Stratigraphy

The Leonardian succession in the Permian Basin area accumulated on shallow-water carbonate platforms and in deep subtidal environments (Figure 2.2; Ruppel & Jones, 2006). The platform succession is predominantly shallow-water peritidal to subtidal facies. In the slope and basinal areas, the deposits are dominantly deep-water sandstone turbidites and carbonate debris flows (Ruppel & Jones, 2006). Eustatic sea level changes controlled the high cyclicity of sediment deposition during the Leonardian Stage (Silver & Todd, 1969).
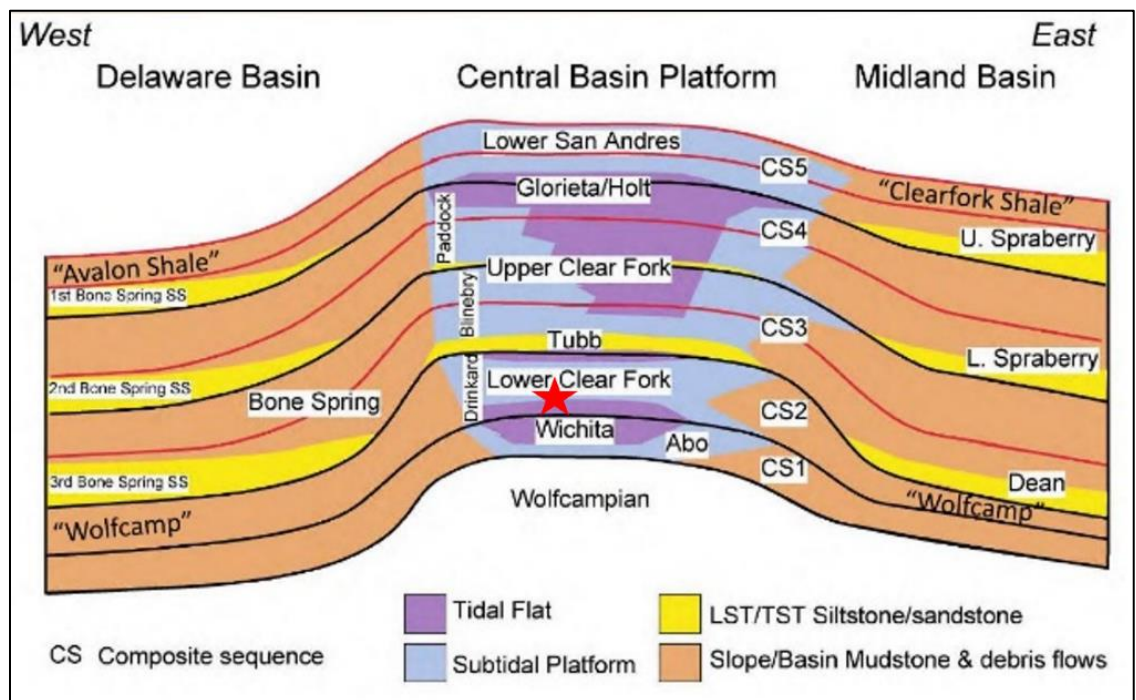
Figure 2.4. Regional stratigraphic cross-section of the Leonardian carbonates in the Permian Basin. The red star indicates the study formation (Lower Clear Fork). Figure modified from Ruppel (2017).

Authors including Atchley et al., (1999); Montgomery, (1998); Ruppel et al., (2000, 2002); Ruppel & Harrington, (2012); and Ruppel & Jones, (2006) carried out detailed studies of the subsurface Clear Fork platform carbonates and its equivalent outcrop analogs along the Diablo Platform in West Texas using core, wireline logs, and seismic data. These studies have led to the establishment of a well-defined stratigraphic framework for the Leonardian carbonates on the Central Basin Platform and the broader Permian Basin region. These extensive studies stem from the active interest in these reservoirs in the context of oil and gas exploration and production, a focus that has persisted throughout the last century.

In the Central Basin Platform, the Wichita/Abo Group, Clear Fork Group (Lower, Tubb, Upper Clear Fork), the Glorieta Sandstones, and the lowest part of the San Andres Formation constitute the Leonardian carbonates (Figure 2.5). In the Tex-Mex, S.E. Field, the productive reservoirs include the San Andres, Wichita, and the Lower Clear Fork. However, in this study, San Andres and Wichita were not examined. The approximately 338.9 feet (103.3 m) of core from the Peterson 1P well consists of dolomite and interbedded anhydrite with a minor amount of clay and siliciclastics (Figure 2.5). This observation from analysis of the core is consistent with conclusions reported by Ruppel et al., (2002) on the outcrop equivalent of the Lower Clear Fork at the Sierra Diablo Platform. Within the Clear Fork Group, the Tubb Formation separates the Lower and Upper Clear Fork. The Tubb Formation acts as a seal to the Lower Clear Fork and Wichita reservoirs (Jenkins, 1987).

Stage	Tex-Mex, S.E. Field - CBP			Depth (ft)	Lithology	Descriptions
Permian	Leonardian	Guad.	San Andreas	4328.0	Anhydrite	Nodular and bedded Anhydrite
					Dolomite	mix with sands and interbedded
				4656.0	Sand	with dolomite
			Glorieta			Interbedded siltstone, silty dolomite, and anhydrite
		Clear Fork Group	U. Clear Fork			Anhydrite/Dolomite
			Tubb			Sandstone/Dolomite/Anhydrite
			Lower Clear Fork Fm.	6885.0		Higher concentration of sands/silts & anhydrites
						Predominantly dolomite with interbedded anhydrite
						Higher concentration of sands / silts
						Predominantly dolomite with interbedded anhydrite
						Higher concentration of anhydrite in section
		Abo	Wichita Group	7223.9		Limestones and anhydrite dominated top with interbedded dolomite. Dolomite dominated base.
		Wolf	Wolfcamp			Limestones, Conglomerate, and Shales

Legend: Dolomite, Anhydrite, Sand, Cored Section

Figure 2.5. Stratigraphic units of the Central Basin Platform in the Permian Basin. The description of the lithological composition of the Lower Clear Fork cored interval from this study from Tex-Mex, S.E. Field is shown. Stratigraphic and lithology information adapted from Atchley et al., (1999); Montgomery, (1998); Ruppel et al., (2000, 2002); Ruppel & Harrington, (2012); and Ruppel & Jones, (2006).

22

2.3. Depositional Setting

Generally, the Leonardian carbonate succession on the Central Basin Platform was deposited under an open marine environment in a shallow-water carbonate platform environment. (Figure 2.2; Figure 2.6). The facies are predominantly shallow-water peritidal and downdip subtidal carbonates. The thickness of the Leonardian carbonate interval is up to 2,500 ft (762m) (Ruppel et al., 2000). Ruppel et al. (1995), from using established facies relationships, developed a 3D deposition model that relates the facies to the platform geography (Figure 2.6). In their geological model, four distinct facies were used and represented. Tidal-flat facies including fenestral mudstones, and evaporites occupy the innermost section of the platform. These facies show characteristics of frequent exposure. The middle platform is characterized by mud-dominated skeletal and peloidal wackestones with low wave energy. The ramp crest facies display evidence of high-energy settings dominated by grain-dominated packstones and oolitic grainstones (Ruppel et al., 1995). The outer ramp areas are dominantly fusulinid wackestone and packstones with some locally by small buildups with associated crinoid wackestone/packstones. The outer platform marks the transition from shallow to deeper water conditions. This setting is dominated by fusulinid wackestone/packstones and small local buildups of associated crinoid wackestone/packstones. The Outer ramp marks the transition from a shallow water condition to deeper water (Ruppel & Ward, 2013).
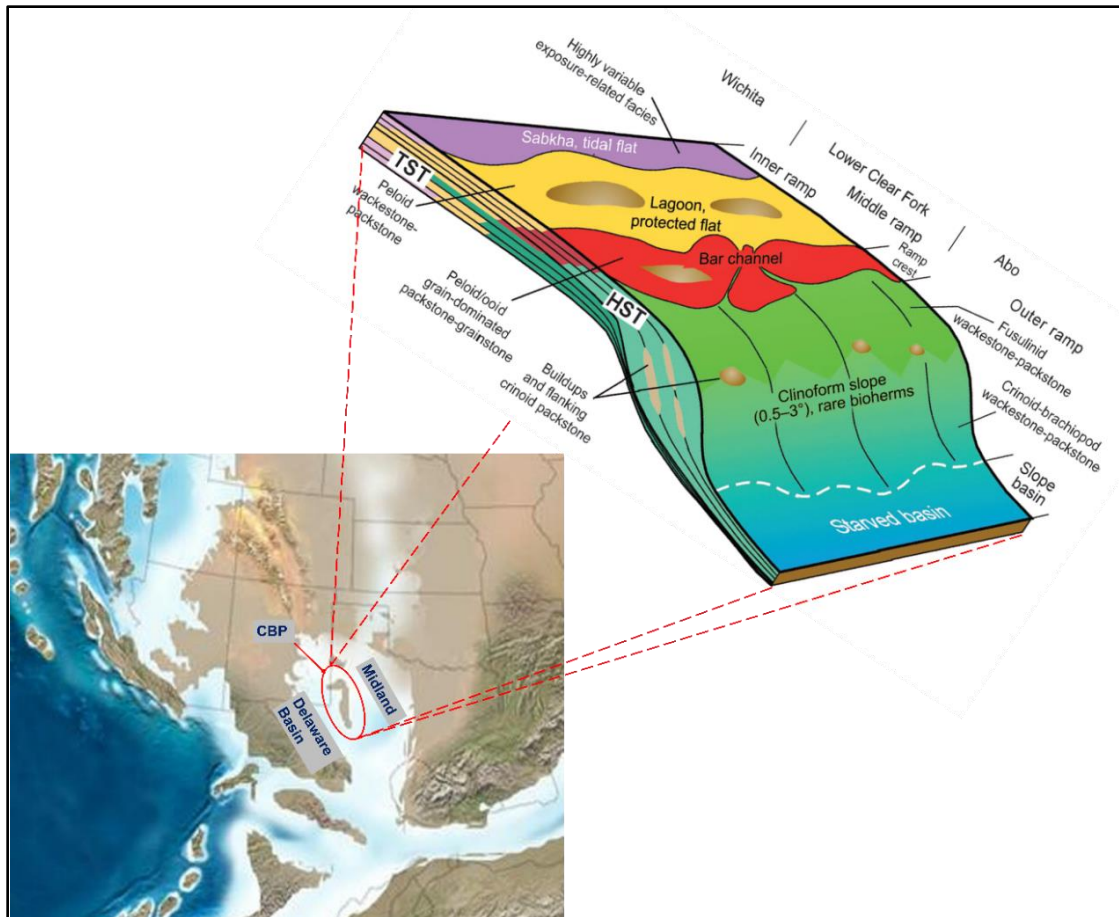
Figure 2.6. Depositional model for shallow-water carbonate platforms in the Permian. This model applies to most Leonardian carbonate platform successions in the Permian Basin. Depositional model modified from Ruppel et al., (1995); paleogeographic map modified from Blakey, (2013).

2.4. Sequence Stratigraphic Framework

The Leonardian reservoirs located on the Central Basin Platform in the Permian Basin exhibit a sequence stratigraphic framework that reflects the interplay of various sedimentary processes and eustatic sea level changes. Integrated studies conducted on outcrops and subsurface core and well data by authors including Ruppel et al., (2000) at Sierra Diablo Mountains, Ruppel & Harrington, (2012) at Fullerton Field, and Ruppel et al., (2002) using cycle and sequence stratigraphic analysis of the South Wasson Clear Fork reservoir have established the sequence stratigraphic framework for the Leonardian Clear Fork reservoirs. The Clear Fork reservoirs from these fields provide excellent analogs for the Clear Fork reservoir units at Tex-Mex, S.E. Field. The facies changes within the Lower Clear Fork interval in the Tex-Mex, S.E. Field is similar to the sequence stratigraphic framework developed by Ruppel et al., (2000); Ruppel & Harrington, (2012) and Ruppel et al., (2002) for the analogous reservoirs situated in the Central Basin Platform and in the Northern Shelf of the Permian Basin. From these studies, the stratigraphic sequences that were established and recognized for the Leonardian succession are shown in Figure 2.7 (Ruppel et al., 2000).

In the established stratigraphic framework, Abo/Wichita which is the basal stratigraphic unit of the Leonardian succession on the Central Basin Platform corresponds to Leonardian sequence one (Leo 1), the Lower Clear Fork unit corresponds to Leonardian sequence two (Leo 2), and the overlying Tubb corresponds to Leonardian sequence three

(Leo 3) sequence (Ruppel et al., (2000); (Kerans et al., 2000). The stratigraphic units of the

Leonardian succession and their sequence stratigraphic relationship from analogous units

are shown in Figure 2.7.
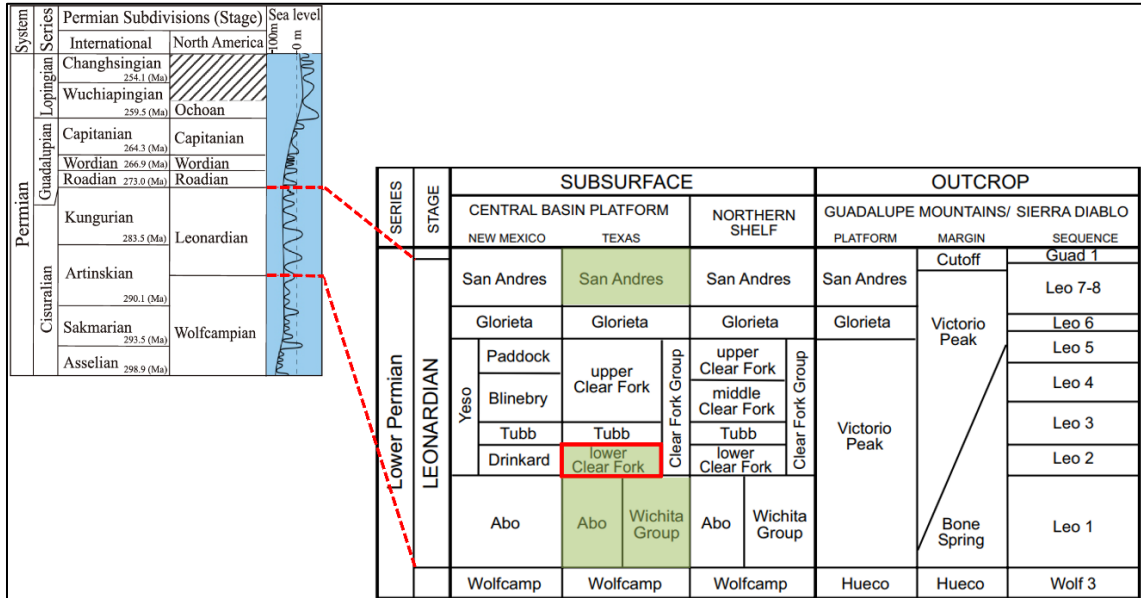
Figure 2.7. Chart showing the Lower Permian stratigraphic units and their corresponding sequences in the Permian Basin. The interval of interest in this study (Lower Clear Fork) is shown in the red outline. The chart also shows analogous units in New Mexico, the Northern Shelf, and the outcrop equivalent from the Sierra Diablo/Guadalupe Mountains. Productive reservoir intervals in the study area are shaded in a light green color. Stratigraphic chart modified after Ruppel, (2002). Sea-level curves adapted from Haq & Schutter, (2008).

The Lower Clear Fork in analogous Sierra Diablo outcrops recorded gradual flooding of the previously exposed Abo platform and a continued, although punctuated, increase in accommodation space and water depth. The Lower Clear Fork deposits consisting of alternating peritidal tidal-flat, and inner-to-ramp crest facies successions document cyclic rise and fall of sea level at the high-frequency sequence (HFS) and cycle scale (Mazzullo & Reid, 1989; Ruppel et al., 2000; Silver & Todd, 1969).

3. RESEARCH METHODOLOGY

3.1. Dataset

This research was conducted using core and wireline log data from Peterson 1P well located in the Tex-Mex, S.E. Field in Gaines County, on the Central Basin Platform (Figure 1.1). This well is located 21 miles (33.8 km) southwest of Seminole township in Gaines County, west Texas. The true vertical and measured depths for the well are 8,387 ft (2,556 m) and 8,391 ft (2,558 m), respectively. The cored sample for this study was provided to the East Texas Core Repository by Sozo Natural Resources and is housed at Stephen F. Austin State University. The Peterson 1P core consists of the San Andres and the Lower Clear Fork intervals. However, the Lower Clear Fork cored section, 338.9 ft (103.3 m) used in this study was recovered from the interval between 6,885 ft (2,099 m) and 7,224 ft (2,202 m). Provided data associated with the core and used in this study included digital open-hole wireline logs, petrographic thin sections, X-ray diffraction mineralogical data (whole rock powdered XRD), core-derived porosity, permeability (Klinkerberg), grain density, and fluid saturation (oil and water). These sets of data are summarized in Table 3.1. This study employed two general methods: defining the depositional facies and interpretation of the depositional environments, and petrophysical assessment of the Lower Clear Fork interval using data from core, wireline logs, and XRD (Table 3.1).

These methods helped determine the depositional facies and assessment of the petrophysical and mineralogical characteristics of the Lower Clear Fork Formation in the Tex-Mex, S.E. Field.

Table 3.1. Summary of data available for the Peterson 1P well studied.

Well	Wireline logs*	Input curves	Wireline log interval (ft)	Total cored length (ft)	Type of Core Data and Number of Sampling Points					
					XRD	Porosity	Permeability	Saturation	Grain Density	Thin section
Peterson 1P	GR, RHOB, NPHI, SGR, CAL, DT, LLS, LLM, LLD.	11	6900	338.9	30	81	81	77	81	50

* GR: Gamma Ray; **RHOB**: Density; **NPHIL**: Neutron Porosity; **SGR**: Spectral Gamma Ray; **CAL**: Caliper; **DT**: Sonic; **LLS, LLM, LLD**: Shallow, Medium, and Deep Resistivity; **XRD**: X-Ray Diffraction.

3.2. Core/Facies Analysis

Available lithology descriptions by Aim GeoAnalytics located in Missoula, Montana provided with the Peterson 1P core were reviewed and matched with the slabbed core, core photographs (in white light and UV light), and petrographic thin sections to

determine and define the main facies. Fifty (50) thin sections sampled from different depths of the Lower Clear Fork interval prepared by Core Laboratories were examined under a polarizing microscope to determine mineralogy, fossil presence, and diagenetic changes. Thin-section photomicrographs were taken using the electronic microscope in plane and cross-polarized light.

Features such as mineralogy, fractures and pore types, anhydrite structures, evidence of bioturbation, and fossils were noted. Thin section data were utilized to focus on the finer details of the facies (depositional texture, diagenetic texture, and pore types). The Dunham classification, (Dunham, 1962) system was used in classifying the carbonate rock types while the classification of the carbonate porosity types was based on Choquette & Pray, (1970). The results of the thin sections analysis, combined with the interpretation of core descriptions, helped establish the depositional facies, paleoenvironments, and their characteristics.

3.3. Whole Rock Mineralogical Analysis (XRD)

Previously collected X-ray diffraction data from thirty (30) sampled depths over the Lower Clear Fork interval by Core Laboratories were provided with the core. Analysis of the sampled XRD mineralogical data provided a quantitative estimation of core-based measurement of whole rock mineralogy. The results of the whole rock mineralogical analysis were matched with the facies identified in cores and thin sections. These data helped to determine the distribution of mineralogy within the Lower Clear Fork interval.

The XRD data were also useful in confirming the accuracy of the mineral modeling result obtained from petrophysical wireline logs.

3.4. Routine Core Analysis (RCA)

Routine core analysis was performed on eighty-one (81) core samples over the Lower Clear Fork interval, to estimate key petrophysical parameters such as porosity, water saturation, permeability, and grain density. The RCA was conducted by Core Laboratories and the data was provided with the core samples. The porosity measurements, obtained through standard laboratory methods, offer insights into the pore space within the rock, crucial for understanding fluid storage capacity. Water saturation data, reflecting the fraction of pore space filled with water and hydrocarbon fluids, is vital for assessing hydrocarbon potential. Permeability data, indicating the ability of the rock to transmit fluids, and grain density measurements, crucial for rock matrix characterization, further complement the understanding of the Lower Clear Fork reservoir. These core-derived data also helped in calibrating the results of the petrophysical calculations derived from wireline log data.

3.5. Petrophysical Analysis/Mineral Modeling

The goal of the petrophysical analysis was to construct a petrophysical mineral model of the Lower Clear Fork interval in Tex-Mex, S.E. Field using the Peterson 1P wireline and core-derived data. The calibrated mineral model helped to determine the

mineral composition and petrophysical properties including porosity and water saturation.

The petrophysical analysis and mineral modeling were carried out using the software *Interactive Petrophysics 2021* under an academic license from Geoactive Limited (formerly Lloyds Register) (called IP throughout this research). The wireline logs were prepared and uploaded into the IP software, and quality control checks were conducted on the imported logs to identify any data issues. Subsequently, the logs were preprocessed, which involved depth matching to ensure that all the well log data were on a consistent depth scale and properly aligned. Figure 3.1 shows a typical log of Clear Fork reservoirs at Fullerton Field from Ruppel & Harrington (2012) (left) matched with log plots generated from the Peterson 1P well in Tex-Mex, S.E. Field (right). Both fields are located on the Central Basin Platform and sit adjacent to each other (refer to Figure 1.1) and have been established to have similar depositional and stratigraphic sequences.
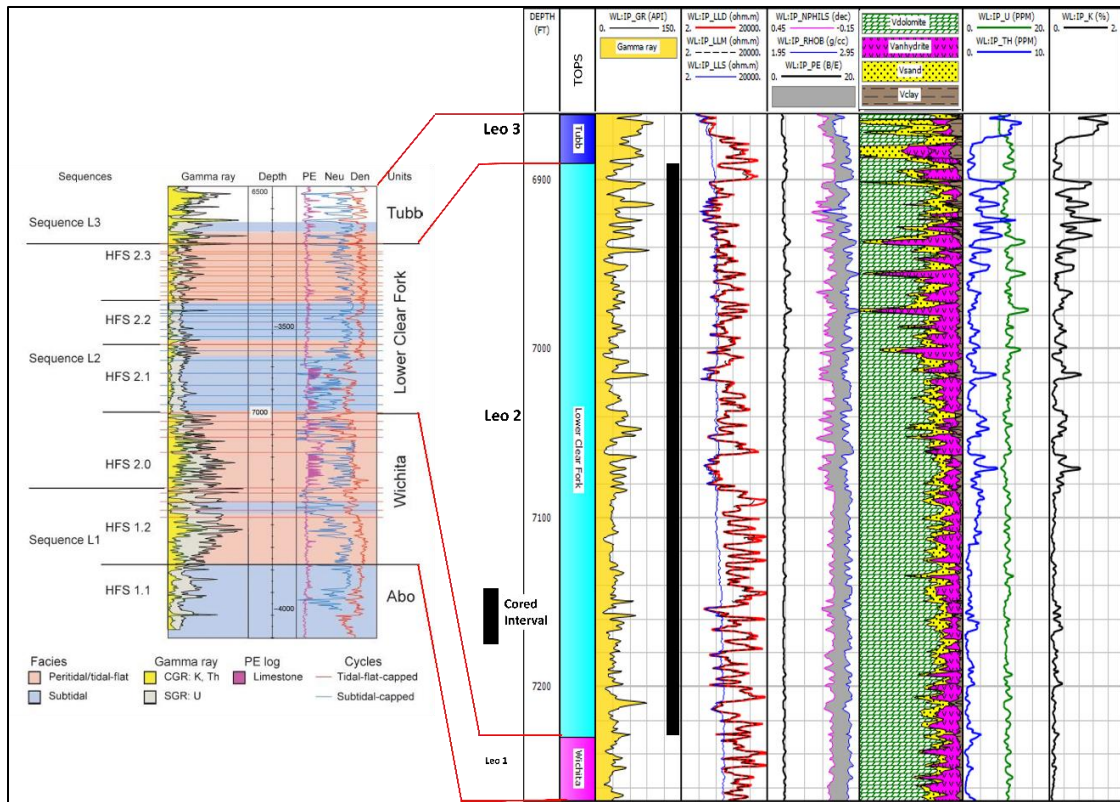
Figure 3.1. Type log of Clear Fork reservoirs at Fullerton Field (left) matched with log plots generated from the Peterson 1P well in Tex-Mex, S.E. Field (right). The Clear Fork reservoirs at Fullerton Field adjacent to Tex-Mex, S.E. Field on the CBP serve as an excellent reservoir analog as established by Ruppel & Harrington, (2012); Ruppel & Jones, (2006). The Lower Clear Fork interval is generally characterized by lower Gamma Ray (GR), thorium (Th), Uranium (U), and potassium (K). However, high spikes in GR and SGR values correspond to zones of silts and clay. The interval shows high dolomite and anhydrite content. The scale of the generated log is 1: 600ft. Fullerton Clear Fork type log (left) is modified from Ruppel & Harrington, (2012).

3.5.1. Clay Content Analysis

Computing the volume of clay is essential to understanding the clay distribution in the Lower Clear Fork interval for petrophysical calculations (porosity, water saturation) and mineral modeling purposes. The process involved identifying the Gamma Ray clean value, GR_{clean} (little to no clay) and Gamma Ray clay, GR_{clay} (100% clay) from the Gamma Ray log. The clay volume module in Interactive Petrophysics software was used to compute for minimum volume of clay (V_{clay}) over the interval. The volume of clay (V_{clayGR}) was computed utilizing the single clay indicator Gamma Ray log. Clay volume computation from the double clay indicator (neutron-density) logs method was not used as clay volume computation (V_{clayND}) results did not fit the core-derived clay content. The clay volume calculation from Gamma Ray, V_{clayGr} was based on the linear method in Equation 3.1 below.

$$V_{clayGR} = \frac{GR_{log} - GR_{clean}}{GR_{clay} - GR_{clean}}$$

Equation 3.1

where: GR_{log} = Gamma Ray value at the depth of interest.

GR_{clean} = Gamma Ray value in the clean zone.

GR_{shale} = Gamma Ray value in the pure shale zone.

After V_{clayGR} was calculated, the results were compared with core-derived XRD clay content.

3.5.2. Mineral Modeling, Porosity, and Water Saturation Determination

Once the V_{clay} parameters were defined and computed over the Lower Clear Fork, the mineral module in IP, "*Mineral Solver*" was used to determine the mineral proportions, porosity, and fluid saturations in the Person 1P well. The "*Mineral Solver*" comprises two modules, the "*Mineral Preprocessor*" and the "*Mineral Solver*". The modeling process involves entering a model of the minerals encountered in the formation penetrated, the logging tools, equations or constants to be used, and the parameters relating to the logging tool equations to the mineral model. The mineral solver module will solve the setup as a system of equations and return the most probable lithologies and fluid results for the depth of interest (Senergy Ltd, 2008). The mineral preprocessor and mineral solver workflow following the IP help manual involves the following.

A mineral preprocessing module was run to ensure the accuracy of the model results by calculating the volumetric cross-section, U from the input of density and photoelectric log. The equation representing this step is shown in Equation 3.2 below.

$$U = PEF * (RHOB + 0.1883) * 0.93423$$

Equation 3.2

where: U = Volumetric Cross Section   PEF = Photoelectric Factor

RHOB = Bulk Density.
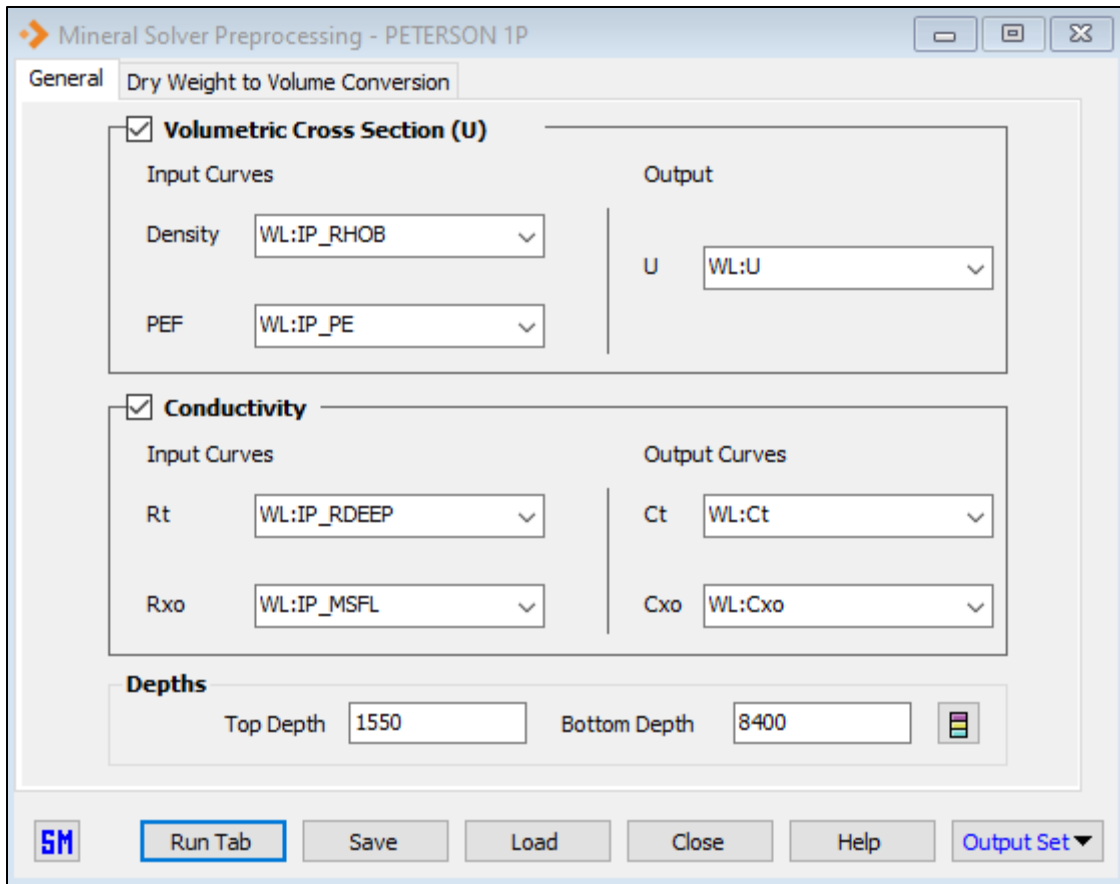
Figure 3.2. The interface of the Mineral Solver during mineral preprocessing (General Tab Interface).

The volumetric cross section, U is a parameter that indicates the volume occupied by a certain mineral or rock in a given cross-sectional area of the subsurface. It is a derived parameter that integrates data from density and photoelectric factor logs. Photoelectric Factor, (PEF) is a parameter obtained from well logging that indicates the electron density of a formation. It is sensitive to the atomic number of the elements in the rock, and hence,

to the mineral composition. Bulk Density, (RHOB) represents the density of the rock formation, including the pores and the material filling those pores. It is a direct measure of the mass per unit volume of the rock. Mineral conductivity (C_t and C_{xo}) curves were computed from Deep resistivity (R_t) and Micro Spherical Formation Log (R_{xo}). Figure 3.2 shows the interface and the settings used for this step of the modeling process.

Under the mineral preprocessing module, the '*dry weight to volume conversion*' tab was used to convert the elemental volume fractions from mineral dry weight fractions. Here, the dry mineral weight percentages from core XRD mineral analysis data were converted to mineral volume fractions. The output from this step serves as input into the actual mineral modeling. Figure 3.3. shows a screenshot of the mineral preprocessing tab with the settings used. The mineral dry weight conversion process in IP is governed according to Equation 3.3.

$$Wet\,Vol\,\% = \frac{(Dry\,Weight\,\%) * (1 - Porosity) * (Rock\,GD)}{Mineral\,Grain\,Density} \qquad \textbf{Equation 3.3}$$

The rock grain density and porosity data were from core-derived data (Routine Core Analysis) while the mineral grain density was fixed values in IP for a particular mineral. The XRD dry weight percentages, the core porosities, and rock grain densities were imported into IP from MS Excel using the interval/spreadsheet importer. This mineral pre-processor setting was run and saved for recall in the mineral modeling.
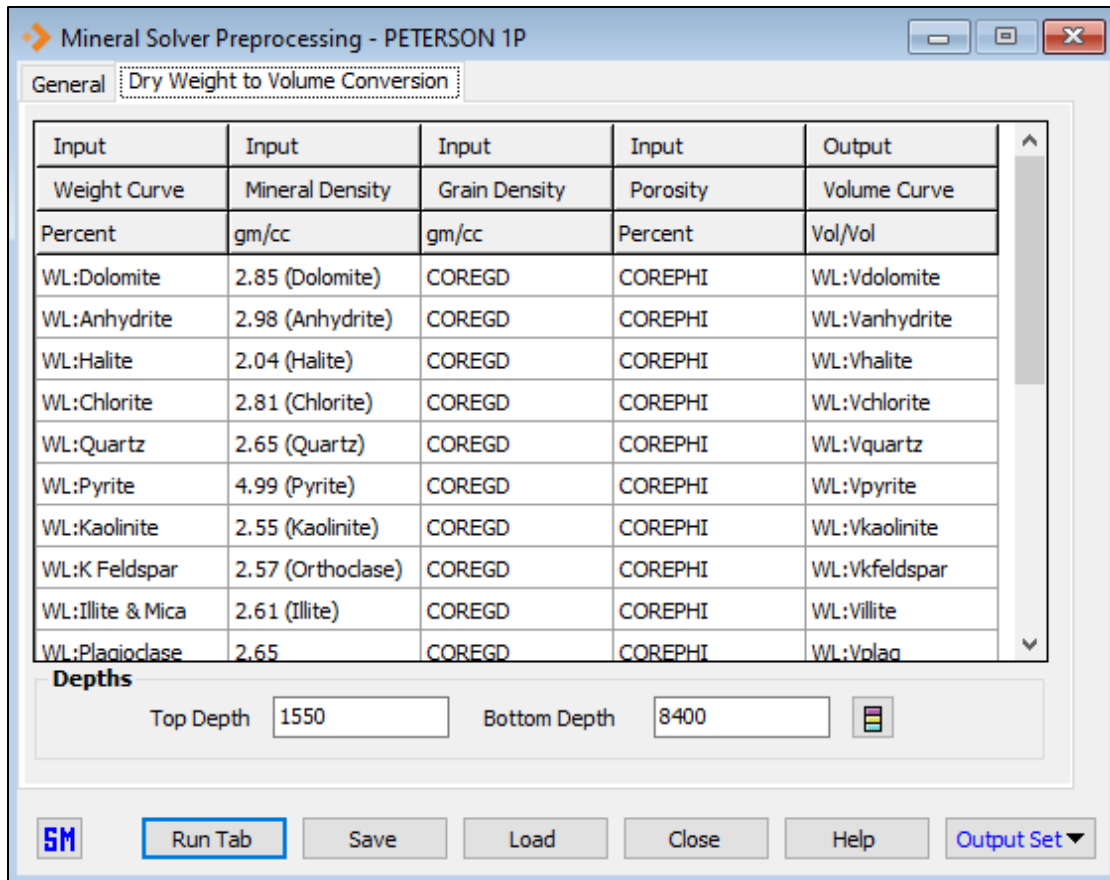
Figure 3.3. Dry weight to volume conversion interface in mineral preprocessing module (used to convert core XRD mineral dry weight to wet weight for mineral modeling).

The "*Mineral Solver*" interpretation module was then initialized. The interface comprises four tabs including '*Curves*', '*Parameters*', '*Models*', and '*Mixings*' tabs. The '*Curves*' tab was used for setting the input curves for the calculation of water saturation. The temperature curve was set here to convert input resistivity parameters, Rw and Rmf to downhole values. Formation resistivity, Rt and flushed zone resistivity (MSFL), and Rxo were input logs to calculate water saturation, Sw and Oil saturation, and Sxo. The output

curves for each separate model by default in IP were set here (Figure 3.4).
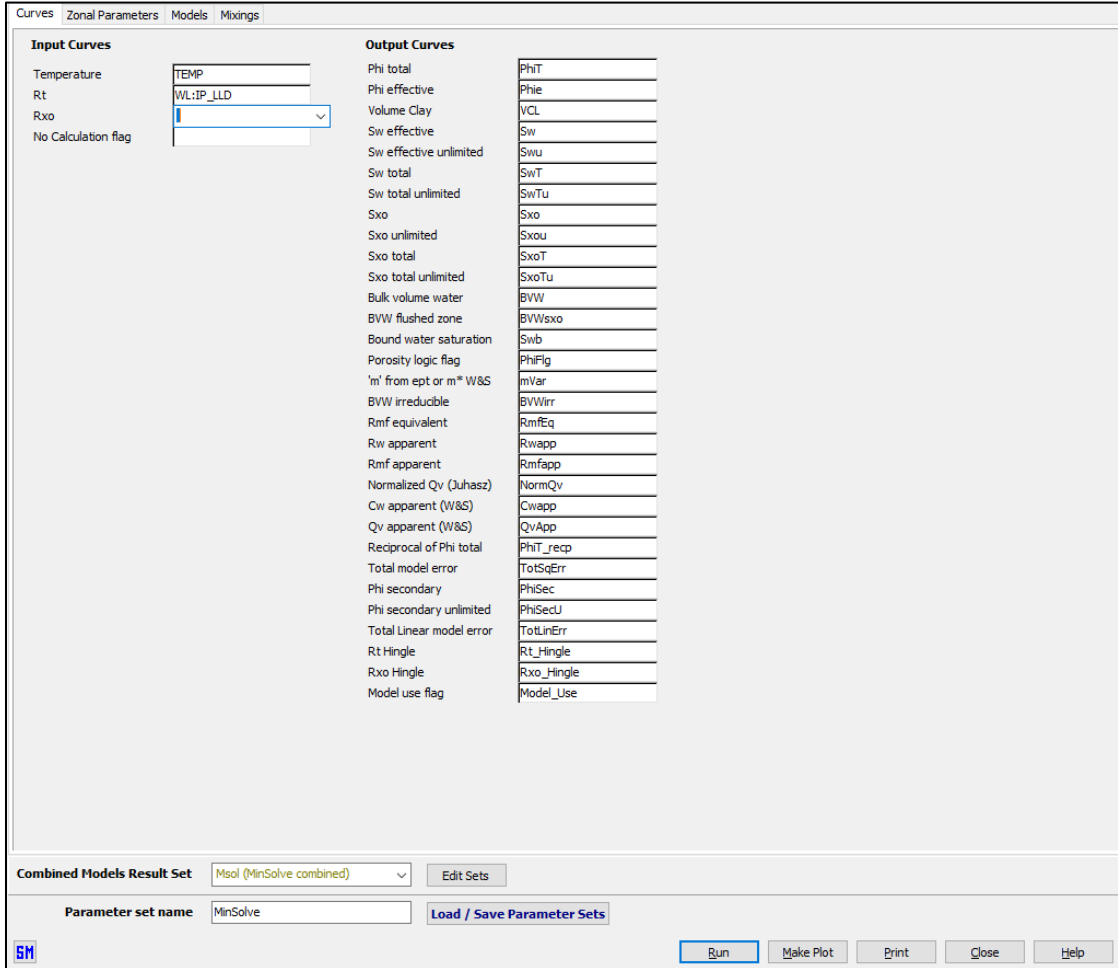
Figure 3.4. The interface of the Mineral Solver's inputs and output curves settings in IP.

Under the '*Parameters tab*', the zone/mixing module was set to perform the modeling over the entire interval. The 'water clays' sub-tab was used for setting water saturation and clay content calculations and parameters such as (porosity, water, clay

resistivity, and temperature) for the Lower Clear Fork well. The water saturation Logic/Limits sub-tab allowed for the selection of the saturation equation to be used (Archie modified, ArchiePhiT was chosen as the Peterson well had deep resistivity log data). The Archie PhiT equation computes total porosity and is given mathematically below.

$$\frac{1}{Rt} = \frac{(PhiT)^m * (Sw^n) * (n)}{a.Rw}$$ **Equation 3.4**

Where R_t = Formation resistivity; PhiT = Total porosity

Rw = Resistivity of water in the pores; Sw is the water saturation of the rock (the fraction of the pore space filled with water); a, m, and n are empirically derived constants ('a' is the tortuosity factor, 1 used; 'm' is the cementation exponent, 2 used and 'n' is the saturation exponent, 2 used).

In the water saturation parameters sub-tab, (sw parameters), the sw parameters were maintained. The sonic/neutron sub-tab allowed for selecting a sonic equation for calculating sonic porosity. The Hunt Raymer equation was chosen to calculate the sonic porosity. For the logging contractor, Halliburton was selected as they were the contractors. The interface and parameter settings used are shown in Figure 3.5.

Zones / Mixings | Waters Clays | Sw Logic / Limits | Sw Params | Sonic / Neutron / Density

Zone #	Zone Name	Zone Top	Zone Bottom	Zone Color	Lock Zone	Zone Mixing	Mdl Merge Dist.
1		1500	8400	Default		Mix 1	0

Zones / Mixings **Waters Clays** Sw Logic / Limits Sw Params Sonic / Neutron / Density

Zone #	Rw	Rw Temp	Rw Salinity Kppm	Rmf	Rmf Temp	Rmf Salinity Kppm	Rw bound	Rwb Temp	Rwb Salinity Kppm	Rmf bound	Rmfb Temp	Rmfb Salinity Kppm	Res Clay	Rxo Clay	PhiT Clay
1	0.3	120	12.3	0.0574	180	50	0.1	60	87.8	0.1	60	87.8	1	1	0.15

Curves **Zonal Parameters** Models Mixings

Zones / Mixings Waters Clays **Sw Logic / Limits** Sw Params Sonic / Neutron / Density

Zone #	Sat Equation	Sw Method	Sxo Method	OBM ?	Sw Sxo Inv Logic	m vari wth Vcl	Vcl cutoff	Sxo Limit ?	Sxo Limit	Invasion factor	Phi Sw Limit	Vcl Sw Limit	Swi Limit
1	Archie PhT	Rt	Rxo		✓		0.6	✓	0.2	2	0	1	0

Curves **Zonal Parameters** Models Mixings

Zones / Mixings Waters Clays Sw Logic / Limits **Sw Params** Sonic / Neutron / Density

Zone #	m source	n source	a factor	m exponent	n exponent	min m value	max m value	m plus value	B fact Juhasz	B fact W&S	Qv	Qv 'a' Const	Qv 'b' Const	Cm*
1	Param	Param	1	2	2	1.5	3	0	1			0.5	-3	1

Curves **Zonal Parameters** Models Mixings

Zones / Mixings Waters Clays Sw Logic / Limits Sw Params **Sonic / Neutron / Density**

Zone #	Sonic Equ	Sonic Cp	Neu Form Sal	Neu Log Cont	Neu Tool Type	Den Hy Model
1	Raymer	1	✓	Halliburt	Neutron	Modified

Figure 3.5. Mineral solver's zonal parameters tab settings in IP.

Finally, in the '*models*' tab, the mineral models were set up to describe the main minerals (dolomite, anhydrite, quartz, clay, and halite) and fluids (oil and water) for the interval. These modeled minerals were selected based on results from XRD mineralogical data and backed by reported mineralogies of the Lower Clear Fork interval. The curves and logging equations (well logs – Density (RHOB), Gamma Ray (GR), Neutron (NPHILS), Sonic (DT), Grain Density (GD), volumetric cross-section, (U)) were added to the model. The equation mode was selected as a "model" to allow the system to use the various equations in solving the probabilistic equations (resolving the mineralogies). The confidence interval was set individually for each logging tool. Also, the invasion factor of 1.0 was selected for each curve to indicate the tool was reading into the flushed zones. The mineral endpoints were defined (i.e. 100% mineral readings) for each mineral. That is, setting the known log responses for pure minerals. For instance, the known density, neutron porosity, and other log responses for minerals like quartz, dolomite, oil, and clay were predefined in IP. For instance, the density for 100% dolomite was 2.85g/cc, quartz was 2.65g/cc, and freshwater was 1.0 g/cc.

The model was run and the responses were compared with the initial log responses. The model was rerun for the second time and the results were calibrated with core-derived data from XRD mineralogy, porosity, and water saturation. The settings and parameters defined for the various stages of the actual mineral modeling are shown in Figure 3.6 below.

Equation	Eq. Mode	Use	Confidence	Inv. Fact.	Result	Quartz	Dolomite	Anhydrite	Oil Sxo	Water Sxo	Halite	Clay
					Mineral	Quartz	Dolomite	Anhydrite	Oil Sxo	Water Sxo	Halite	Clay
					Type	Matrix	Matrix	Matrix	Hyd. Sxo	Water Sxo	Matrix	Wet Clay
					Shading							
					Use	✔	✔	✔	✔	✔	✔	✔
					Result	VQuartz	VDol	VAnhydrite	VOil	VWater	VHalite	VClay
Unity	Model	✔	0.01	1		1	1	1	1	1	1	1
Density	Model	✔	0.04	1		2.65	2.85	2.98	0.6	Auto	2.04	2.78
Neutron	Model	✔	0.1	1		Auto	Auto	-0.02	0.8	Auto	0.03	0.3
Sonic	Model	✔	0.1	1		55	42	50	200	189	67	100
GammaRay	Model	✔	5	1		10	9	15	0	0	0	234.4
U	Model	✔	5	1		4.8	9	14.95	0.8	Auto	9.7	10
Linear	Model	✔	0.04	1		0	0	0	0	0	0	1
GrainDensity	Output	✔				2.65	2.85	2.98	0	0	2.04	0

Figure 3.6. Setup of model tab in IP mineral module, showing the input logs, the model minerals, and their respective values used for the mineral calculations.

The modeling steps utilized guidance from the mineral solver workflow (Senergy Ltd, 2008) and helped guide in current IP version. A summary of the workflow used in the study of the Lower Clear Fork Formation is shown in Figure 3.7.
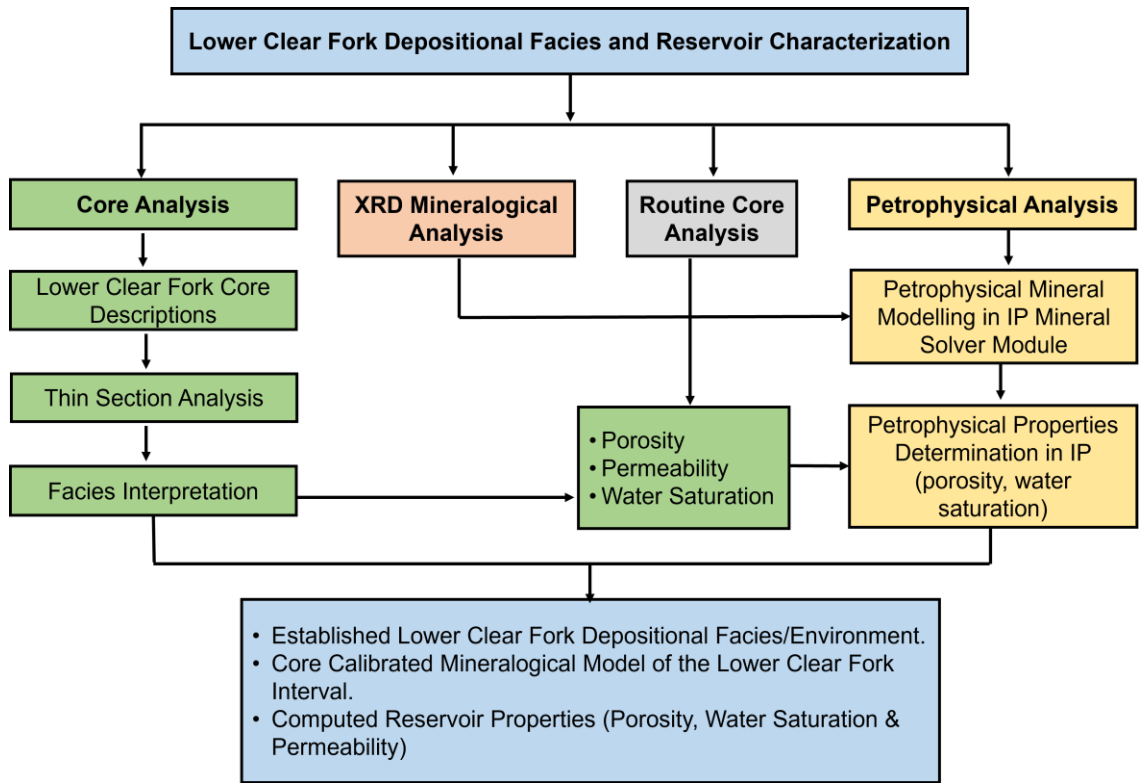
Figure 3.7. Workflow deployed in the study of the Lower Clear Fork Formation.

4. RESULTS

The primary objective of this study was to identify the depositional facies, interpretation of their paleoenvironments, and assessment of the petrophysical and mineralogical characteristics of the Lower Clear Fork Formation. To conduct a thorough petrophysical analysis and modeling, an understanding of the facies and mineralogy is needed. This section examines the different facies identified in the Peterson 1P core studied. It also provides an overview of the mineralogical characteristics associated with each different facies in the Lower Clear Fork interval, followed by the petrophysical analyses.

4.1. Lower Clear Fork Facies in Tex-Mex, S.E. Field

Outcrop and subsurface facies studies by Kerans et al., (2000) and Ruppel, (2002) established that the Leonardian succession in the Permian Basin consists of shallow-water peritidal tidal flat and subtidal facies. Those studies were used as a framework for this research. In this core, the Lower Clear Fork facies are very similar to those established from previous studies. The analysis of the core and thin sections revealed seven (7) distinct depositional facies, regrouped into four (4) facies associations. Each major depositional facies, their interpretation, and depositional environment are summarized in Table 4.1 and discussed below.

Table 4.1. Summary of depositional facies, their characteristics, and their related depositional environment of the Lower Clear Fork interval in the Peterson 1P core.

Facies Association	Facies	Interpretation (Environment)	Characteristics			
			Grain Types	Pore Types	Fossils/ Structures	Mineralogy
Dolomudstone	Silty - dolomudstone Argillaceous - DM	Tidal flat	Intraclasts, Peloids.	Micropores, Intercrystalline, Moldic.	Laminations Bioturbated, Stylolite.	Dolomite, Anhydrite
Dolowackestone	Peloidal - DW Skeletal - DW	Inner ramp, Middle ramp	Peloids, Coated grains, skeletal debris.	Micropores, Intercrystalline, Moldic, vuggy.	Bioturbation, Wispy laminations, Bivalves, Ostracods	Dolomite, Anhydrite
Dolopackstone	Mud-dominated DP. Grain-Dominated DP	Inner, Middle ramp, Ramp crest.	Intraclasts, peloids, ooids, coated grains.	Vuggy, Moldic, Micropores, Intercrystalline, Interparticle.	Fenestral fabrics, Rare Ostracods and Bivalves	Dolomite, Anhydrite
Anhydrite	Anhydrite	Sabkhas, Restricted lagoons	—	No visible pores	Massive and Nodular anhydrite	Anhydrite

DM – Dolomudstone   DP - Dolopackstone   DW - Dolowackestone

4.1.1. Dolomudstone

The dolomudstone facies contain laminated clay (dark gray to black) and mud-rich rocks. These facies are dominantly dolomitized with grain types including coated grains, intraclastic grains, and recrystallized dolomites with no observable peloids. Laminations and bioturbation are common. Mineralogy as observed in cores, thin-section photomicrographs, and XRD analysis revealed the dominance of dolomite and anhydrite. XRD mineralogy showed the absence of calcite minerals in the dolomudstone facies. Clay minerals, specifically illite, and smectite, correlated with elevated Gamma Ray and Spectral Gamma Ray responses in the well log data (Figure 3.1). Importantly, thin sections revealed massive moldic pores developed within the recrystallized dolomite crystal grains (Figure 4.1c). Other porosity developments in these facies include intercrystalline, vugs, and micropores (Figure 4.1d). These zones may display high porosities as a result of the neomorphism of the dolomites.

Additionally, anhydrite appears to have precipitated within the fractures and pore spaces, indicating it is a diagenetic product. Primary porosity remains visually absent, implying it has been modified as a result of the dolomitization and anhydrite precipitation. Stylolites are evident within the dolomudstone facies indicating compaction actions after deposition (Figure 4.1b). The dolomudstone facies show evidence of subaerial exposure, indicating an exposed tidal flat environment (Figure 2.6) where sediments were deposited above mean sea level with infrequent exposure to flooding.
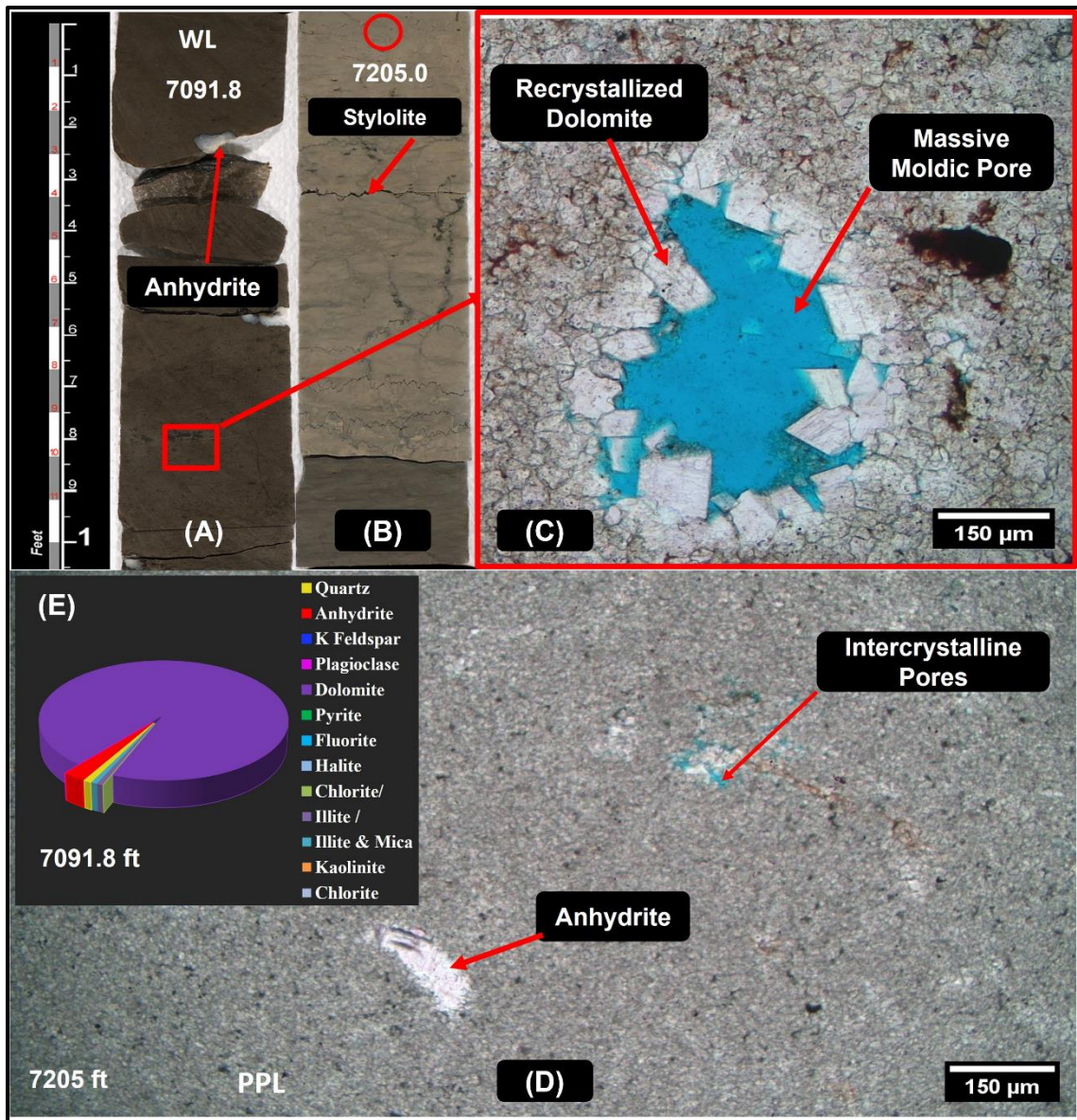
Figure 4.1. Core and thin-section photomicrographs of dolomudstone facies in the Lower Clear Fork interval. (A) and (B) are slabbed photographs (taken in white light) of dolomudstone showing anhydrite and stylolite structures. (C) Photomicrograph of dolomudstone facies in (A) (PPL) showing massive moldic pores and subhedral recrystallized dolomite. (D) Photomicrographs of dolomudstone facies in (B) (PPL), showing intercrystalline pores and anhydrite. (E) Mineral abundances (XRD) at 7091.8 ft (2161.6 m). Note: Red circles show where thin sections were taken. Core depths were 7091.8 ft (2161.6 m) and 7205.0 ft (2196.1 m) respectively.

4.1.2. Dolowackestone

This facies association consists of peloidal and skeletal dolowackestones. The facies contain some amount of mud just like the tidal flat dolomudstone facies. It is characterized by distinct features such as wispy laminations, peloidal grains, bioturbation structures (burrows), fenestral fabric filled with anhydrite cement, and the presence of skeletal debris (Figure 4.2). The primary sediment grains consist of intraclasts and fecal pellets (peloids), which are attributed to the activities of faunal burrowers. Skeletal debris (bivalves and ostracods) were present in the facies (Figure 4.2d).

From thin-section photomicrographs and XRD mineralogical analysis, the dominant minerals were dolomite and anhydrite (Figure 4.2). Dominant pore types in the facies include intercrystalline, moldic, micropores, and minor occurrences of vuggy pores. Notably, the anhydrite nodules were precipitated within pore spaces and fractures, indicating post-depositional infiltration by sulfate-rich diagenetic fluids into permeable pathways within the precursor limestones (Figure 4.2a). The facies characteristics and sedimentary attributes show their association and deposition in low-energy, well-oxygenated inner to middle ramp on the carbonate platform.
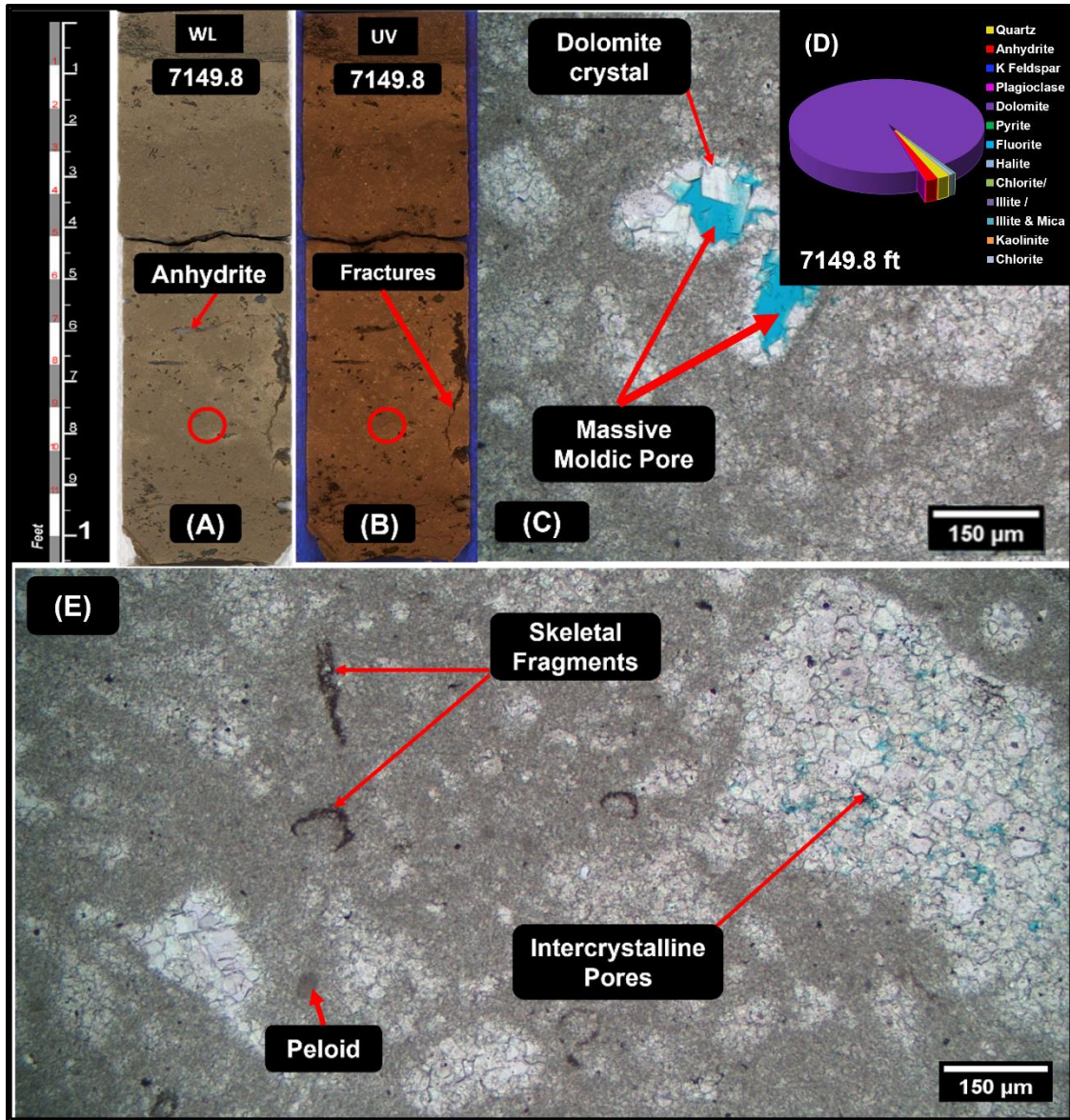
Figure 4.2. Core and thin-section photomicrographs of peloidal/skeletal dolowackestone facies in the Lower Clear Fork interval. The core depth was 7149.8 ft (2179.3 m). (A) and (B) slab photographs of dolowackestone in plain and ultraviolet lights, respectively, showing anhydrite and fractures. (C) PPL photomicrographs of dolowackestone facies in (A), showing massive moldic pores and recrystallized dolomite. (D) Mineral abundances (XRD) at 7149.8 ft (2179.3 m). (E) PPL photomicrographs of dolowackestone facies in (A), showing intercrystalline pores, skeletal fragments, and peloids. Note: Red circles show where the thin section was taken.

4.1.3. Dolopackstone

The dolopackstone facies association consists of mud-dominated and grain-dominated dolopackstones. As the names mud-dominated and grain-dominated packstone imply, they are mud and grain-supported, respectively. These sedimentary facies exhibit an abundance of coated grains and peloidal grains, primarily composed of fecal pellets generated by burrowing fauna. Localized occurrences of skeletal debris, including ostracods and bivalves were observed in thin section photomicrographs. Sedimentary structures such as fenestral fabrics have been infilled with anhydrite cement. The lithological transition within this interval extends to wackestone facies when carbonate mud increases. Mineralogically, the facies is dominated by dolomite and anhydrite (Figure 4.3c). Pore characteristics within this interval are predominantly manifested by the presence of moldic, micropores, intercrystalline, interparticle, and vuggy pores (Figure 4.3d). Additionally, the presence of stylolites highlights the significant intense burial and compaction (post-diagenetic processes) that have transpired. Notably, there is a continuous gradation from poorly defined peloids to clearly discernible pellets, exhibiting diverse textures spanning from wackestone to packstone. Figure 4.3 shows the dolopackstone core and associated thin section photomicrograph (WL). The facies' characteristics and attributes put their environment of deposition in the high-energy ramp crest of the carbonate platform.
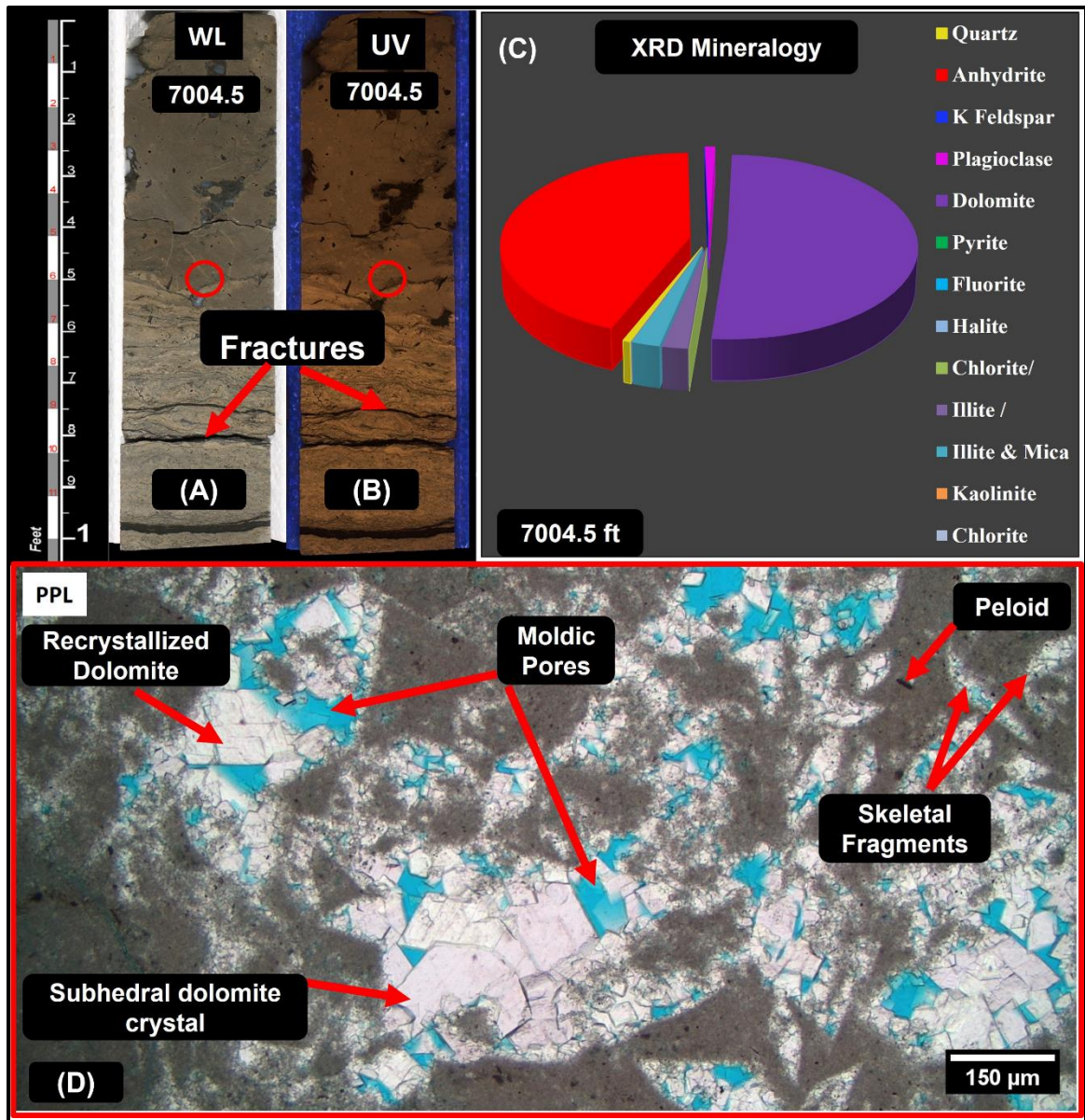
Figure 4.3. Core and thin-section photomicrographs of dolopackstone facies in the Lower Clear Fork interval. The core depth was 7004.5 ft (2135 m). (A) and (B) slab photographs of dolopackstone in plain and ultraviolet lights, respectively, showing fractures and stylolites. (C) Mineral abundances (XRD) at 7004.5 ft (2135 m) (D) PPL thin section photomicrographs of dolowackestone facies in (A), showing moldic pores, recrystallized dolomite crystals, skeletal fragments, and peloids. Note: Red circles show where the thin section was taken.

4.1.4. Anhydrite

The anhydrite facies occur as massive and nodular in structure (at least a foot thick) and are dispersed within other facies within the Lower Clear Fork interval (Figure 4.4). Early Permian marine circulated water contains abundant magnesium, sulfate-rich (SO_4^{2-}) brines, and calcium ions (Ca^{2+}). With the arid and warm climate conditions during the Early Permian, high evaporation of sea water prevailed in the shallow and restricted marine environment resulting in the deposition of calcium sulfate in the form of gypsum. Evidence from cores suggests the gypsum was deposited in shallow restricted lagoons and inland, coastal, and subaerially exposed sabkhas. Increases in salinity levels, temperature, and deep burial from subsequent depositions resulted in the formation of anhydrite at deeper depths The nodular and massive structure of the anhydrite suggests dehydration of gypsum during burial at deeper depths. The characteristic nature of the anhydrite facies in the Lower Clear Fork indicates their formation in warmer to semi-arid climates such as the inland sabkha and restricted lagoon environments of the carbonate platform (Figure 4.4b; Table 4.1).
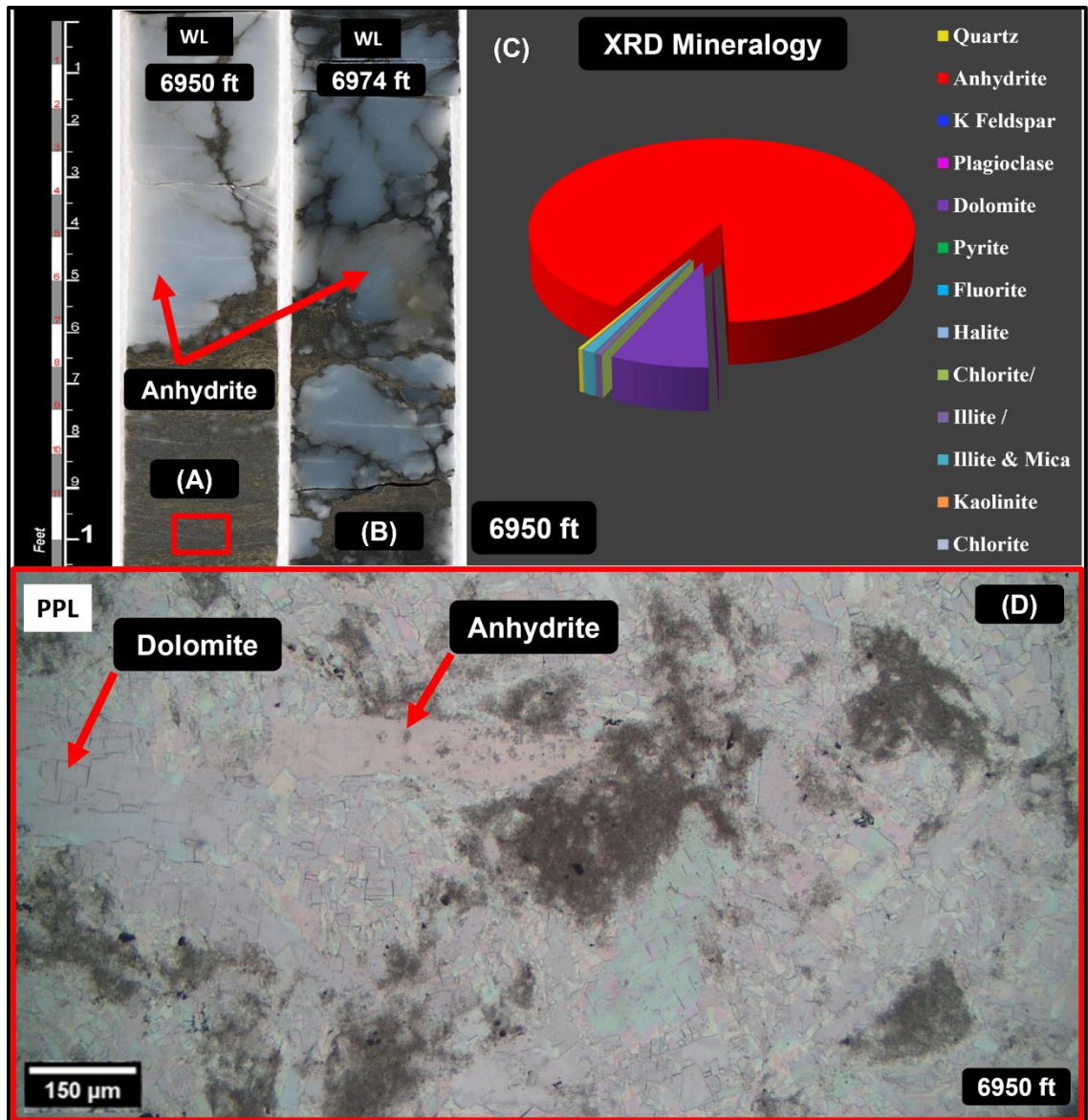
Figure 4.4. Core and thin-section photomicrographs of anhydrite in the Lower Clear Fork interval. Core depths were 6950.0 ft (2118.4 m) and 6974.0 ft (2125.47 m), respectively. (A) and (B) slabbed core photographs showing massive anhydrite and nodular (in WL). (C) Mineral abundances (XRD) at 6950.0 ft (2118.4 m) (D) PPL thin section photomicrograph showing anhydrite and dolomite (D) PPL photomicrographs of packstone facies in (A) showing moldic pores, peloids, subhedral Note: Red rectangle denotes depth where the thin section in (D) was taken.

A constructed chart of the distribution of the facies across the Lower Clear Fork interval is shown in Figure 4.5. The chart also shows the facies composition and how the Gamma Ray, photoelectric, neutron, and density porosity logs correlated with the facies across the interval.
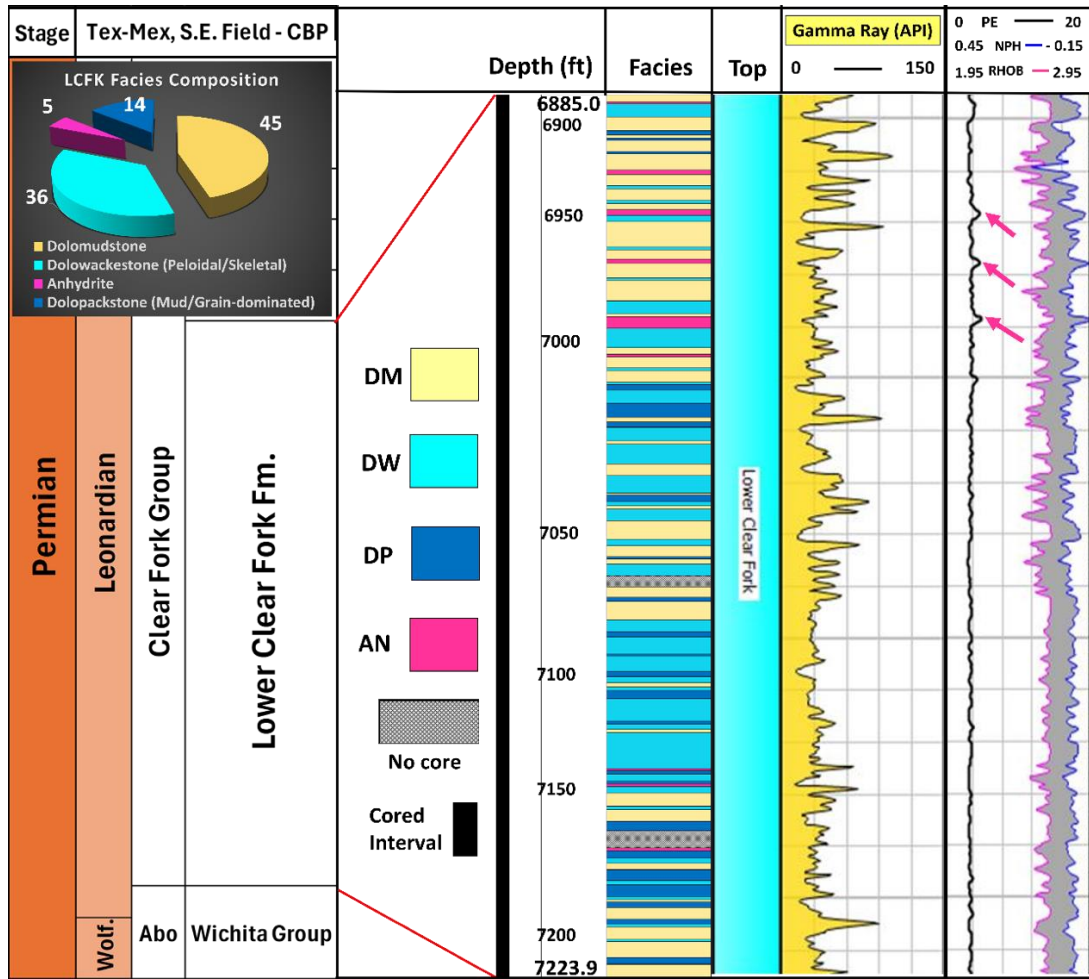
Figure 4.5. Facies distribution in the Lower Clear Fork Formation from Peterson 1P core. The percent composition of the major facies found in the core is shown in the pie chart (Upper left corner). Gamma Ray, Photoelectric, Neutron, and Density Porosity logs have been added to show their correlation to the core facies. Red arrows show anhydrite-dominated zones (the typical PE value of anhydrite is 5.1 barns/e)

4.2. Mineralogy of the Lower Clear Fork

The data extracted to conduct this mineralogical analysis were obtained from whole rock XRD analysis. The process involved determining the mineral weight percent present in the rock at a specific depth. Based on the XRD analysis, the Lower Clear Fork core from the Tex-Mex, S.E. Field is composed of the following minerals: dolomite, anhydrite, quartz, pyrite, plagioclase, K-feldspar, clay (illite/smectite, illite and mica, and chlorite), and halite. Figure 4.6 shows a plot of XRD whole rock mineral abundances and their distribution within the Lower Clear Fork.

The Lower Clear Fork interval, 6880 – 7225 ft (2072.6 – 2202.2 m) is composed of dolomite and anhydrite, with typical values in the range of 7.3% – 98.7% for dolomite and 0.4% – 90.9% for anhydrite. Values of clay content and quartz vary between 0.3% – 51.4% and 0.6% – 17%, respectively. The XRD data show a clear absence of calcite within the interval indicating that almost all the calcite from the parent rock, limestones had been replaced with dolomite within the Lower Clear Fork interval. This supports the intense dolomitization within the Clear Fork reservoirs as reported by authors including Kerans et al. (2000); Ruppel et al. (1995); Ruppel & Harrington (2012); Ruppel & Jones (2006) associated with the shallow-water carbonate on the Central Basin Platform.
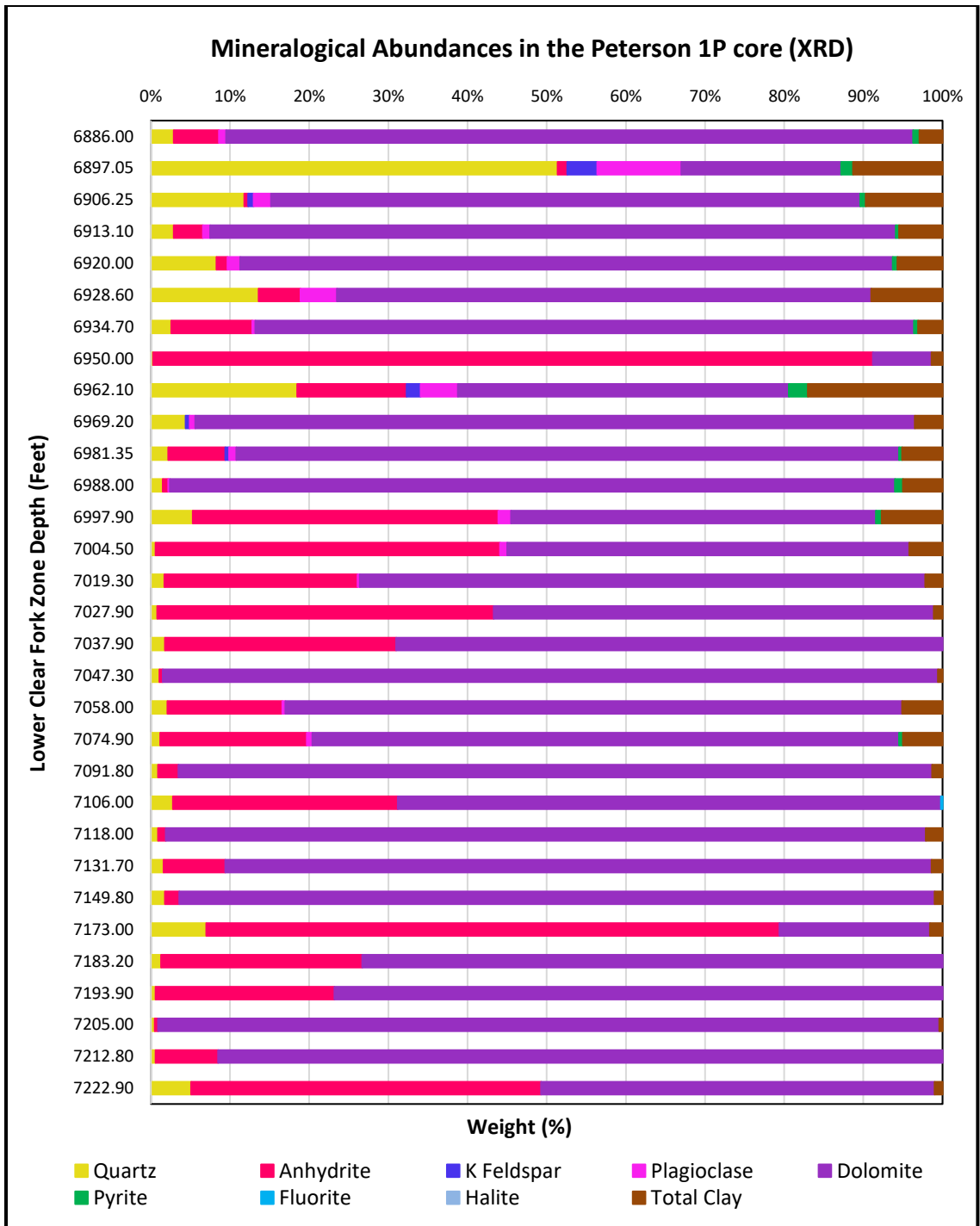
Figure 4.6. Whole rock X-ray Diffraction (XRD) mineral distribution within the Lower Clear Fork Interval.

To better understand the clay phyllosilicate minerals and their distribution, the different clay minerals estimated from XRD analysis were plotted with depth. The clay mineralogy across the Lower Clear Fork interval demonstrates significant variations in clay mineral compositions, predominantly marked by the presence of illite and mica, illite/smectite, and chlorite, with a notable absence of kaolinite. At the top of the Lower Clear Fork, 6886.00 ft (2098.9 m) (Figure 4.7), illite and mica comprise 55.2% of the total clay mineral, and interlayered illite/smectite comprise the remaining 44.8%, with no chlorite, or kaolinite. Down depth, a compositional shift is observed, with the appearance of chlorite, reaching 15.93% of total clay at 6897.05 ft (2102.2 m) and progressively increasing in subsequent depths. This trend continues, with illite and mica and illite/smectite remaining primary components, but with fluctuating proportions of chlorite. At 6950.00 ft (2118.3 m), the assemblage simplifies to mainly illite and mica (64.29%) and illite/smectite (35.71%), with no chlorite. This pattern, with varying dominance of illite and mica and illite/smectite, persists at several depths. Overall, the clay mineralogy in this interval is characterized by the predominance of illite and mica and illite/smectite, with variable chlorite presence.
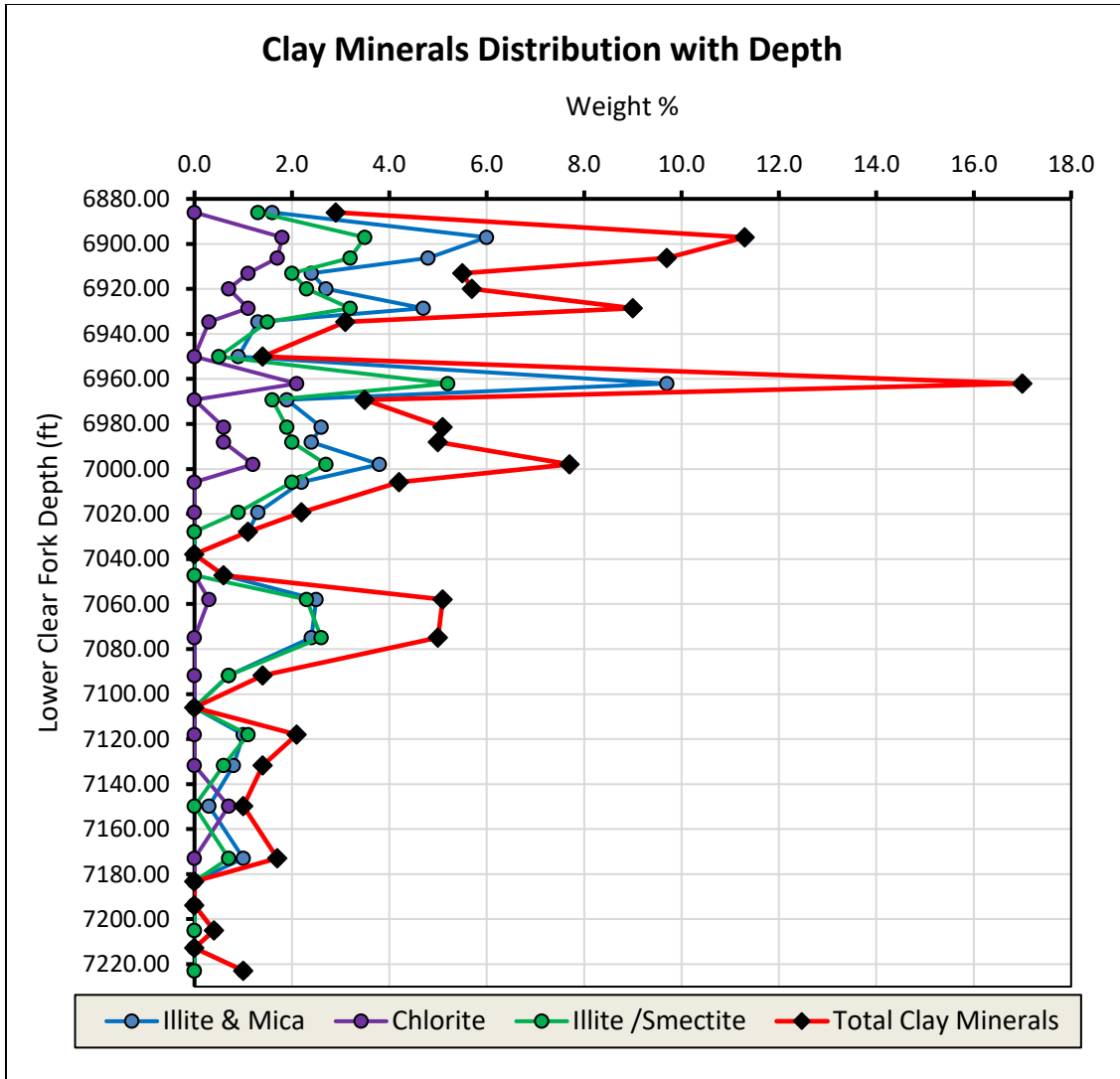
Figure 4.7. Clay mineralogical distribution over the Lower Clear Fork. (Note: Mixed layer of Illite/Smectite contains 10-20% Smectite).

Figure 4.8 shows the mineralogical and corresponding lithological distribution associated with the observed facies groups within the Lower Clear Fork interval.
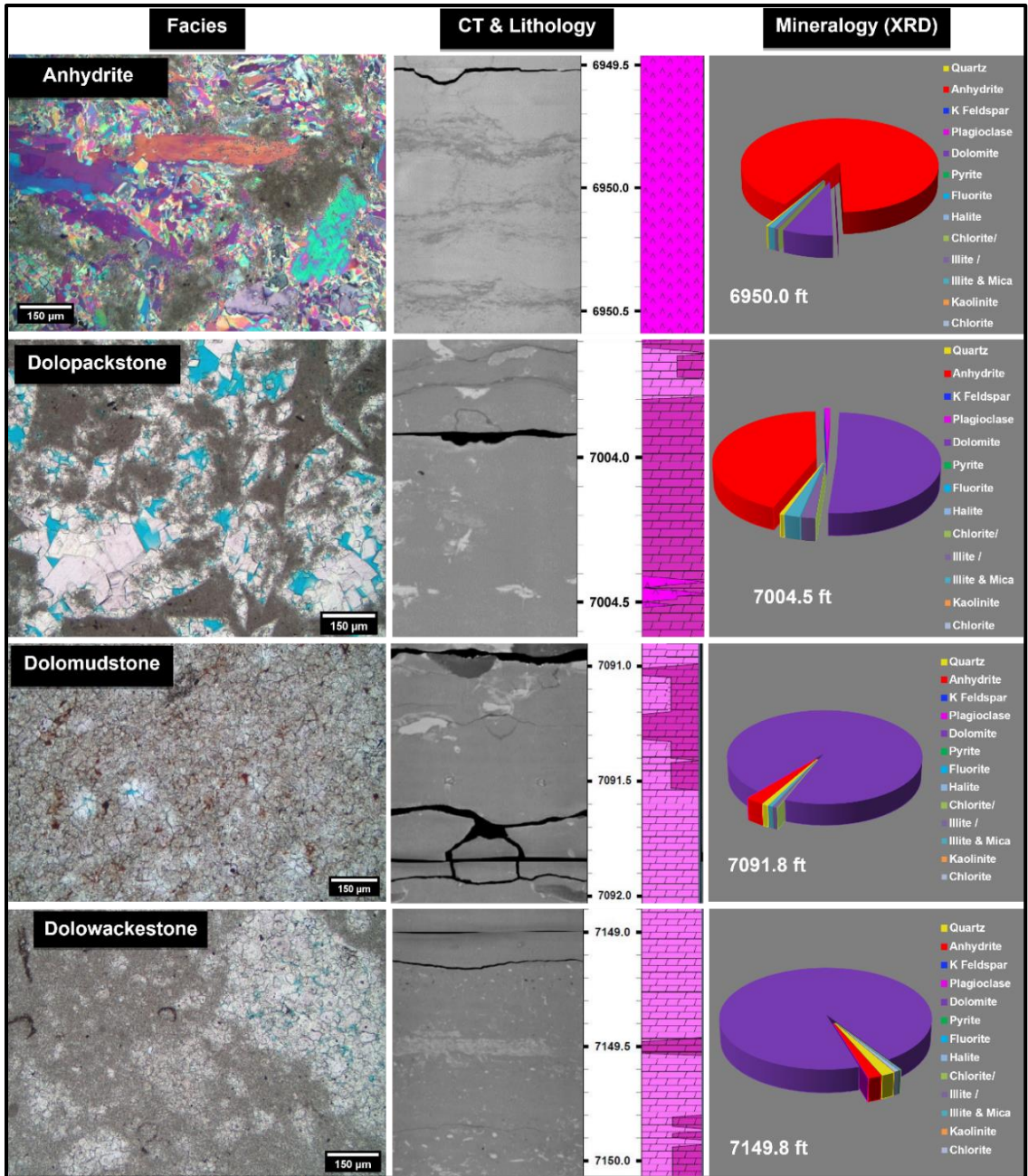
Figure 4.8. Mineralogical and major facies distribution within the Lower Clear Fork interval. (Computed Tomographic (CT) images were taken by Core Laboratories in 2018).

Dolomite and anhydrite were noted to be the dominant minerals in the Lower Clear Fork interval based on XRD mineralogical data. Observations from the plot in Figure 4.8 point to a higher intensity of dolomitization in dolowackestone and dolomudstone facies than observed in the dolopackstone facies. Conversely, anhydrite content is lowest in dolowackestone and dolomudstone facies, moderate in the dolopackstone, and highest in the anhydrite facies. A cross-plot of the dolomite against anhydrite to identify trends or relationships between the two minerals shows a negative correlation (Figure 4.9). Lower values of anhydrite correspond to intensely dolomitized zones. The negative relationship between the dolomite and anhydrite resulted from the complex diagenetic processes that altered the original mineral composition of the precursor limestone.
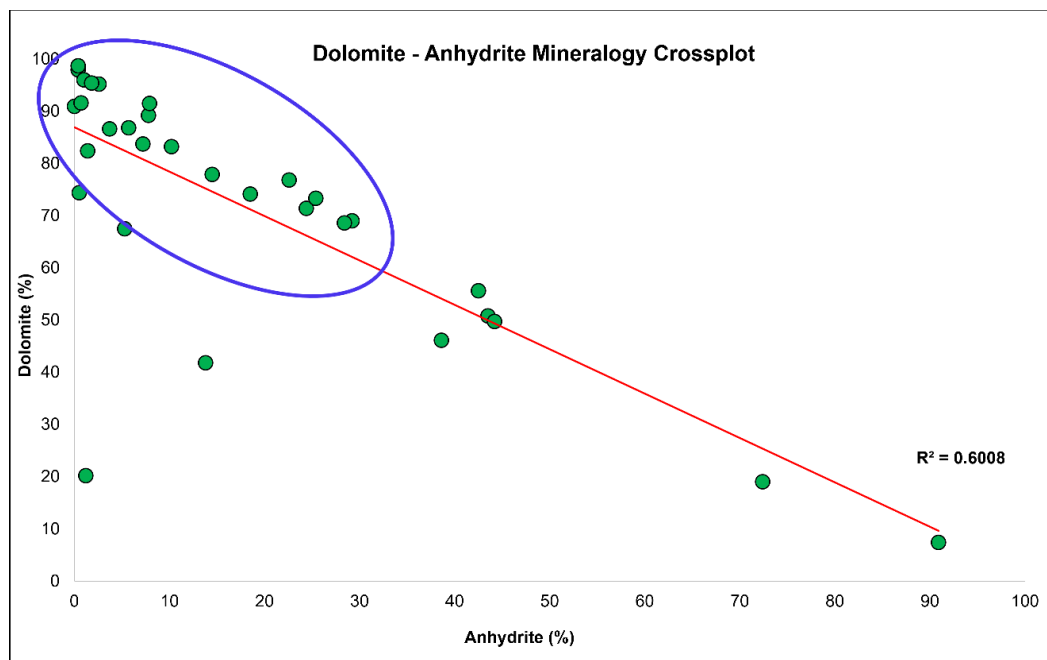
Figure 4.9. Cross-plot of dolomite versus anhydrite mineralogy (XRD) showing a negative correlation.

4.3. Petrophysical Analysis

The goal of the petrophysical analysis in this study was to build a mineral model and estimate the petrophysical parameters (porosity, water saturation, and permeability) of the Lower Clear Fork reservoir interval, 6880 – 7225 ft (2072.6 – 2202.2 m) in the Tex-Mex, S.E. Field using the Peterson 1P well and core-derived data. Core-derived data (XRD, porosity, water saturation) were used to calibrate the mineral modeling result. The results were interpreted regarding the different facies. The mineral modeling was conducted using the "*Mineral Solver*" module in Interactive Petrophysics software.

4.3.1. Clay Content Determination

The clay volume was computed using the *Clay Volume Module* in IP - "single clay Gamma Ray indicator". The single clay Gamma Ray indicator averaged the clay volume ($Vclay_{GR}$) based on only the Gamma Ray curve. Based on the Gamma Ray response for the interval, the baseline for little to no clay was established to be 10 API units while the clay line corresponding to 100% clay to a Gamma Ray value of 110 API units. The cross plot of clay volume from the Gamma Ray log compared with the core-derived XRD clay content shows a moderate correlation with an R-squared value of 0.6468 (Figure 4.10). This moderate correlation indicates that while the Gamma Ray log provides a reasonable estimate of clay content, there are other factors influencing the GR readings, or potential discrepancies between the logs and the core-derived measurements.
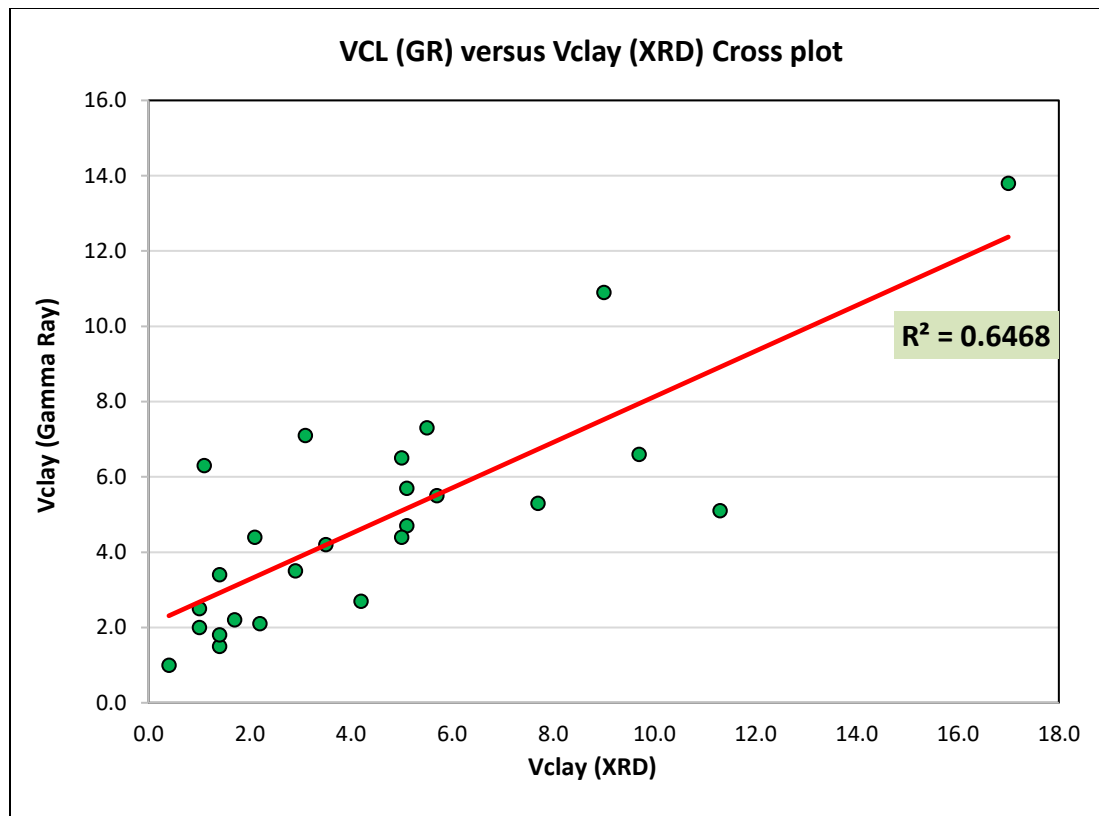
Figure 4.10. A cross-plot of clay content from Gamma Ray versus XRD-derived clay content mineralogy (XRD) shows a positive correlation.

The range of clay content within the Lower Clear Fork interval, as shown in Figure 4.11, varies from 0.4% to 17.4%. This suggests that the Lower Clear Fork Formation exhibits variable clay content, with certain depths exhibiting higher concentrations of clay. Zones of elevated clay volume corresponded with a high abundance of clay minerals, specifically illite, and smectite. The variations in clay content, as indicated by the data, suggest that there is significant heterogeneity within the interval. Adams, (1965) suggested that during the Early Wolfcamp, the basin experienced rapid subsidence permitting the

deposition of limestones and siliciclastics (shales and fine-grained sandstones) that came from the rising mountains on the northwest, west, and southwest. The calculations were calibrated with core-derived data, providing a more accurate interpretation of the clay volumes for the Lower Clear Fork interval.
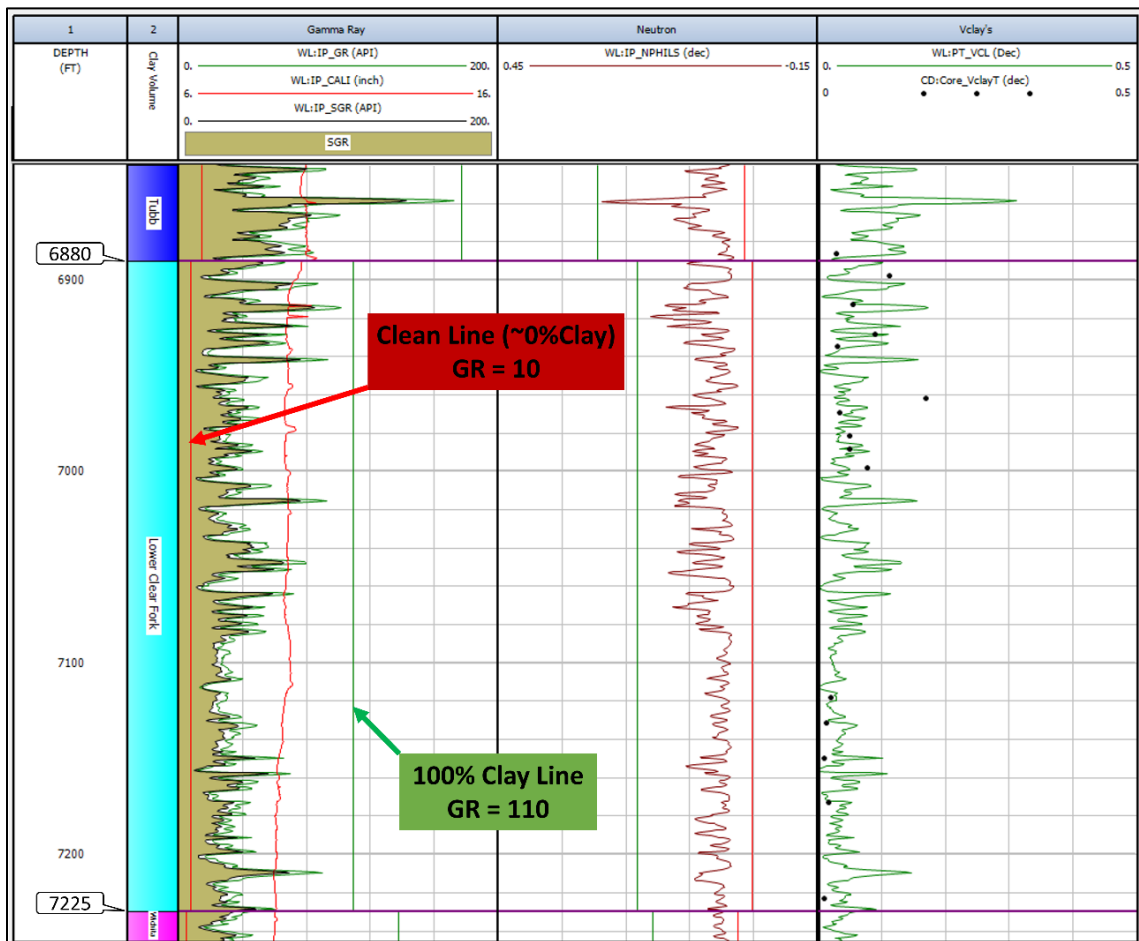
Figure 4.11. A plot illustrating clay volume calculation from a single clay indicator (Gamma Ray) for Peterson 1P. The first track shows the GR clean line (red) and the 100% clay line (green). Scale of the log plot: (1: 600ft). The second track shows the Neuton Porosity log. The third track shows the calculated clay volume with compared XRD clay content values. The shaded curve in tan is Spectra Gamma Ray (SGR) plotted to match the Gamma Ray.

4.3.2. Mineral Modeling

Characterization of a reservoir interval requires a consistent evaluation of the volumes of minerals present in the formation of interest. However, identification of these minerals by normal wireline log interpretation presents challenges due to the presence of clay, kerogen, and smaller grains. Furthermore, similar log responses can be obtained from different combinations of minerals. Overall, mineral modeling can be a challenge. The application of multiple mineral petrophysical models provides the best solution to tackle this challenge (Jadoon et al., 2016).

Based on mineralogical results from the XRD analysis, the desired minerals were selected and modeled using the *Mineral Solver* module in Interactive Petrophysics (IP). The study utilized a suite of wireline logs, including the Gamma Ray curve for clay content indication and resistivity for fluid content and rock matrix identification. The interactive petrophysics software synthesized these logs using the mineral inversion model, calibrated against core data, to quantitatively predict the mineralogies of the formation. After two iterations, the required mineral volumes, porosity, and saturation were obtained. Figure 4.12 shows the mineral model generated in the IP mineral solver. Note: The complete XRD data utilized in this work is proprietary and therefore not available for display in the appendix.
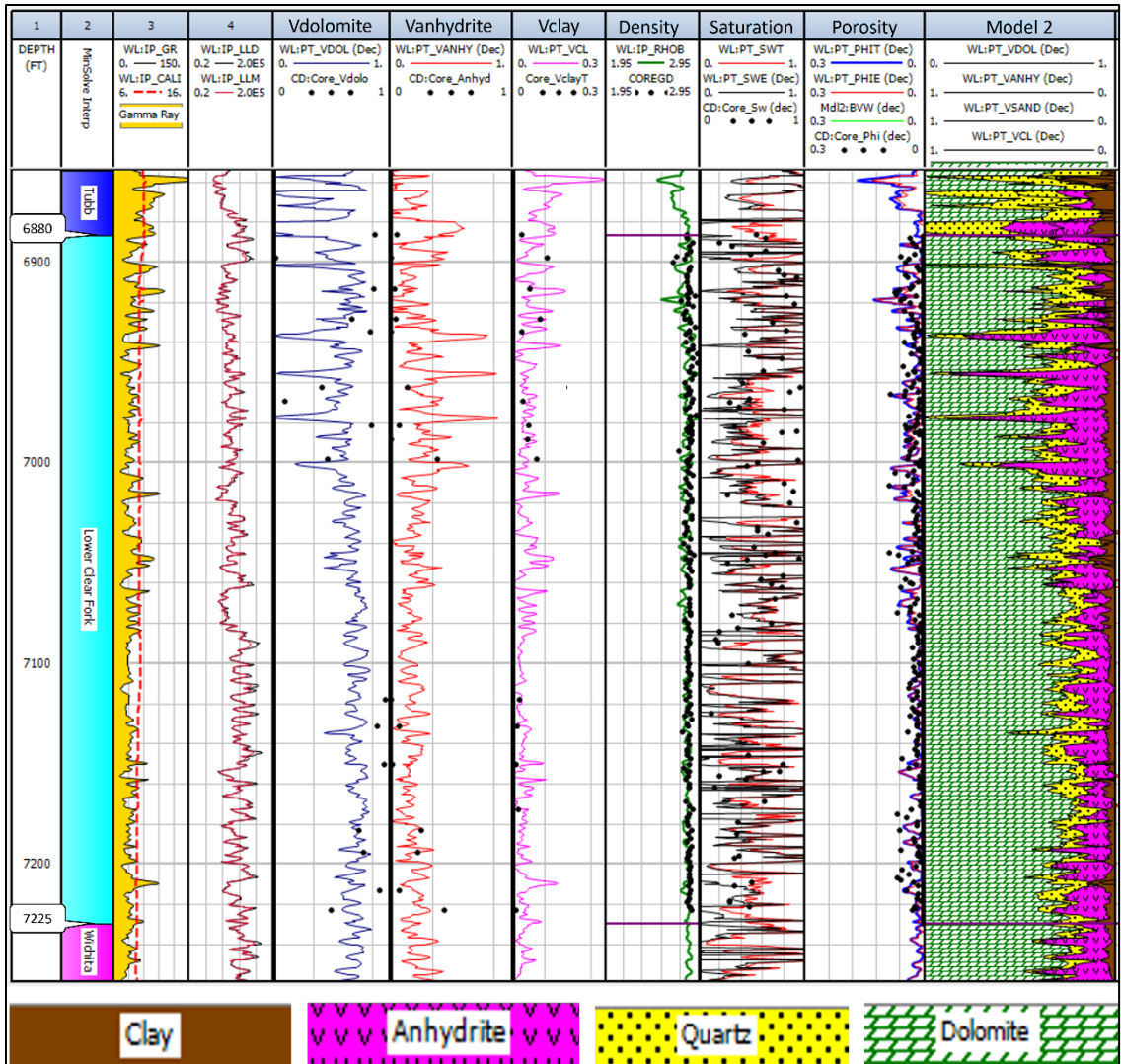
Figure 4.12. Mineral model for the Lower Clear Fork interval. The black dots represent the core data used to calibrate the modeling results. The plot also displays the volume of the dominant minerals (Vclay, Vanhydrite, Vdolomite); porosity (PhIT, PHIE, Core Phi), and saturation (SWT, SWE, Core SW).

Analysis of the result from mineral modeling suggests that the Lower Clear Fork interval, 6880 – 7225 ft (2072.6 – 2202.2 m) is highly dolomitized (over 70% dolomite on average consistent over the interval) and anhydrite (10 - 20% on average). However, the top of the interval, 6935 – 7000 ft (2113.8 – 2133.6 m) shows spikes of anhydrite (80 – 90%). The modeling results calibrated with core-XRD mineral abundances, are shown in Figure 4.12. The dominance of dolomite and anhydrite suggests extensive diagenetic processes took place throughout the entire Lower Clear Fork. This is indicative of pervasive brine-rich fluid that dolomitized the carbonate rock of the Lower Clear Fork. The paleoenvironment during the Early Permian provided arid and warmer climatic conditions that facilitated high evaporation of seawater and subsequent precipitation of gypsum. Also, the significant presence of gypsum later dehydrated to anhydrite within the interval points towards episodes of evaporitic conditions, potentially reflecting periodic restriction and isolation of the depositional environment from open marine conditions.

The minor spikes of siliciclastics (quartz) within the upper portions of the interval, 6880 – 6920 ft (2097 – 2109.2 m) suggest remnants of siliciclastic influxes. During the low stand of the sea, terrigenous sands carried by wind or fluvial were deposited on the carbonate platform and along the shelf margins. They were subsequently moved towards the basinal areas through incised valleys and channels. The presence of clay in minor amounts represents periods of reduced sedimentation energy, allowing for the deposition of finer clastic materials.

4.3.3. Porosity and Permeability

In evaluating the reservoir properties of the Lower Clear Fork, a bivariate plot of porosity and permeability was generated to visualize the relationship between these two critical reservoir parameters based on the different depositional facies and pore types. The facies included dolomudstone, dolowackestone, dolopackstone, and anhydrite, each demonstrating a unique porosity and permeability signature.

The core-derived porosity and permeability data were collected from one-inch core plugs taken from the Peterson 1P well containing the Lower Clear Fork interval. From the petrophysical analysis in IP, the porosities were calculated and the results were calibrated with core porosity data. A histogram distribution of the core-derived porosity based on the identified major facies is shown in Figure 4.13. The core-derived porosity data from the Lower Clear Fork interval revealed the average porosity for dolomudstone, dolowackestone, and dolopackstone facies, as 3.20%, 3.04%, and 4.53%, respectively. The porosity value averaged for all the different facies (representing the entire Lower Clear Fork interval) is 3.23%, indicating a relatively low porosity attribute of the Lower Clear Fork reservoir. The range of porosities is 0.54 – 9.09% (dolomudstone); 0.49 – 8.31% (dolowackestone); 0.77 – 7.22% (dolopackstone) and 0.49 – 9.09% (for all facies in the interval). Anhydrite facies, while not extensively measured, showed a notably lower porosity value at 0.94%, which is consistent with its tighter and less porous framework.
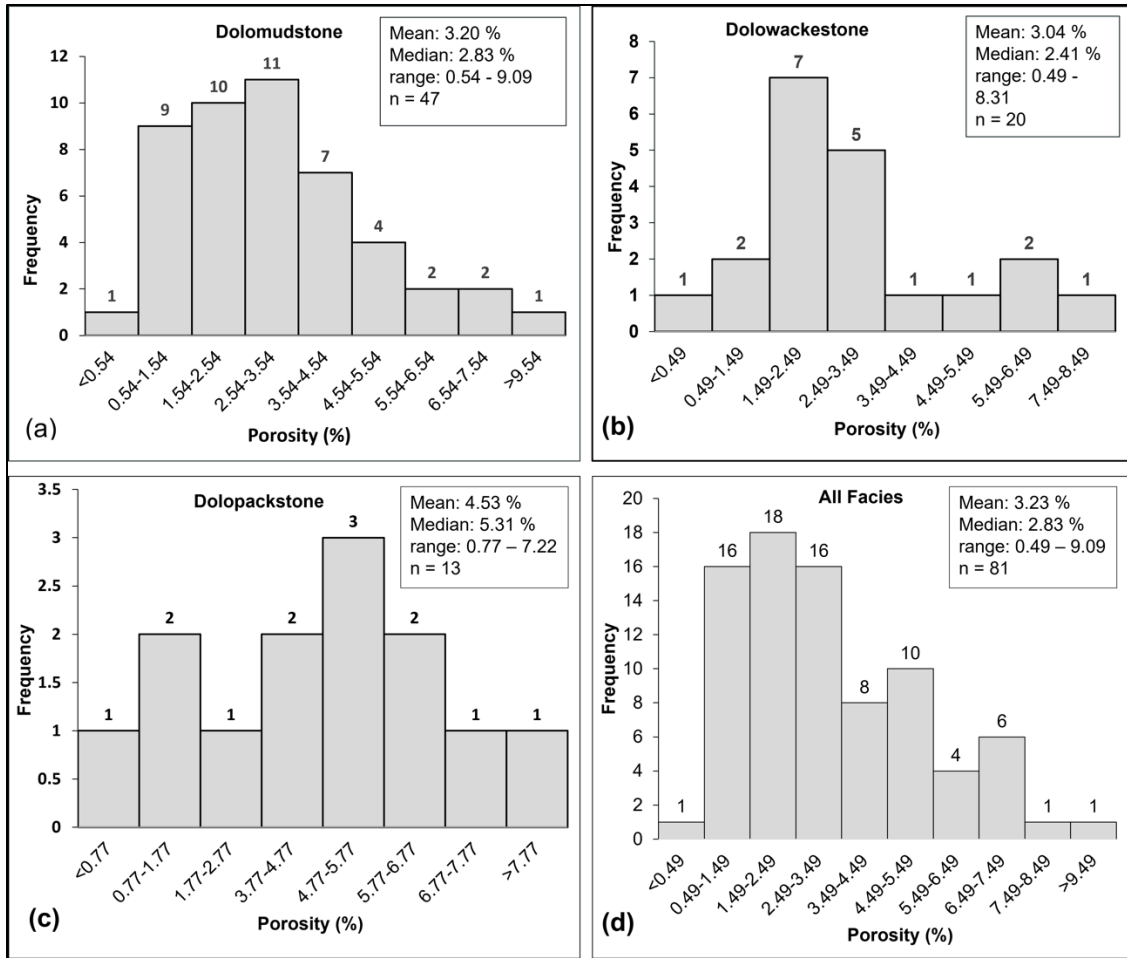
Figure 4.13. Column plots of core-derived porosity data showing heterogeneity in facies in the Lower Clear Fork interval in the Tex-Mex, S.E. Field. The histogram shows the porosity distribution in (a) dolomudstone; (b) porosity distribution in dolowackestone; (c) porosity distribution in packstone; Note: Not enough porosity data points to plot histogram data for anhydrite; (d) porosity distribution in all the identified facies.

While the range of porosities in dolomudstone facies ranges between 0.54 – 9.09% which is consistently low (Figure 4.13a), the corresponding permeability values range between .0003 – 1.6 mD (Figure 4.14). From the data, however, about ninety percent of the permeability values for the dolomudstone facies were below 1 mD (Figure 4.14).
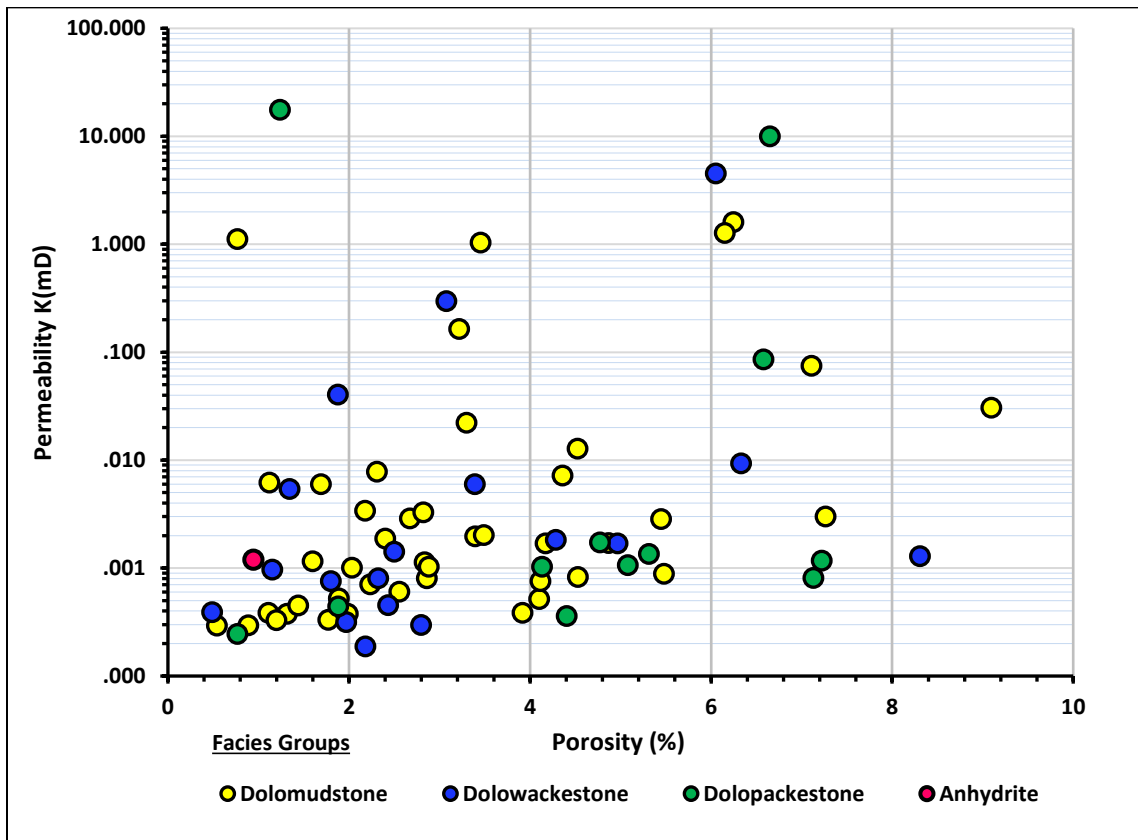
Figure 4.14. Peterson 1P core-derived permeability versus porosity cross-plot for all the different facies (predominantly dolowackestone) in the Lower Clear Fork interval.

The porosity and permeability results of the dolomudstone facies suggest compacted and tightly packed dolomite fabrics. The occurrence of gypsum, which later converted into anhydrite, occluding vuggy pores and fractures within the finely recrystallized dolomite matrix, has significantly impacted pore connectivity, as depicted in Figure 4.15. This phenomenon has adverse implications for fluid flow within the rock formation.
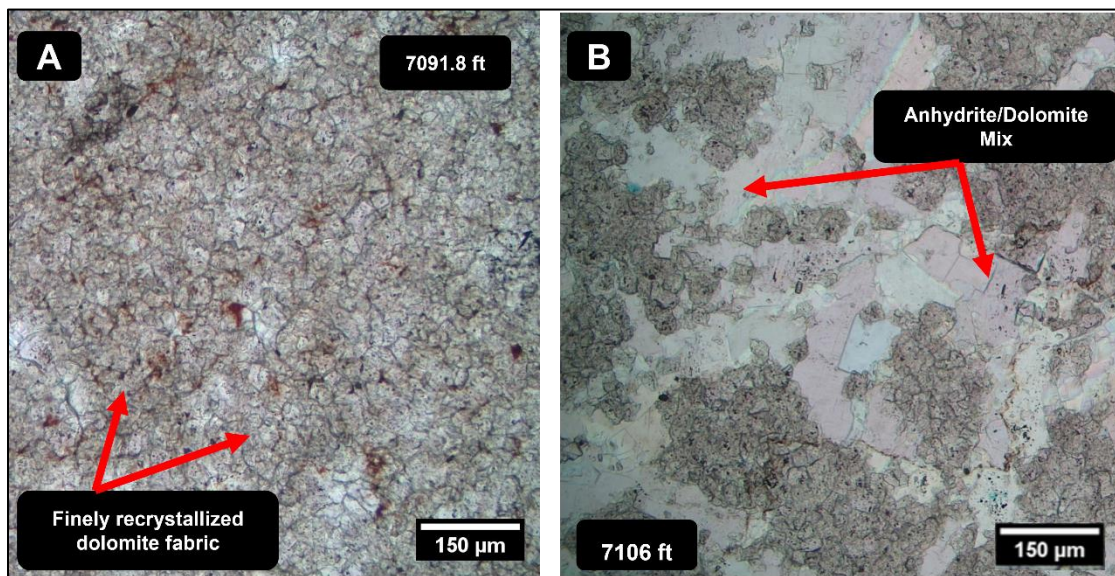
Figure 4.15. Thin section photomicrographs of dolomudstone facies showing fine dolomite crystals in A and recrystallized dolomite and anhydrite fabric in B. Depths of thin sections in A and B were taken at the depth of 7091.8 ft (2161.6 m) and 7106 ft (2165.9 m) respectively. Both thin sections were taken in Plain Polarized Light.

In the dolowackestone facies, while the values of porosity range from $0.49 - 8.31\%$, the dominant porosities lie in the range of $2.49 - 3.49\%$ (Figure 4.13b). Corresponding permeability values for this facies class range between .0002 to 4.52 mD (Figure 4.14). The contributing pores types to these porosities include micropores, intercrystalline, and moldic pores (Figure 4.16).
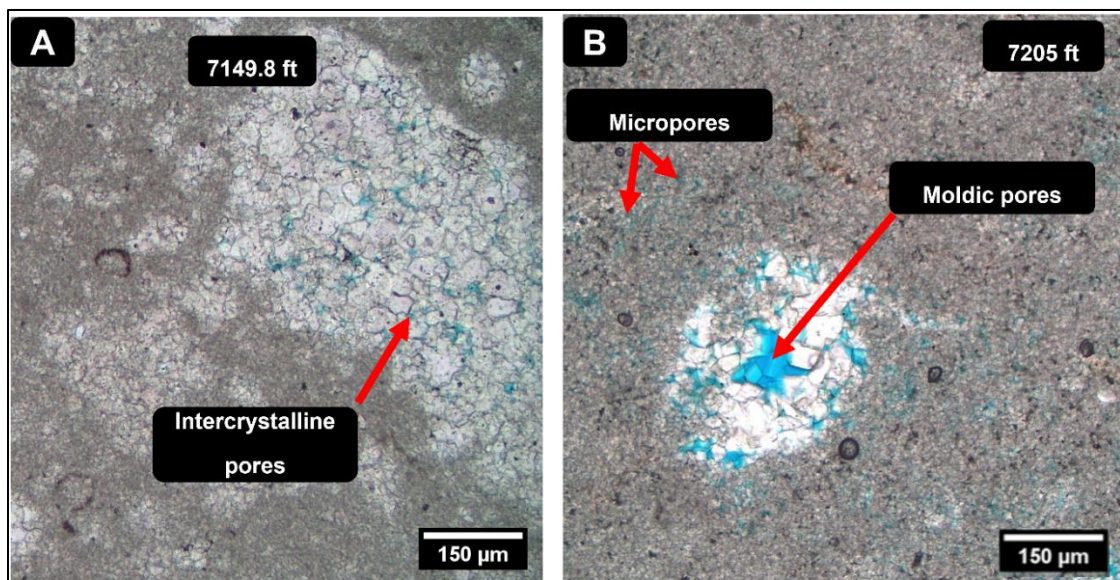
Figure 4.16. Thin section photomicrographs of dolowackestone facies showing intercrystalline pores in A; and moldic and micropores in B. Depths of thin sections in A and B were taken at the depth of 7149.8 ft (2179.3 m) and 7205.0 ft (2196.1 m)respectively. Both thin-section photomicrographs were taken in Plain Polarized Light.

Like the dolomudstone and dolowackestone, the dolopackstone facies exhibited a broad range of porosity (0.77 – 7.22%) (Figure 4.14) with an average porosity value of 4.53% (Figure 4.13c). The permeability values range between 0.0002 and 17.6 mD (Figure 4.14). The instance of a higher permeability value, 17.6 mD occurred at the depth, of 7104.8 ft (2165.8 m) which has vuggy pores. The occurrence of vuggy pores offers a favorable pore geometry and the potential interconnection of pore spaces hence the high value of 17.6 mD. With the anhydrite facies, only one porosity and permeability data point was available (0.94%, 0.001 mD) at a depth of 6950 ft (2118.4 m) (Figure 4.14). The anhydrite facies are characterized by low porosity and permeability values validating their characteristic tightness. Their low porosity and permeability values and occurrences within pores and fractures contributed to impacting fluid flow and reservoir compartmentalization.

The bivariate cross plot of porosity and permeability based on the major facies showed a broad range of porosities and permeability values as stated above (lack of trend or correlation), suggesting significant lithologic heterogeneity existing in the different facies of the Lower Clear Fork interval. The spread and ranges of the porosities and permeability values in the different facies across the Lower Clear Fork are indicative of the diagenetic modifications of the facies and pores (dolomitization, compaction, fracturing, and dissolution) after sediment deposition.

The pore types revealed through thin-section analysis included micropores, intercrystalline pores, fracture pores, vuggy pores, and moldic pores, each imparting distinct influences on the reservoir's permeability. Intercrystalline and micropores, dominant across the interval, highlighted the low to moderate porosity and permeability values observed across the interval. In contrast, fracture, and moldic porosity deviate from this trend, often associated with moderate to high porosity and permeability values (Figure 4.17). The vuggy pores showed low to high porosity and permeabilities across the different facies. The different pore types highlight their contribution to fluid flow through secondary porosity, which is directly not linked to the primary depositional characteristics of the rock.
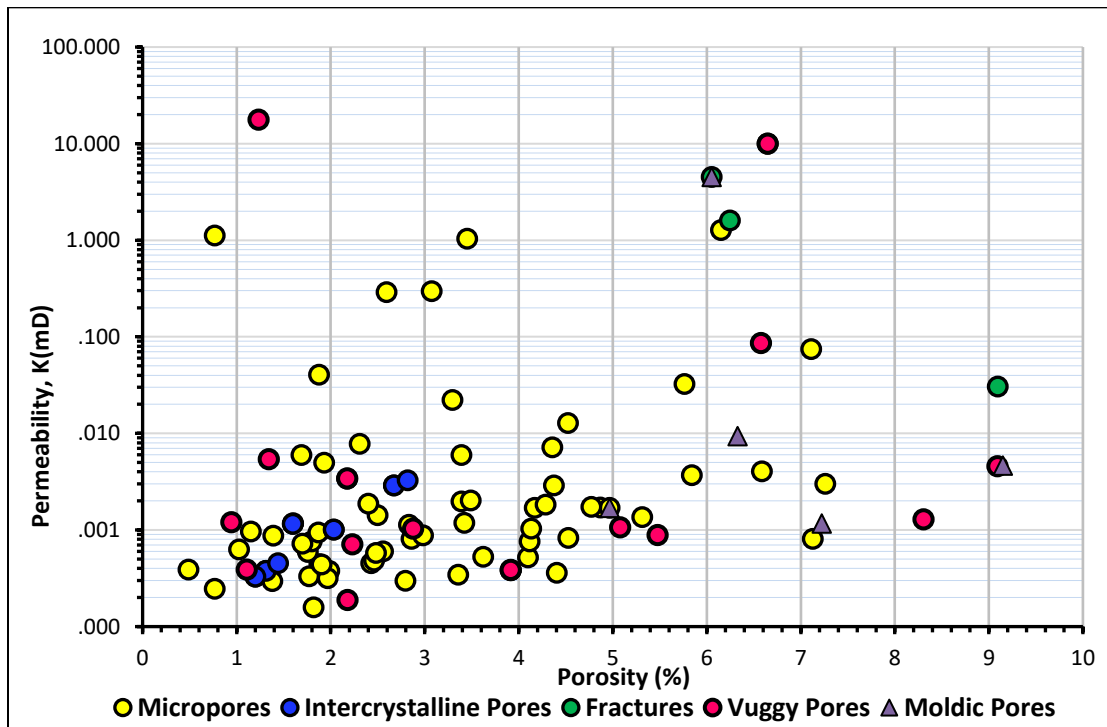
Figure 4.17. Peterson 1P well core-derived permeability versus porosity cross plot by pore types within the Lower Clear Fork interval.

The porosity and permeability results indicate that the Lower Clear Fork facies are significantly heterogeneous in both porosity and permeability. This heterogeneity is a direct consequence of the variable diagenetic modifications that took place in the different facies of the Lower Clear Fork reservoir, including dolomitization, gypsum and anhydrite formation, fracturing, compaction, grain leaching, and dissolution. The anhydrite that later formed within the pore spaces and fractures acting as barriers to fluid flow could be targeted for hydraulic fracturing to increase interconnectivity within the interval.

The porosity estimation from the petrophysical analysis in IP software, when compared with core-derived data, enabled a more comprehensive understanding of the Lower Clear Fork reservoir. The result of porosity measurements from routine core analysis (RCA) was critical for calibrating and validating the petrophysical results, ensuring that the Lower Clear Fork subsurface evaluation was as accurate as possible. The Lower Clear Fork interval demonstrates a complex interplay between porosity, permeability, and facies, influenced by secondary diagenetic alterations. Figure 4.18 shows the core-derived porosity values plotted to assess the quality of the porosity computations from the petrophysical modeling of the Lower Clear Fork. Generally, both measured and calculated porosity values range between 1 to 10% (see Figure 4.14; Figure 4.18).
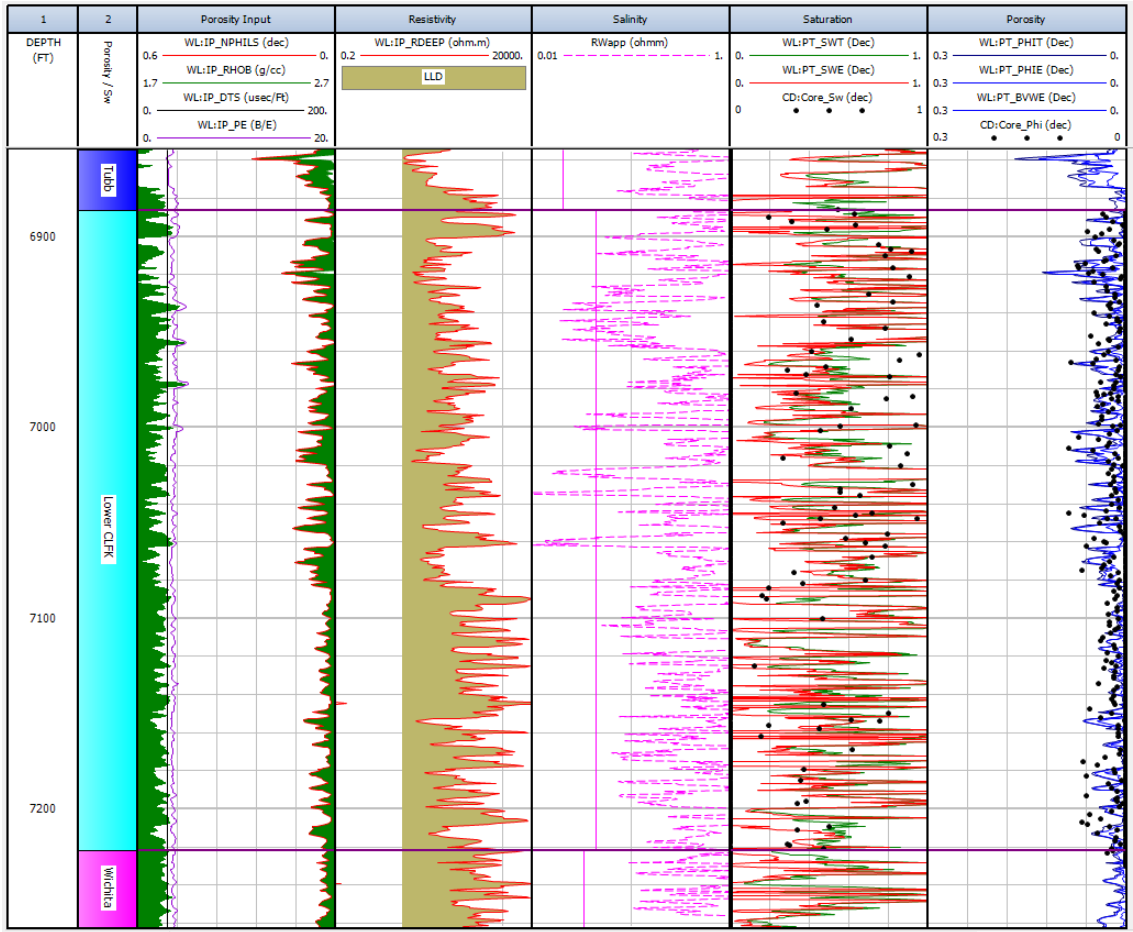
Figure 4.18. Log plot of porosities computed for the Lower Clear Fork interval. The wireline porosities were calibrated with core-derived porosities to ensure the accuracy of the petrophysical calculations. Black dots in the porosity track (far right) represent core-derived porosity values. Scale of plot: 1:600ft

4.3.4. Water Saturation

The analysis of the core-derived saturation data yielded a distribution profile of oil and water across the Lower Clear Fork interval. The saturation plot, Figure 4.19, displays the percentage of pore volume occupied by oil and water at various depths.
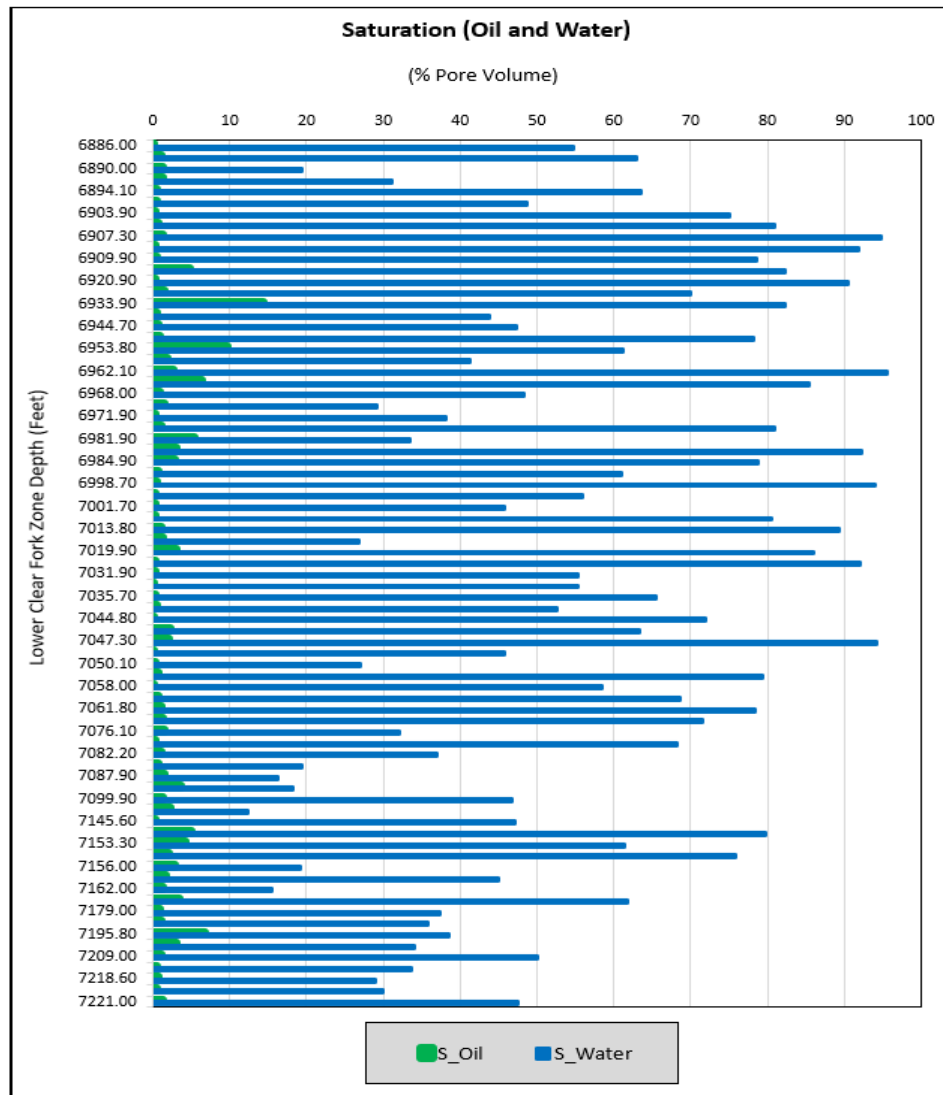
Figure 4.19. Oil and water saturation profile over the Lower Clear Fork interval.

The pore spaces of the Lower Clear Fork reservoir are dominantly saturated with water, particularly at a depth, of 6907.3ft (2105.3 m), where it accounted for approximately 94.7% of the pore volume. Conversely, oil saturation in the interval was consistently low (0.1 – 6.7% of pore volume) and a high of 14.4% occurring at a depth of 6933.9 ft (2113.2 m) (Figure 4.19). At the depths, 6933.9 - 6964.4 ft (2113.2 – 2122.7 m), the moderate increase in oil saturation (Figure 4.19, green bars) suggests a zone of increased hydrocarbon accumulation. The predominance of anhydrite facies across the interval is a likely factor to account for the low oil saturation, as anhydrite acts as an effective seal, limiting hydrocarbon migration and trapping fluids below. The heterogeneity in fluid distribution within the interval suggests a complex interplay between depositional environments and diagenetic processes that impacted the reservoir connectivity and fluid flow. A petrophysical plot of the water saturation obtained using the Archie PhiT equation in IP software is shown in Figure 4.20. The water saturation calculations were calibrated with core analysis data to determine the validity of the method for calculating water saturation within the interval.
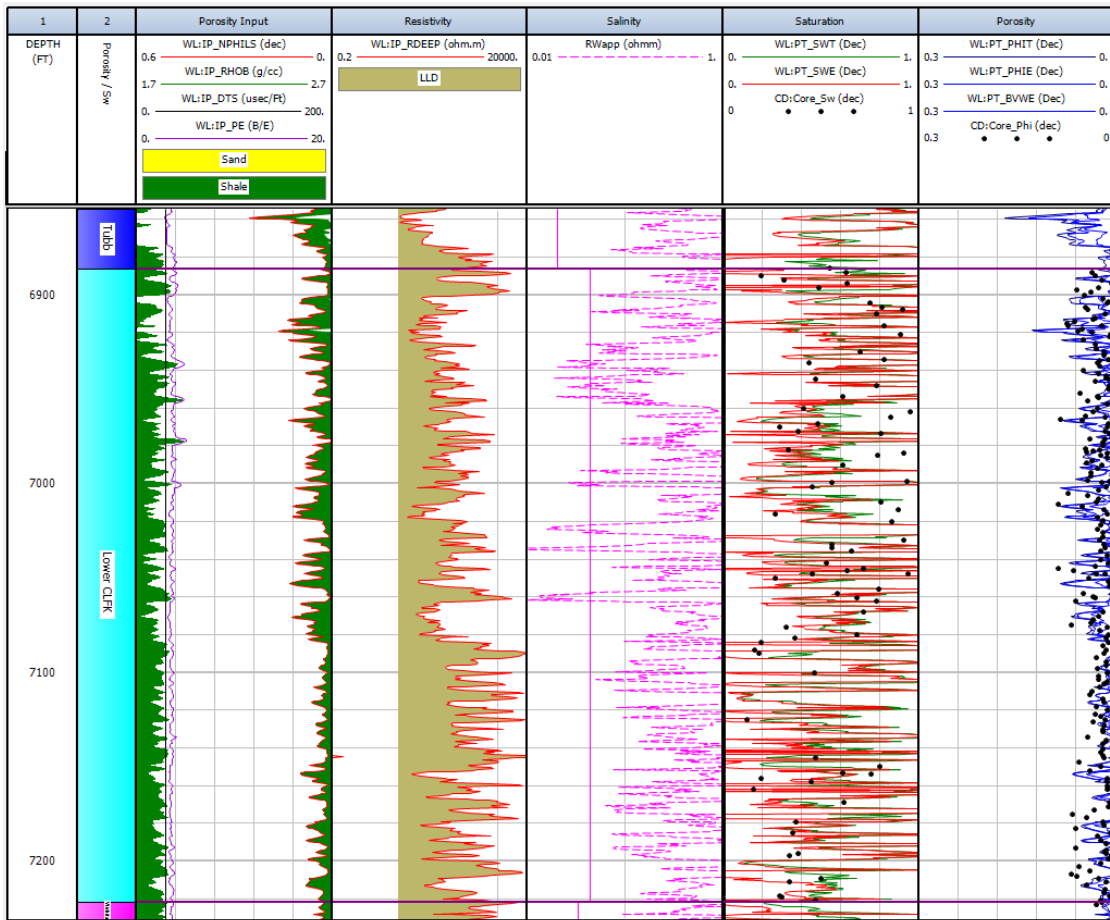
Figure 4.20. Calibrated log plot of water saturation computed for the Lower Clear Fork interval. The core-derived saturation data were plotted to ensure the accuracy of the computations. Scale: 1:600ft. The black dots represent core data.

From water saturation results calibrated with core-derived data (Figure 4.20), the range of water saturation for the entire interval lies within 12.4 – 95.4%, with a mean water saturation of 63.2% (Figure 4.21; Table 4.2). For the volume of pore space occupied by water based on the facies type, dolomudstone accounted for 12.4 – 95.4%; 19.4 – 94.2% for dolowackestone, and 58.4 – 94.7% for dolopackstone. The water saturation, however,

for the entire interval lies in the range of 12 – 95.4% (Figure 4.21). The corresponding mean values of water saturation for dolomudstone, dolowackestone, dolopackstone, and the entire facies were 57.2, 62.6, 75.4, and 63.2 % respectively (Figure 4.21).
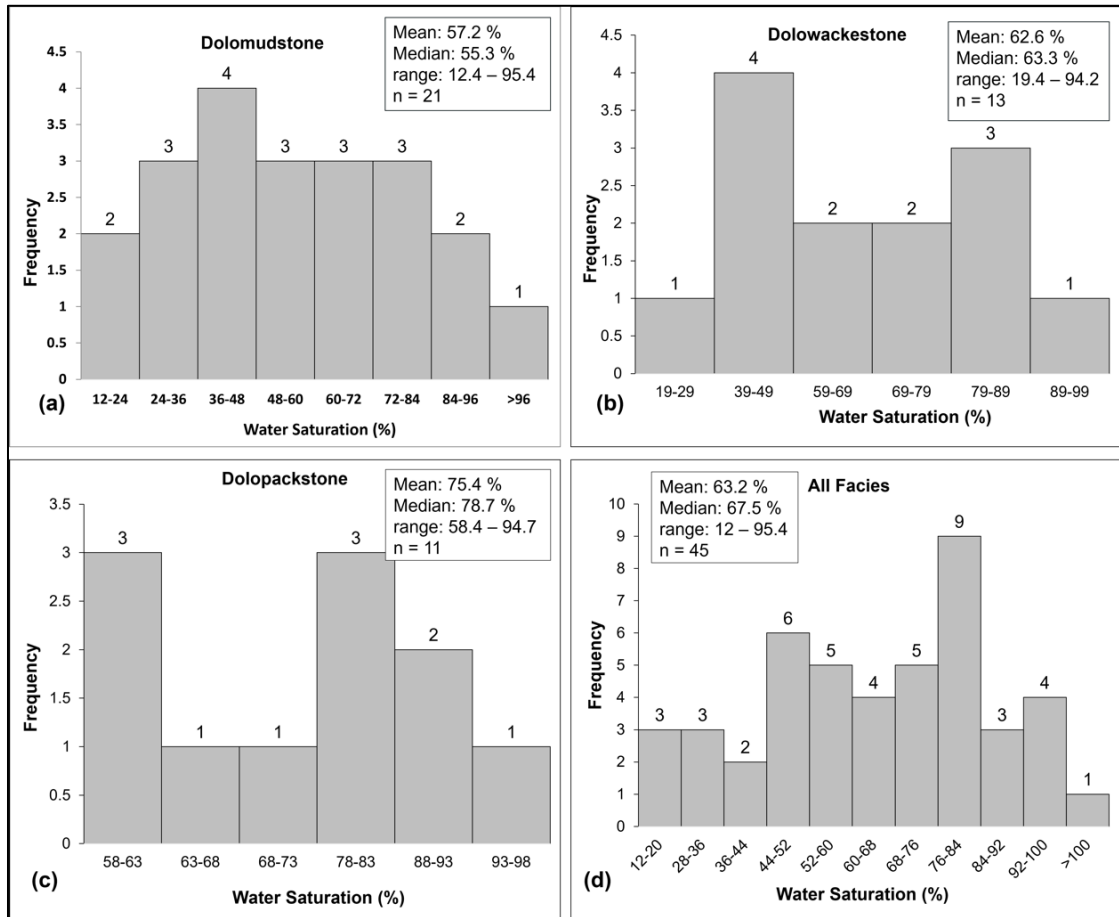
Figure 4.21. Column plots of water saturation over the Lower Clear Fork interval were obtained from the core analysis. The histogram shows the water saturation distribution in (a) dolomudstone. (b) water saturation distribution in dolowackestones. (c) water saturation distribution in packstones. Note: Not enough porosity data points to plot histogram data for anhydrite. (d) water saturation distribution in all the identified facies.

The high percentages of water saturation across the interval suggest corresponding low oil saturation in the pore spaces. From the oil saturation plot, the highest oil saturation within the interval was 14.4% (Figure 4.20). Overall, the low oil saturation results underscore the facies heterogeneity of the Lower Clear Fork Formation. The data from core analysis and petrophysical analysis points to a highly saturated water reservoir.

Table 4.2. Summary table of petrophysical computations for the Lower Clear Fork interval.

Well Name	Porosity (%)	Water Saturation (%)	Oil Saturation (%)	Perm, K (mD)	Vclay (%)	Vdolomite (%)	Vanhydrite (%)
Peterson 1P	0.5 - 10	12.4 – 95.4	0.1 – 14.4	10^{-4} – 17.6	0.4 – 17.4	7.3 – 98.7	0.2 – 90.9

4.3.5. Limitations to the Petrophysical Study

The analyses presented in this study integrated data from core analysis and those calculated from petrophysical modeling in IP software. Analytical results from core-based measurement and petrophysical calculations exposed fundamental differences that can be attributed to a mix of factors within subsurface geological formations. Data from the core, offering direct measurements, usually do not comprehensively represent reservoir heterogeneity. Petrophysical calculations, while valuable for broader reservoir characterization, are subject to uncertainties stemming from modeling approaches, equations, techniques, and assumptions used in petrophysical modeling. Assumptions

about rock properties, mineralogy, and well-log parameter selection influence the accuracy of petrophysical predictions. Moreover, core damage, contamination, and uncertainties in fluid saturation estimation can further contribute to disagreements between core-derived data and petrophysical models.

In determining the mineralogy of the Lower Clear Fork, the selection of minerals for the petrophysical mineral modeling was based on the mineralogical results from the XRD analysis. The outcomes of the mineral modeling (refer to Figure 4.12) showing the modeled mineralogy and their volumes were calibrated with mineralogy data obtained from X-ray diffraction (XRD). A visual observation of agreement, when the mineral volumes of dolomite, anhydrite, and clay from XRD were plotted on the mineral result from petrophysical mineral modeling, revealed about 70% of results agreement (refer to the core-calibrated mineral modeling result in Figure 4.12). Also, clay volume calculated from the IP software when crossplotted with total clay result from XRD revealed a 65% extent of correlation.

With regards to the assessment of porosity and water saturation across the Lower Clear Fork interval, petrophysical modeling outcomes were calibrated with results from core-based measured porosity and water saturation data. The core-calibrated plots of porosity and water saturation are shown in Figure 4.18 and Figure 4.20 respectively. Acknowledging the complex nature of estimating carbonate reservoir rock properties, factors that contributed to disagreement of results from petrophysical and core-base data

include variation in sample lithology, diagenetic modifications of the carbonate system, and assumptions inherent in the petrophysical modeling process. Potential sources of error from core analysis techniques include core damage and contamination, alongside uncertainties associated with petrophysical modeling, including simplifications in petrophysical models, and equations. Additionally, human errors stemming from experience (which is gained over time) in using petrophysical models and IP software, may introduce errors. The integration of the core data and petrophysical modeling results in this study represents a significant contribution to reservoir characterization efforts.

5. DISCUSSION

The Lower Clear Fork Formation at the Tex-Mex, S.E. Field was analyzed to define the depositional facies, mineralogical, and petrophysical properties. Across the interval, the Lower Clear Fork comprises four major facies dominated by dolomite and anhydrite with a minor amount of clay and siliciclastics. A mineralogical analysis of the Lower Clear Fork interval revealed dolomitization occurred early in the sediments after deposition. In this chapter, the depositional environment of the facies, the mineralogy, and the implications of the facies attributes on the Lower Clear Fork reservoir are discussed.

5.1. Depositional Environments

The facies attributes of the Lower Clear Fork interval at Tex-Mex, S.E. Field as revealed in cores, thin sections, and mineralogical data point to shallow-water carbonates deposited in a warm and restricted marine environment during the Early Permian (Figure 5.1). The facies from this field are closely related in character and mineralogically with the other Clear Fork carbonates examined and documented from outcrops and subsurface studies by Ruppel et al. (1995); Kerans et al. (2000) and Ruppel (2002), across the carbonate platform. Landward (up-dip) on the platform, the Lower Clear Fork stratigraphic unit at the Tex-Mex, S.E. Field is characterized by peritidal tidal-flat deposits (dolomudstone and anhydrite) and inner, middle to ramp crest facies (wackestones and

packstones (Figure 5.1; Table 4.1). The alternation of these deposits across the interval is consistent with the cyclicity in the eustatic rise and fall of sea level during the Early Permian.
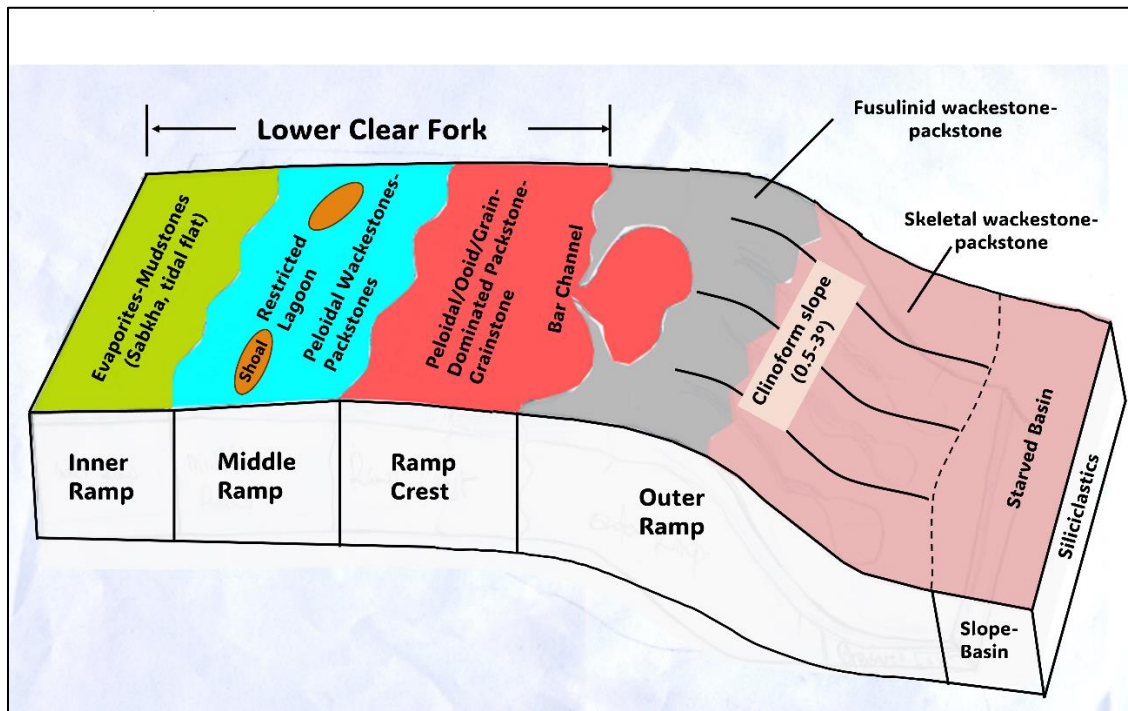
Figure 5.1. Idealized depositional model for shallow-water platform carbonates based on facies encountered in the Lower Clear Fork core study and from previous studies in the Central Basin Platform. The different facies and their related depositional are shown in colors. The modified depositional model incorporated some information adapted from Ruppel et al., (1995).

5.1.1. Tidal Flat Environment

The Lower Clear Fork dolomudstone facies, comprising silty to argillaceous variants, are indicative of deposition in a very shallow restricted marine environment where hypersaline brines persisted with arid and warmer climates (Figure 5.1; Figure 5.2). These sediments were deposited during highstand. These areas of the platform do not experience frequent flooding of the sea except during high tides. This interpretation is supported by the presence of mud-rich rocks that are massive and laminated with intraclastic grains and few peloidal grains. The dolomitized facies are characterized by a range of pore types including micropores, intercrystalline, moldic, and fractures.

Ruppel & Harrington (2012), in their published work on the Clear Fork reservoir at the Fullerton Clear Fork Field, an analogous equivalent of the Lower Clear Fork at Tex-Mex, S.E. Field, concluded that the tidal flat dolomudstones were highly dolomitized and those areas are likely to display porosities to about 15%. The highest porosity recorded in this study for dolomudstones, however, was 9.09%. This fell short of the 15% projected porosity value by Ruppel & Harrington, 2012 due to the compact framework of the finely crystallized dolomite followed by anhydrite occurrence in pores and fractures. Their work, however, argued that, because the facies were dominated by intercrystalline pores with finely-crystallized dolomite and anhydrite, they exhibited low permeability values. The porosity values from this study for the tidal flat facies fell below 2.0 mD. The crystalline dolomite crystal and the occurrence of anhydrite point towards a diagenetic overprint in a

hypersaline environment (reflux dolomitization). The prevalent mineralogy of dolomite and anhydrite minerals within these facies further supports a tidal flat/sabkha environment with restrictive marine water circulation and exposure to arid and warmer climates. This environment favored significant evaporation of seawater rich in sulfate ions (SO_4^{2-}) and brines with a high concentration of dissolved salts, including magnesium ions (Mg^{2+}) and calcium ions (Ca^{2+}). The evaporative action during the Early Permian initiated gypsum precipitation in the shallow tidal flat environment and reflux dolomitization. With further evaporation, increased salinity levels, burial, and compactive actions, anhydrite began to precipitate, typically replacing the gypsum layers at depth within the sediments.

5.1.2. Inner, Middle to Ramp Crest Environments

The skeletal wackestone-packstone facies are characterized by the presence of skeletal debris, primarily composed of mollusk fragments (ostracods and bivalves). Peloids are commonly found throughout the facies, which transition into peloidal wackestones and packstones. There were occurrences of burrowing activities, indicating bioturbation activity. The skeletal wackestone-packstone facies exhibit low porosity, with pore spaces comprising skeletal molds and intercrystalline pores. The prevalence of mollusk fragments (ostracods and bivalves) and the notable absence of typical marine organisms (fusulinids) suggest a low-energy depositional environment situated within the inner-platform setting.

The peloidal wackestone-packstones facies present facies distinct from rocks of

peritidal mudstone facies, particularly in their associated sedimentary structures and environments. The predominant grains are peloids containing fecal pellets formed by infaunal burrowers. The absence of skeletal allochems suggests their interpretation of a low-energy, potentially restricted, inner to middle ramp setting of the carbonate platform. Anhydrite nodules are frequently observed within these rocks, indicating the infiltration of sulfate-bearing diagenetic fluids post-deposition. These nodules often occupy permeability pathways created by burrowers and fractures. Porosity in these rocks is predominantly associated with intercrystalline pores, with less common skeletal moldic pores contributing to the overall porosity characteristics. This distribution of porosity types suggests a complex interplay between depositional processes, early dolomitization alterations, and subsequent lithological properties.

The grain-dominated (or grain-rich) peloidal packstones represent a departure from the mud-rich peloid facies previously discussed. Unlike their mud-dominated counterparts, these packstones often exhibit characteristics indicative of wave-related transport. They are typically well-sorted and feature interparticle pores that may be either open or filled with anhydrite cement. Ruppel & Harrington (2012), noted that the presence of interparticle pores suggests that these peloids functioned as true grains rather than pellet mud, distinguishing them from the intercrystalline and moldic pores typical of mud-dominated facies. These facies' characteristics and attributes put their environment of deposition in the high-energy ramp crest setting of the carbonate platform. These facies typically

exhibited the highest porosity values when compared with other facies, coupled with the well-sorted nature of the rocks, making them particularly desirable to transmit hydrocarbon fluids.

In summary, the dolowackestone and dolopackstone facies suggest an environment of deposition to an inner, middle to ramp crest facies (Figure 5.1; Figure 5.2;). The grain types present, such as intraclasts, peloids, and coated grains, suggest low energy conditions conducive to sediment reworking and transport. The occurrence of fenestral fabrics and fossils such as ostracods and bivalves within the mud-dominated dolopackstone facies particularly denotes a low-energy, well-oxygenated setting with open circulation, likely representing the middle ramp. The occurrence of grain-dominated packstones is evidence of wave transport of high energy associated with the ramp crest.

5.1.3. Sabkha/Restricted Lagoon Environments

The anhydrite facies align with deposition in a restricted coastal lagoon or exposed tidal flat/sabkha environment (Figure 5.1; Figure 5.2), typified by limited marine water circulation and high evaporation rates, leading to the precipitation of gypsum and subsequently replacement by anhydrite. The lack of visible porosity and the presence of massive and nodular anhydrite are characteristics of such settings where salinity levels are elevated and the arid to warmer climatic conditions conducive to gypsum precipitation. During the Early Permian, there was a mix of conditions conducive to gypsum precipitation

(arid/warmer climate, hypersaline brines rich in sulfates, restricted circulation of marine water to the lagoons/tidal flat environment). The massive and nodular anhydrite interbedded within the carbonate facies and in most cases precipitating in pores spaces and fractures suggest diagenetic pore infilling having implications on porosity and permeability development. A study by Mohammed-Sajed & Glover, (2020) highlighted that anhydrite cement has the potential to seal pores and fractures affecting the resulting reservoir quality. Contrary to their common contribution to poor reservoir quality, some studies by Lucia, (2004); Lucia, (1999); Lucia & Ruppel, (1996), have documented that a significant presence of anhydrite in some cases might not necessarily affect its quality, and even in some instances may improve the quality of the reservoir.
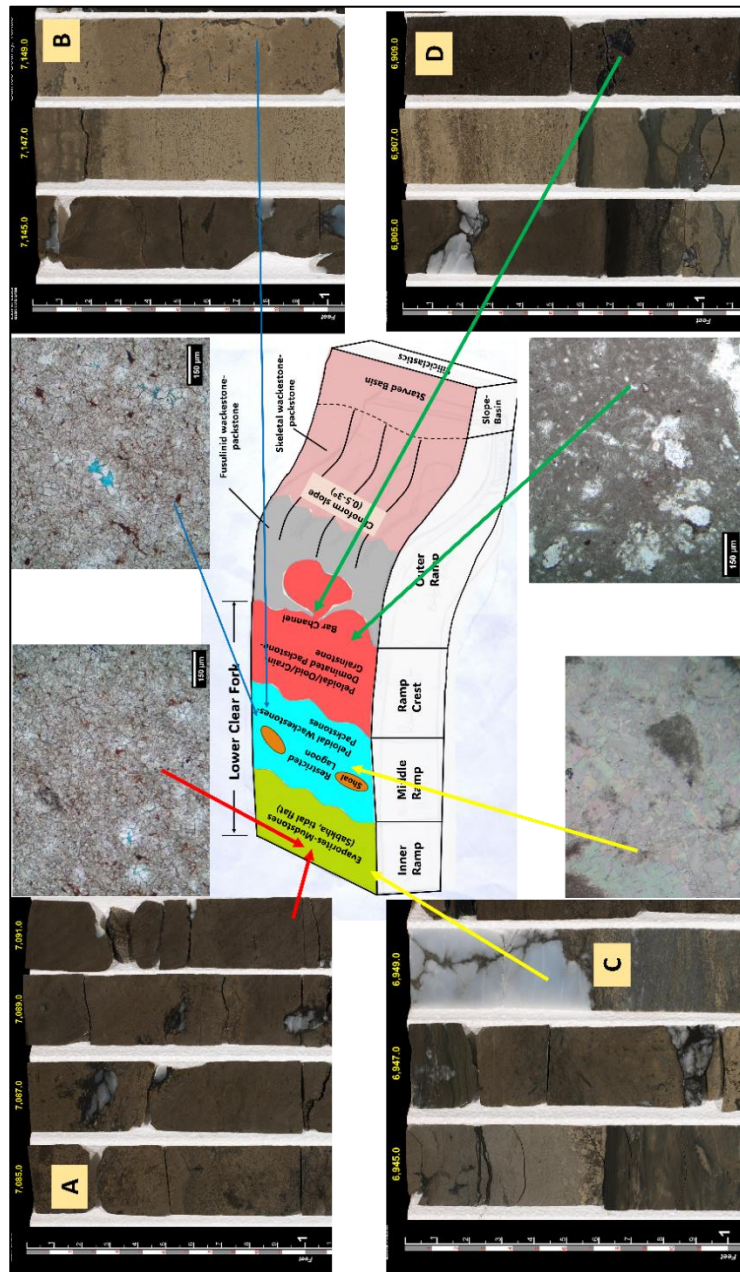
Figure 5.2. Schematic diagram for the shallow-water carbonate in the Permian Basin (after Ruppel et al., 1995). The associated cores and thin-section photomicrographs show the main facies characteristics in relation to the depositional environments established for the Lower Clear Formation. A (Dolomustone); B. (Dolowackestone); C. (Anhydrite); D. (Dolopackstone). Pictures of cores and thin sections of photomicrographs were taken in WL and PPL respectively.

5.2. Mineralogy of the Lower Clear Formation

The Lower Clear Fork facies are composed of dolomite, anhydrite, and a minor amount of clay and siliciclastics (quartz) (refer to Figure 4.6; Figure 4.12). The entire Lower Clear Fork interval contains a high amount of recrystallized dolomites (over 80% dolomite over the interval) and anhydrite. The work of Ruppel & Harrington (2012) on the Clear Fork reservoir at Fullerton Field supports this finding that, the entire Lower Clear Fork contains anhydrites and dolomites that were matrix replacive and pore-filling. The XRD data reflected an absence of calcite minerals in the interval. This suggests that the calcite ($CaCO_3$) in the precursor limestones have been replaced by dolomite.

Evidence of early dolomitization was observed in the thin section photomicrographs showing recrystallized dolomite crystals (Figure 5.3). Ruppel et al., (2002) in their work on the Clear Fork Group reservoirs on the Sierra Diablo Mountains in Texas, a proven outcrop analog to the subsurface Clear Fork reservoirs in the Permian Basin recognized that the Clear Fork successions including the Lower Clear Fork exhibited a notable deficiency in calcite, attributed to reflux dolomitization. The Lower Clear Fork mineralogy from Tex-Mex, S.E. Field shows a well-noted deficiency of calcite from the facies as early-stage dolomitization led to the replacement of the precursor calcites. Their work pointed out that calcite, if any remaining in the Clear Fork reservoirs, might be formed during the late stage of diagenesis. A specific diagenetic model is discussed in the next section.
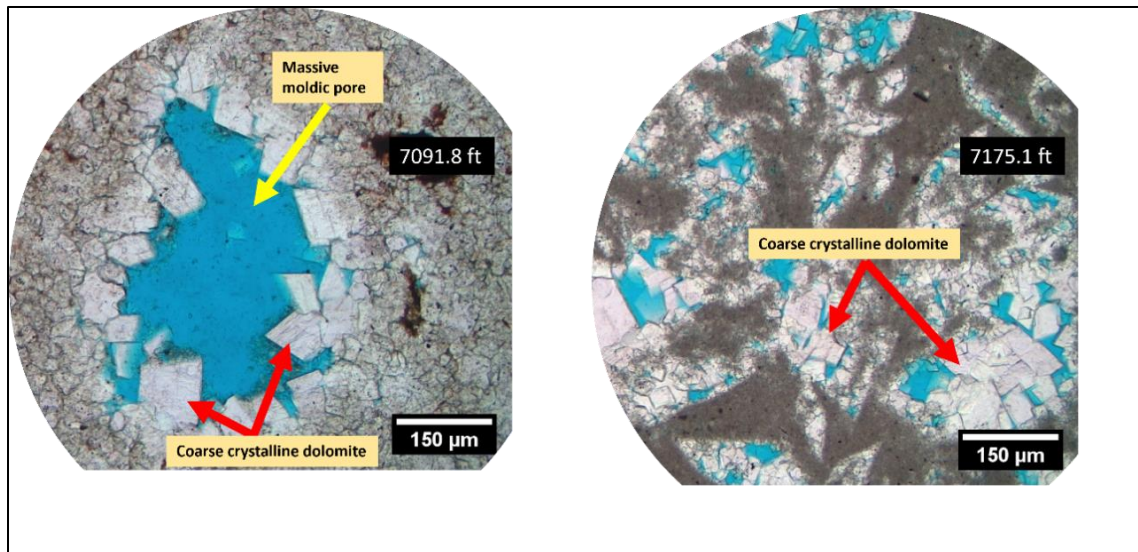
Figure 5.3. Photomicrographs of thin sections (in PPL) showing recrystallized dolomite minerals (red arrows) within the Lower Clear Fork interval. Note the crystalline dolomite fabric in the left image that has eliminated the precursor calcite. Depths of thin sections were 7091.8 ft (2161.6 m) (left) and 7175.1 ft (2186.9 m)(right). The top left yellow arrow points to a massive moldic pore.

The Clear Fork reservoirs contain massive and nodular anhydrites. The work of Ruppel, et al. (2002), however, noted that while the subsurface Clear Fork reservoirs contain anhydrite, they were missing in their outcrop equivalent at Apache Canyon due to the late dissolution and removal of the anhydrite by meteoric waters. This conclusion was based on the presence of anhydrite-sized vugs (left behind from anhydrite dissolution) exposed on the Apache Canyon outcrops. However, in the equivalent subsurface Clear Fork, as seen from this study as well, the vugs were commonly occupied with anhydrite. The Lower Clear Fork core with anhydrite-filled vugs is shown in Figure 5.4.
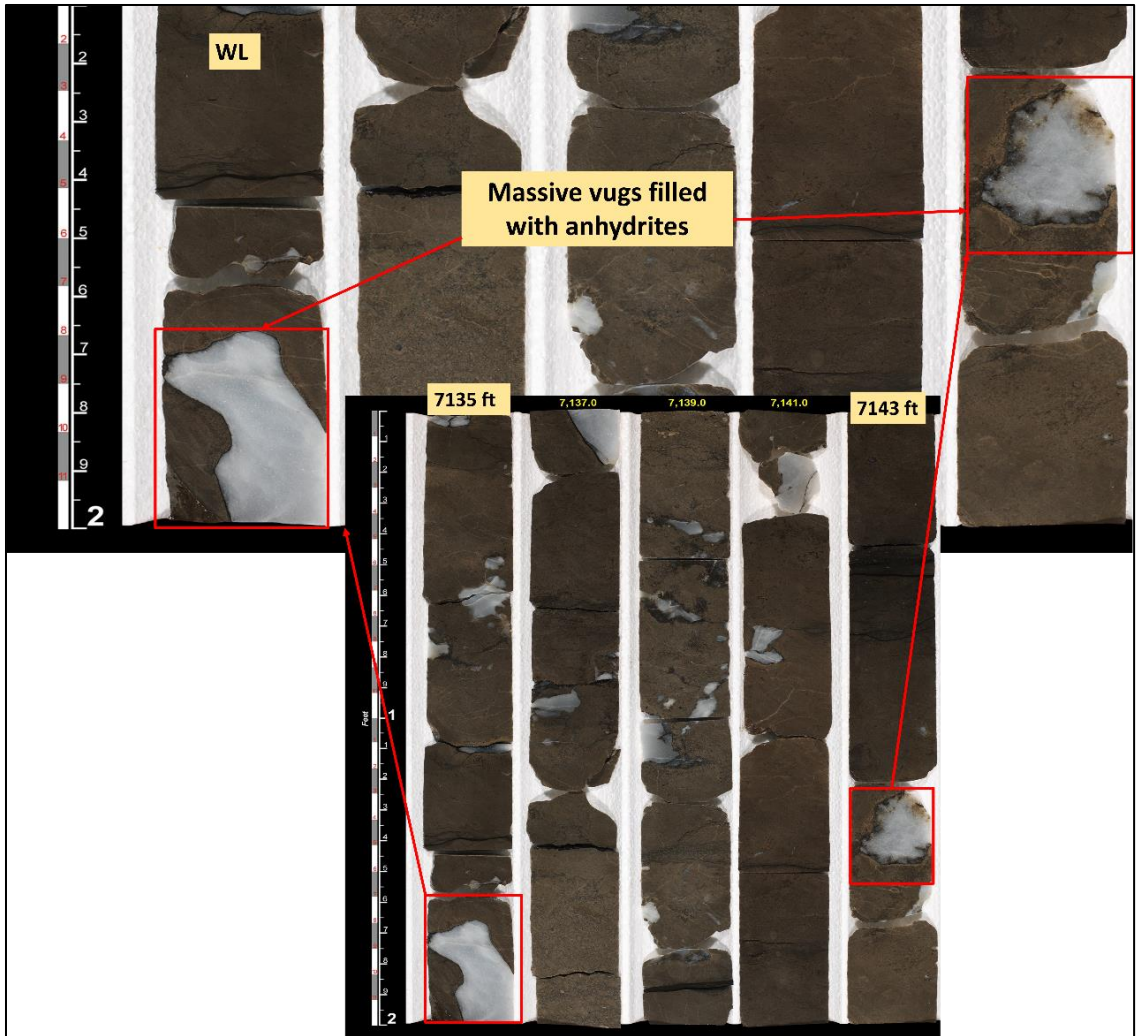
Figure 5.4. Slabbed core picture of Peterson 1P core showing massive vugs filled with anhydrite. The depth range of the core was between 7135 to 7143 ft (2174.7 – 2177.2 m). The core picture was taken in white light (WL).

5.2.1. Diagenesis in the Lower Clear Fork

The precipitation of evaporites is commonly associated with the dolomitization of shallow water carbonates, owing to either seawater evaporation or sulfate dissolution (Melim & Scholle, 2002; Qing et al., 2001). According to (Flügel, 2010; Tucker & Wright, 1990), various variables influence the order of diagenesis in carbonate formations, including mineral composition, grain size, texture, characteristics of pore fluids, and climatic conditions. Reflux dolomitization of the Permian carbonate platform occurred as a result of high evaporation of hypersaline brine-rich seawater. Evidence of this model (seepage reflux dolomitization) as applicable to the Permian carbonates was first proposed by Adams and Rhodes in 1960. To date, the seepage reflux model as proposed by Adams and Rhodes (1960) in their work on the Permian dolomite distribution in west Texas remained widely accepted to be the dolomitization process that modified most of the Permian carbonates (Longman, 1982).

In their model (refer to seepage reflux diagrams in Figure 5.5), high rates of evaporation from the coastal environment (restricted lagoons/tidal flats environment) in a restricted marine water circulation concentrated highly dense saline brine rich in Mg^{2+} ions. The source of magnesium ions is from the seawater. As the evaporation of the seawater progressed, the Ca^{2+} ions were liberated from the solution due to the precipitation of calcium sulfate in the form of gypsum. The resulting hypersaline brine rich in Mg^{2+} becomes denser than the sea water causing it to percolate downward and seaward under

gravity influence (seepage reflux).
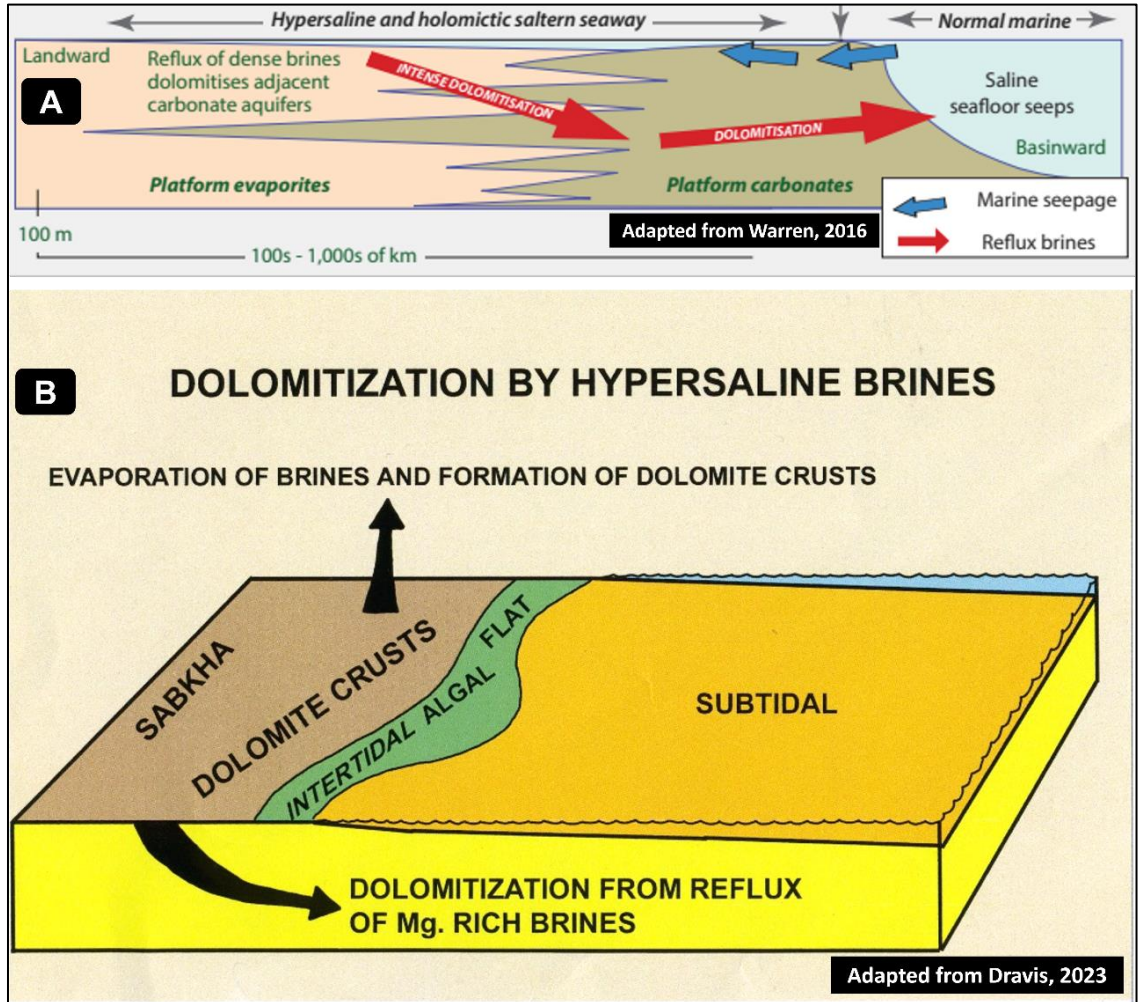
Figure 5.5. Hypersaline seepage reflux model for the dolomitization and gypsum precipitation. A. Modified Adams and Rhodes (1960) seepage reflux (Warren, 2016). B. Block model of hypersaline brine showing depositional environments (adapted from Dravis, 2023).

The percolation of the dense magnesium-rich fluids fills the pores of the carbonate sediments underlying the lagoons/ tidal flats. The hypersaline brine rich in Mg^{2+} reacts with pore fluids in the carbonate sediments and replaces the Ca^{2+} in the precursor limestones (Adams & Rhodes, 1960). The resulting process led to the formation of dolomite. Additionally, as saline-rich brine percolates through the pores, some gypsum precipitates within the carbonate matrix. With deeper burial and compaction, the gypsum dehydrates transforming into anhydrite. (refer to Figure 5.6). Restricted circulation of water from the seawater supplied Mg^{2+} ions to the restricted lagoon and coastal tidal flat replenishing the water lost to evaporation and refluxion (refer to Figure 5.5a). The strength of reflux dolomitization was aided by the salinity of the dolomitizing fluid (seawater), the permeability of the underlying carbonate sediment, density gradient, topography, and reactivity of the sediments (Adam and Rhodes, 1960).

The early dolomitization and gypsum precipitation were accelerated by favorable conditions present during the Permian period. The presence of the restricted lagoon/tidal flats overlying the porous deposited carbonates (precursor limestones), the marine water circulating brines-rich fluids (seawater), and the prevalent high evaporation as a result of the arid and warmer climatic regimes during the Early Permian facilitated the reflux dolomitization of the platform carbonates and gypsum precipitation. Over time, burial, compactive actions, and other diagenetic processes led to the transformation of the initially deposited gypsum into anhydrite through the loss of water molecules. The dolomite and

gypsum precipitation processes affected not only the mineral composition by increasing the magnesium content but also significantly produced broad ranges of porosity and permeability values within the facies identified (Figure 5.4 and Figure 5.6). Within the Lower Clear Fork interval, the dominance of dolomite over anhydrite is directly tied to the early dolomitization, shallow gypsum precipitation, and later replacement of gypsum by anhydrite processes. The high dolomite composition to low anhydrite precipitation (negative relationship between the dolomite and anhydrite observed; see Figure 4.9) resulted from the dolomitization and gypsum precipitation that altered the original mineral composition of the precursor limestone. The early dolomitization process converted limestone (calcite or aragonite - $CaCO_3$) to dolomite ($CaMg(CO_3)_2$), involving the replacement of calcium ions in the precursor limestone by magnesium ions (Equation 5.1). As the seawater evaporated, the calcium ions (Ca^{2+}) were liberated from the solution as a result of gypsum precipitation (refer to Equation 5.2 and Equation 5.2 represent the chemical reaction pathway for the dolomite formation and gypsum precipitation respectively.

$$2CaCO_3 + Mg^{2+} \rightarrow CaMg(CO_3)_2 + Ca^{2+}$$

Equation 5.1

$$Ca^{2+} + SO_4^{2-} + 2H_2O \rightarrow CaSO_4.2H_2O$$

Equation 5.2
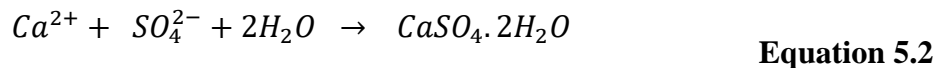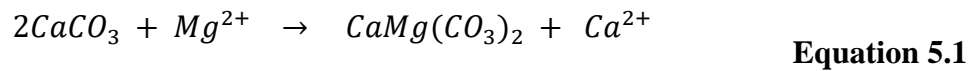
While gypsum precipitation releases significant Ca^{2+}, the resulting hypersaline brine becomes highly concentrated with magnesium (Mg^{2+}) ions for dolomitization. This

significantly raises the concentration of the magnesium ions when compared with the concentration of the calcium ions in the resulting hypersaline brine (Mg^{2+}/Ca^{2+} ratio) contributing to the overall relationship as shown in Figure 4.9 (Yaseen & Khan, 2018).

In summary, the depositional environments of the Lower Clear Fork Formation during the Permian contributed to early-stage dolomitization and gypsum precipitation that occurred in the Lower Clear Fork facies. The Early Permian was characterized by arid and warmer climatic conditions with a restricted marine water circulation enhancing high evaporation of seawater, leading to the formation of dolomite and gypsum (later transformed into anhydrite).
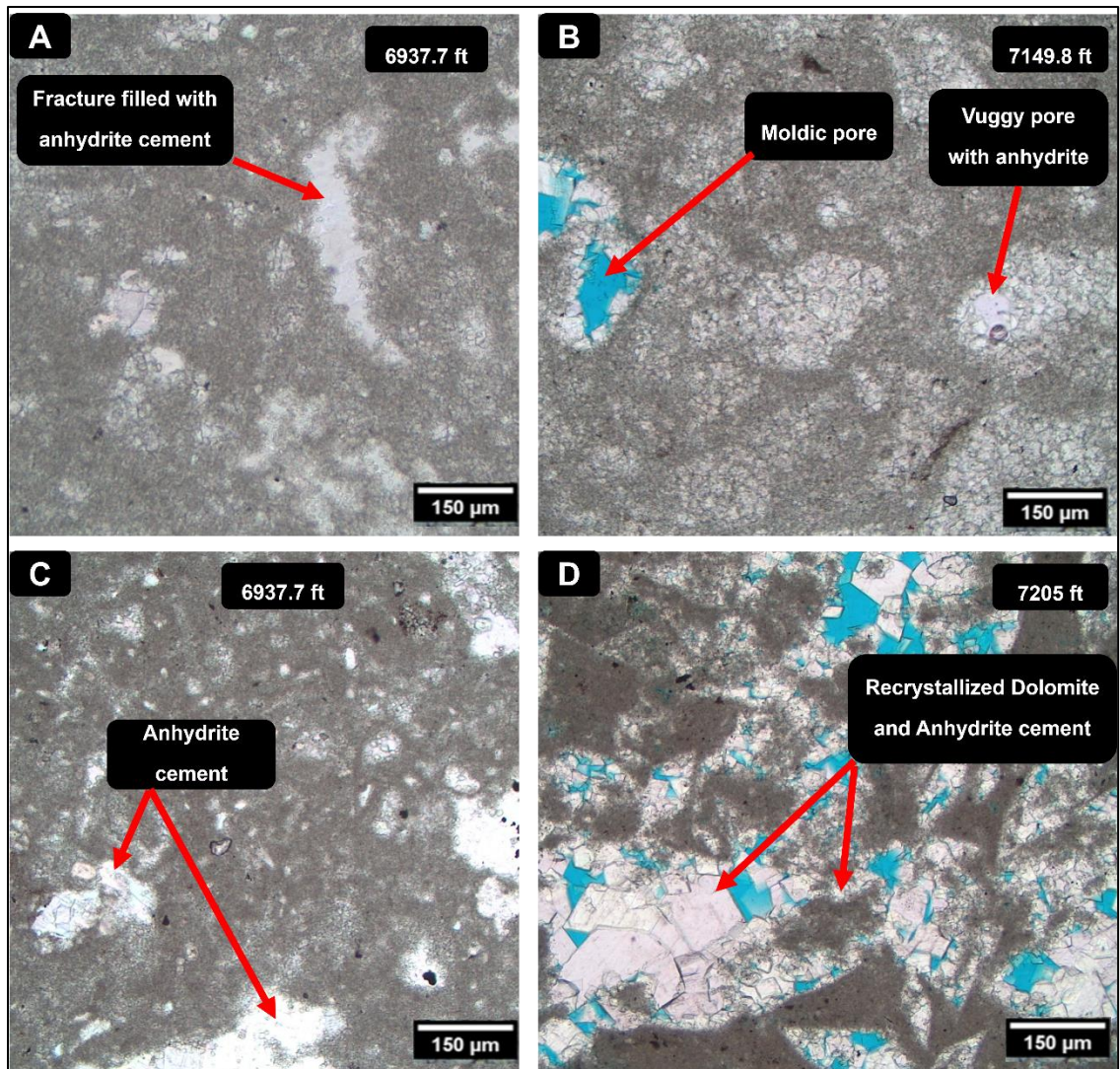
Figure 5.6. Thin section photomicrographs (PPL)) of dolomite-anhydrite diagenetic features in the Lower Clear Fork. (A) Fracture filled with anhydrite; (B) Vuggy pore filled with anhydrite; (C) Anhydrite cement in facies; (D) Recrystallized dolomite and anhydrite cement.

5.2.2. Paragenesis in the Lower Clear Fork

The deposition of the Lower Clear Fork occurred on a shallow marine water platform during the Permian period. The work of Landreth (1977) on the Lower Clear Fork carbonate from Mitchel County, Texas suggested that the carbonates were originally composed of aragonite with a minor amount of high Mg-calcite and calcite. His work noted that some of the carbonate grains were coated by algae forming a dense micritic coating.

Diagenetically, early dolomitization took place in the coastal tidal flat and restricted lagoon environment where calcites in precursor limestones were replaced by dolomite. As pointed out earlier in this work, the early dolomitization was caused by the evaporation of seawater from the coastal environment during the arid and warmer environment during the Early Permian leaving behind dense hypersaline brines. The resulting dense hypersaline brines percolated through the pores of the carbonates, reacting with the precursor calcite to produce dolomite. Following the lithification of the sediments, erosion of the peritidal tidal flat environment caused hard crust structures to be broken by storm tides (Landreth, 1977). During high tides, mud was moved from the subtidal environment and deposited in the peritidal tidal flat surfaces, filling in the low spots of the erosional surface. Subaerial exposure of the tidal flats/restricted lagoon environment during the arid to warmer climate precipitated shallow gypsum within the Lower Clear Fork.

After early dolomitization, the inner to subtidal sediments experienced burial saturated by seawater due to seawater progradation. The discharge of saline water

percolating into the sediments created a refluxing zone with seawater, leading to the dolomitization of unstable carbonates. The dolomitization process intensified during basinward migration of the mixing zone, resulting in the formation of drusy cements. Dolomite crystal size increased distally as the dolomitization process progressed (Landreth, 1977).

The Ca^{2+} ions liberated during dolomitization likely led to high sulfate concentration in saline brine, leading to the formation of gypsum as evaporation took place, including replacement nodules and massive replacement of dolomite (Landreth, 1977). Over time, intensified evaporation, burial, compactive actions, and other diagenetic processes caused the initially precipitated gypsum to be replaced by anhydrite through the loss of water molecules. Finally, from Landreth (1977), the last step of diagenesis involving the Lower Clear Fork involved the freshwater dissolution of anhydrite, evidenced by moldic and vuggy pores that formed from the dissolution of sparry replacement.

5.3. Reservoir Quality of the Lower Clear Fork

The analysis of facies, mineralogy, and petrophysical properties (porosity, permeability, water, and oil saturation) of the Lower Clear Fork reservoir suggests that the quality of the Lower Clear Fork reservoir in the Tex-Mex, S.E. Field presents a complex scenario influenced by a dynamic interplay of geological processes and lithological heterogeneities. The Lower Clear Fork interval exhibited high water saturation and low oil saturation in pore spaces presenting possible challenges in extracting the oil in place, as a

significant portion of the reservoir pore space is filled with water rather than oil (Figure 4.19; Table 5.1). This particular situation tends to potentially impede the efficient recovery of the oil from the pores.

Additionally, the distribution of porosity and permeability in the interval is highly heterogeneous further complicating management of the reservoir, as a result of uneven distribution of reservoir fluids and varying flow characteristics across the formation. Overall, the Lower Clear Fork presents a low-quality reservoir with porosity ranging between 0.5% to 10%, while Klinkenberg permeability varies between 10^{-4} mD to 17.6 mD However, among the facies present in the interval, dolopackstone facies (grain-dominated) exhibit relatively better porosity and permeability, 4.53 % and 17.6 mD (Table 5.1), offering pockets of enhanced reservoir quality within the formation. Ruppel & Harrington (2012) in their study of the Lower Clear Fork at Fullerton Field, an analogous Clear Fork reservoir, suggested that the lower porosity in the updip (peritidal tidal flats and inner ramp environments) facies was probably a result of early dolomitization, compaction, and also due to porosity occlusion by dolomite and anhydrite. However, the dolopackstones deposited on the ramp crest of the platform were least affected by compaction and dolomitization. While significant heterogeneities exist in reservoir properties for all the facies, the porosity, and permeability in the dolopackstones are the highest in this study.

Moreover, the dolomitization and early-stage gypsum precipitation in pores and fractures further complicate the reservoir system. While dolomitization might have

enhanced porosity and permeability in some instances, the precipitation of gypsum and subsequently anhydrite occluded pores and fractures acted as barriers to fluid flow, restricting hydrocarbon movement within the reservoir. The broad ranges of anhydrite and dolomite composition mixed with minor clay and siliciclastics across the different facies suggest a mixed reservoir quality, with areas of potential high productivity interspersed with zones of reduced fluid movement.

Table 5.1. Summary table showing average and ranges of reservoir parameters for the Lower Clear Fork interval from Tex-Mex, S.E. Field.

Facies	ϕaverage (%)	K (mD)	Sw (%)	Soil (%)
Dolomudstone	3.20	$3*10^{-4} - 1.6$	12.4 – 95.4	0.1 – 5.4
Dolowackestone	3.04	$2*10^{-4} - 4.52$	19.4 – 94.2	0.4 – 5.7
Dolopackstone	4.53	$2*10^{-4} - 17.6$	58.4 – 94.7	1.0 – 14.4
Anhydrite	0.94	10^{-3}	-	-

The Lower Clear Fork reservoir heterogeneity is revealed in the broad ranges of lithological, petrophysical properties, and mineralogical distribution. These characteristics point to the cyclicity in sediment deposition and post-depositional processes that affected the facies. The anhydrite facies, representative of the restricted lagoon and coastal tidal flat settings are typically associated with low porosity and permeability. While its presence is crucial from a hydrocarbon trapping perspective, zones where there are dominated could be targeted for hydraulic fracturing to open pores for for hydrocarbon fluid flow.

6. CONCLUSIONS

This study defined depositional and diagenetic characteristics of the Lower Clear Fork Carbonates and completed petrophysical analyses to extrapolate results. The study was based on analysis of core data and wireline logs from Tex-Mex, S.E. Field on the Central Basin Platform of the Permian Basin. Four major facies were identified, differentiated, and interpreted. The mineralogical and petrophysical characteristics of the Lower Clear Fork reservoir have been presented in this work. From the results of the study, the following can be concluded:

1. The Lower Clear Fork unit was deposited in a shallow marine water environment during the Early Permian period. The character of the dolomudstones/anhydrite facies shows close association with high evaporative environments (coastal lagoons/tidal flats) with restricted circulation of hypersaline brines. The dolowackestones were deposited in the inner to middle ramp while the grain-dominated dolopackstones were deposited on the high energy ramp crest of the Central Basin Platform.

2. The Lower Clear Fork facies experienced early dolomitization causing modifications to their mineralogy and depositional textures. These early and complex diagenetic processes have led to heterogeneity in its mineralogy, and

reservoir properties.

3. The identified facies include dolomudstone, dolowackestone, dolopackstone, and anhydrite. Individual anhydrite beds ranged in thickness from less than one inch to a few feet. The anhydrite beds are potential zones for hydraulic fracturing.

4. The Lower Clear Fork interval displays high heterogeneity and low reservoir quality. The interval shows a broad range of porosity and permeability values. Calibrated porosity values ranged between 0.5% to 10%, and permeability (Klingenberg) ranged between 10^{-4} mD to 17.6 mD. Dolopackstone, however, presented the best reservoir quality results when compared to other facies.

5. The Lower Clear Fork Interval exhibited high saturation of water (up to 95.4%) and low oil saturation (highest 14.4%) across the interval. The early-stage gypsum precipitation and its subsequent replacement by anhydrite in other facies is a likely factor to account for the low oil saturation, as anhydrite acts as an effective seal, limiting hydrocarbon migration and trapping of fluids.

6. The Lower Clear Fork pore network is predominantly secondary pore types; intercrystalline, micropores, vugs, molds, and interparticle. Dissolution created the porosities favorable for hydrocarbon migration and extraction. Early-to-late-stage cementation by dolomite and anhydrite significantly reduced reservoir porosity and permeability.

7. FUTURE WORK

This study did not critically assess diagenetic processes and their effects on the evolution of pore systems in the Lower Clear Fork. Future studies should therefore be expanded to unravel the diagenesis and pore-scale modeling to understand pore system evolution in the Lower Clear Fork reservoir. Two other sets of cores are available, which would aid in understanding the spatial distribution of facies in the study area. Finally, the correlation of the facies to multiple wells would allow for the mapping of facies and depositional environments across the study area and platform.

8. REFERENCES

Adams, J. (1965). Stratigraphic-Tectonic Development of Delaware Basin. AAPG Bulletin, 49. https://doi.org/10.1306/A6633888-16C0-11D7-8645000102C1865D.

Adams, J., & Rhodes, L. (1960). Dolomitization by Seepage Refluxion. American Association of Petroleum Geologists Bulletin, 44(12), 1912–1920. https://archives.datapages.com/data/bulletns/1957-60/data/pg/0044/0012/1900/1912.htm?doi=10.1306%2F0BDA6263-16BD-11D7-8645000102C1865D

Atchley, S. C., Kozar, M. G., & Yose, L. (1999). A Predictive Model for Reservoir Distribution in the Permian (Leonardian) Clear Fork and Glorieta Formations, Robertson Field Area, West Texas. AAPG Bulletin, 83, 1031–1055.

Blakey, R. (2013). Regional Paleogeography, North American Paleogeography, Early Permian (280Ma). In https://deeptimemaps.com/north-america/.

Chaney, D., & Dimichele, W. (2007). Paleobotany of the classic redbeds (Clear Fork Group - Early Permian) of north central Texas. Proceedings of the Th International Congress on Carboniferous and Permian Stratigraphy, 357–366.

Choquette, P. W., & Pray, L. C. (1970). Geologic Nomenclature and Classification of Porosity in Sedimentary Carbonates1. AAPG Bulletin, 54(2), 207–250. https://doi.org/10.1306/5D25C98B-16C1-11D7-8645000102C1865D

Cummins, W. F. (1890). The Permian of Texas and its overlying beds. [Available online from the University of Texas-Austin library: http://www.lib.utexas.edu/books/dumble/]

Cummins, W. F. (1891). Report on the geology of northwestern Texas. Texas Geological Survey Annual Report 2. 1890: 357-552.

Dravis, J. J. (2023). Carbonate Play Development in Mesozoic Sequences of the U.S. Gulf Rim: Influences of Physiographic Setting and Structural Controls. East Texas Geological Society Seminar.

Dunham, R. J. (1962). Classification of Carbonate rocks according to depositional texture, 108-121. AAPG Mem., 1.

Dutton, S. P., Kim, E. M., Broadhead, R. F., Breton, C. L., Raatz, W. D., Ruppel, S. C., & Kerans, C. (2004). Play Analysis and Digital Portfolio of Major Oil Reservoirs in the Permian Basin: Application and Transfer of Advanced Geological and Engineering Technologies for Incremental Production Opportunities. https://doi.org/10.2172/828411

Dutton, S. P., Kim, E. M., Broadhead, R. F., Raatz, W. D., Breton, C. L., Ruppel, S. C., & Kerans, C. (2005). Play analysis and leading-edge oil-reservoir development methods in the Permian basin: Increased recovery through advanced technologies. AAPG Bulletin, 89(5), 553–576.

Enverus Inc. (2024). Production data from the Peterson 1P well from Tex-Mex, S.E. Field. Last Accessed on February 23, 2024. Enverus Inc.

Ewing, T. E. (2016). Texas Through Time: Lone Star Geology, Landscapes, and Resources: The University of Texas at Austin, Bureau of Economic Geology Udden Series No. 6, 431 p. 6(431p).

Fairhurst, B., Ewing, T., & Lindsay, B. (2021). West Texas (Permian) Super Basin, United States: Tectonics, structural development, sedimentation, petroleum systems, and hydrocarbon reserves. AAPG Bulletin, 105(6), 1099–1147. https://doi.org/10.1306/03042120130

Flügel, E. (2010). Microfacies of Carbonate Rocks: Analysis, Interpretation, and Application (978th-3rd-642nd-03796–2nd ed.). Springer-Verlag.

Frenzel, H. N., Bloomer, R. R., Cline, R. B., Cys, J. M., Galley, J. E., Gibson, W. R., Hills, J. M., King, W. E., Seager, W. R., & Kottlowski, F. E. (1988). The Permian Basin region. GeoScience World. https://doi.org/https://doi.org/10.1130/DNAG-GNA-D2.261

Galley, J. E. (1958). Oil and geology in the Permian basin of Texas and New Mexico: North America.

Galley, J. E. (1971). Summary of Petroleum Resources in Paleozoic Rocks of Region 5 - North, Central, and West Texas and Eastern New Mexico: Region 5.

Haq, B. U., & Schutter, S. R. (2008). A Chronology of Paleozoic Sea-Level Changes. Science, 322(5898), 64–68. https://doi.org/10.1126/science.1161648

Hills, J. M. (1972). Late Paleozoic sedimentation in west Texas Permian basin. AAPG Bulletin, 56(12), 2303–2322.

Hills, J. M. (1984). Sedimentation, tectonism, and hydrocarbon generation in Delaware Basin, west Texas, and southeastern New Mexico. AAPG Bulletin, 68(3), 250–267.

Holtz, M. H., Ruppel, S. C., & Hocott, C. (1992). Integrated Geologic and Engineering Determination of Oil-Reserve-Growth Potential in Carbonate Reservoirs. Journal of Petroleum Technology, 44(11), 1250–1257. https://doi.org/10.2118/22900-PA

Horak, R. L. (1985). Trans-Pecos Tectonism and its Effect on the Permian Basin: In Dickerson, P. W., and Muehlberger, W.M., eds., Structure and Tectonics of Trans-Pecos Texas, Midland, Texas. West Texas Geological Society Publication 85-8 1, 8 1-87.

Jadoon, Q. K., Roberts, E., Blenkinsop, T., Wust, R. A. J., & Shah, S. A. (2016). Mineralogical modeling and petrophysical parameters in Permian gas shales from the Roseneath and Murteree Formations, Cooper Basin, Australia. Petroleum Exploration and Development, 43(2), 277–284. https://doi.org/https://doi.org/10.1016/S1876-3804(16)30031-3

Jenkins, R. E. (1987). Typical core analysis of different formations. In Petroleum Engineering Handbook. Richardson, TX: Society of Petroleum Engineers.

Kerans, C. K., Kempter, J., Rush, & Fisher, W. L. (2000). Facies and stratigraphic controls on a coastal paleo-karst: Lower Permian, Apache Canyon, West Texas, in R. Lindsay, R. Trentham, R.F. Ward, and A. H. Smith, eds., Classic Permian geology of west Texas and Southeastern New Mexico: 75 years of Permian Basin oil and gas exploration and development: West Texas Geological Society Publication 00-108, p.55–82.

King, P. B. (1942). Permian of west Texas and southeastern New Mexico: American Association of Petroleum Geologists, Bulletin, v. 26, p. 535-763.

King, P. B., Henbest, L. G., Yochelson, E. L., Cloud Jr., P. E., Duncan, H., Finks, R. M.,

Sohn, I. G., & Survey, U. S. G. (1965). Geology of the Sierra Diablo region, Texas; with special determinative studies of Permian fossils. In Professional Paper. https://doi.org/10.3133/pp480

Landreth, R. A. (1977). Depositional Environments and Diagenesis of the Lower Clear Fork Group, Mitchel County, Texas [Published]. Texas Tech University.

Longman, M. W. (1982). Carbonate Diagenesis as a Control on Stratigraphic Traps, with examples from the Williston Basin. https://api.semanticscholar.org/CorpusID:128430340

Lucia, F. (2004). Origin and petrophysics of dolostone pore space. Geological Society, London, Special Publications, 235, 141–155. https://doi.org/10.1144/GSL.SP.2004.235.01.06

Lucia, F. J. (1999). Carbonate Reservoir Characterization: Springer-Verlag, Berlin. 226 pp. In Geological Magazine (Vol. 136, Issue 3). Cambridge University Press.

Lucia, F. J., & Ruppel, S. C. (1996). Characterization of diagenetically altered carbonate reservoirs, South Cowden Grayburg reservoir, west Texas. SPE Annual Technical Conference and Exhibition, SPE-36650.

Mazzullo, S. J. (1982). Stratigraphy and depositional mosaics of lower Clear Fork and Wichita Groups (Permian), northern Midland basin, Texas. AAPG Bulletin, 66(2), 210–227.

Mazzullo, S. J., & Reid, A. M. (1989). Lower Permian platform and basin depositional systems, northern Midland Basin, Texas, in Crevello, P.D., Wilson, J.L., Sarg, J.F. and Read, J.F., eds., Controls on Carbonate Platform and Basin Development: SEPM Spec. Publ. 44, p. 305–320.

Melim, L., & Scholle, P. (2002). Dolomitization of the Capitan Formation forereef facies (Permian, west Texas, and New Mexico): Seepage reflux revisited. Sedimentology, 49, 1207–1227. https://doi.org/10.1046/j.1365-3091.2002.00492.x

Miall, A. D. (2008). The southern Midcontinent, Permian Basin, and Ouachitas, Chapter 8. In A. D. Miall (Ed.), The Sedimentary Basins of the United States and Canada, Elsevier, Amsterdam, The Netherlands (Vol. 5, pp. 297–327). Elsevier.

https://doi.org/https://doi.org/10.1016/S1874-5997(08)00008-7

Mohammed-Sajed, O., & Glover, P. (2020). Dolomitization, cementation and reservoir quality in three Jurassic and Cretaceous carbonate reservoirs in north-western Iraq. Marine and Petroleum Geology, 104256. https://doi.org/10.1016/j.marpetgeo.2020.104256

Montañez, I. P., Tabor, N. J., Niemeier, D., DiMichele, W. A., Frank, T. D., Fielding, C. R., Isbell, J. L., Birgenheier, L. P., & Rygel, M. C. (2007). CO2-Forced Climate and Vegetation Instability During Late Paleozoic Deglaciation. Science, 315(5808), 87–91. https://doi.org/10.1126/science.1134207

Montgomery, S. L. (1998). Permian Clear Fork Group, North Robertson Unit: Integrated Reservoir Management and Characterization for Infill Drilling, Part II-Petrophysical and Engineering Data. AAPG Bulletin, 82, 1985–2002.

Qing, H., Bosence, D., & Rose, E. (2001). Dolomitization by penesaline sea water in Early Jurassic peritidal platform carbonates, Gibraltar, western Mediterranean. Sedimentology, 48, 153–163. https://doi.org/10.1046/j.1365-3091.2001.00361.x

Ruppel, S. C. (2002). Geological Controls on Reservoir Development in a Leonardian (Lower Permian) Carbonate Platform Reservoir, Monahans Field, West Texas: The University of Texas at Austin, Bureau of Economic Geology, Report of Investigations No. 266, 58 p.

Ruppel, S. C. (2017). Applying sequence stratigraphic methods to mudrock systems: when, where, and how? Presentation at the Fort Worth Geological Society held in Fort Worth, Texas, 10 April.

Ruppel, S. C. (2020). Lower Permian (Leonardian) platform carbonate succession: deposition and diagenesis during a waning icehouse period, in Ruppel, S. C., ed., Anatomy of a Paleozoic basin: the Permian Basin, USA (vol. 2, Ch. 20): The University of Texas at Austin, Bureau of Economic Geology Report of Investigations 285; AAPG Memoir 118, p. 227–282.

Ruppel, S. C., & Harrington, R. R. (2012). Facies and sequence stratigraphy: Critical tools for reservoir framework definition, Fullerton Clear Fork Reservoir, Texas.

Ruppel, S. C., & Jones, R. H. (2006). Key role of outcrops and cores in carbonate

reservoir characterization and modeling, Lower Permian Fullerton field, Permian Basin, United States.

Ruppel, S. C., Kerans, C., Major, R. P., & Holtz, M. H. (1995a). Controls on Reservoir Heterogeneity in Permian Shallow Water Carbonate Platform Reservoirs, Permian Basin: Implications for Improved Recovery: The University of Texas at Austin. Bureau of Economic Geology Geological Circular GC9502.

Ruppel, S. C., Kerans, Charles., Major, R. P., & Holtz, M. H. (1995b). Controls on reservoir heterogeneity in Permian shallow-water-platform carbonate reservoirs, Permian Basin: implications for improved recovery. The University of Texas at Austin, Bureau of Economic Geology, Geological Circular 95-2D, 30.

Ruppel, S. C., & Ward, W. B. (2013). Outcrop-based characterization of the Leonardian carbonate platform in west Texas: Implications for sequence-stratigraphic styles in the Lower Permian. AAPG Bulletin, 97(2), 223–250. https://doi.org/10.1306/05311212013

Ruppel, S. C., Ward, W. B., Ariza, E. E., & Jennings Jr, J. W. (2000). Cycle and sequence stratigraphy of Clear Fork reservoir-equivalent outcrops: Victorio Peak Formation, Sierra Diablo, Texas, in R. Lindsay, R. Trentham, R.F. Ward, and A.H. Smith, eds., Classic Permian geology of West Texas and Southeastern New Mexico: 75 years of Permian Basin oil and gas exploration and development: West Texas Geological Society Publication 00-108, p.109–130.

Ruppel, S. C., Ward, W. B., Ariza, E. E., & Jennings Jr, J. W. (2002). Integrated Geological and Petrophysical Studies of Clear Fork Reservoir Analog Outcrops: Sierra Diablo Mountains, Texas. Integrated Outcrop and Subsurface Studies of the Interwell Environment of Carbonate Reservoirs: Clear Fork (Leonardian-Age) Reservoirs, West Texas, and New Mexico, 1–57.

Senergy Ltd. (2008). Interactive Petrophysics Software User's Manual (V3.5). Synergy Ltd.

Silver, B. A., & Todd, R. G. (1969). Permian Cyclic Strata, Northern Midland and Delaware Basins, West Texas, and Southeastern New Mexico. AAPG Bulletin, 53, 2223–2251.

Tucker, M. E., & Wright, V. P. (1990). Carbonate Sedimentology. Blackwell, Oxford,

482 p. http://dx.doi.org/10.1002/9781444314175

Tyler, N., Galloway, W. E., Garrett, C. M. Jr., & Ewing, T. E. (1984). Oil Accumulation, Production Characteristics, and Targets for Additional Recovery in Major Oil Reservoirs of Texas: The University of Texas at Austin, Bureau of Economic Geology, Geological Circular 84-2, 31 p.

Ward, R. F., Kendall, C. G. St. C., & Harris, P. M. (1986). Upper Permian (Guadalupian) Facies and their Association with Hydrocarbons - Permian Basin, West Texas, and New Mexico. AAPG Bulletin, 70(3), 239–262. https://doi.org/10.1306/9488566F-1704-11D7-8645000102C1865D

Warren, J. K. (2016). Evaporites: A Geological Compendium. Springer International Publishing.

Yaseen, M., & Khan, E. U. (2018). Dolomite and dolomitization model - a short review.

9. APPENDIX

The primary dataset used in this research is proprietary. As a consequence, pictures of cores, well information, and core data tables including XRD and routine core analysis data are not displayed. The decision to restrict display is per the proprietary guidelines outlined by the donors of the core and associated data. However, it may be made available upon request to the Core Donors or Stephen F. Austin State University.

10. VITA

Seyram Nyamasekpor was born in Ghana, where he attended Sogakope Senior High School. In 2013, he was admitted into the Bachelor of Science in Geological Engineering program at the Kwame Nkrumah University of Science and Technology and successfully graduated in June 2017. During his undergraduate studies, Seyram served as an engineering intern at the Petroleum Department of the Environmental Protection Agency. Following his graduation in 2017, Seyram returned to the same department. In the Spring of 2022, he began his graduate studies at Stephen F. Austin State University and graduated in May 2024. Seyram's future lies in conducting relevant research into net-zero carbon energy technologies (H_2 storage, CO_2 Sequestration, and Utilization, Critical Minerals, Geothermal Energy, etc.) recognizing their crucial role in achieving the goals of the energy transition.

Permanent Address: Nyamasekpor Bismark Selorm, P. O. Box 89

66 Artillery Regiment, Volta Barracks, Ho, Ghana

Style Manual: Geological Society of America

This thesis was typed by Seyram Nyamasekpor